TFBP-TR-164

for U.S. Nuclear Regulatory Commission

REVISION 2

w/RIL #25

23-249

FRAP-S3 ANALYTICAL MODELS AND INPUT MANUAL
FRAP-S3 A COMPUTER CODE FOR THE STEADY-STATE ANALYSIS OF OXIDE FUEL RODS
VOLUME 1

March 1978

EG&G Idaho, Inc.

IDAHO NATIONAL ENGINEERING LABORATORY

DEPARTMENT OF ENERGY

IDAHO OPERATIONS OFFICE UNDER CONTRACT EY-76-C-07-1570

23-250

FRAP-S3: A COMPUTER CODE FOR THE STEADY-STATE ANALYSIS OF OXIDE FUEL RODS

VOLUME 1

FRAP-S3 ANALYTICAL MODELS AND INPUT MANUAL

M. P. Bohn, Section Leader
Fuel Code Development

J. A. Dearien
FARAD Branch Manager

J. G. Crocker, Manager
Thermal Fuels Behavior Division

THERMAL FUELS BEHAVIOR PROGRAM

EG&G Idaho, Inc.

23-251

FRAP-S3: A COMPUTER CODE FOR THE STEADY-STATE ANALYSIS OF OXIDE FUEL RODS

VOLUME 1

FRAP-S3 ANALYTICAL MODELS AND INPUT MANUAL

By

J. A. Dearien
G. A. Berna
M. P. Bohn
J. D. Kerrigan
D. R. Coleman

PREPARED BY THE THERMAL FUEL BEHAVIOR PROGRAM

EG&G Idaho, Inc.

Date Released - January 1977

Revision - October 1977

ABSTRACT

FRAP-S3 (Fuel Rod Analysis Program - Steady-State, Version 3) is a FORTRAN IV computer code which can be used to solve for the long term burnup response of a light water reactor fuel rod. The coupled effects of fuel and cladding deformation temperature distribution, internal gas accumulation and pressure and material property on the behavior of the fuel rod are considered. Fission gas generation and release are calculated as a function of burnup. The cladding deformation model includes multi-axial elasto-plastic analysis and considers creep. A fuel rod failure subcode, is included which checks for various modes of failure based on the operating conditions.

A material property subcode, MATPRO, which is used to provide gas, fuel and cladding properties to the FRAP-S3 computational subcodes is coupled to FRAP-S3. No material properties need to be supplied by the code user.

FRAP-S3 is a modular code with each major computational subcode isolated within the code and coupled to the main code by subroutine calls and data transfer through argument lists. A major purpose of FRAP-S3 is that it can be coupled to versions of the transient fuel rod code, FRAP-T. FRAP-S3 generates a set of initial conditions used by FRAP-T to initiate analysis of transient accidents such as Loss-of-Coolant (LOCA), Power Coolant Mismatch (PCM) and Reactivity Initiated Accidents (RIA). The code is presently programmed and running on the IBM 360/75 and CDC 7600 computers.

SUMMARY

FRAP-S is a FORTRAN IV computer code developed to describe the steady state behavior of nuclear fuel rods during long-term burnup conditions. FRAP-S includes the coupled effect of thermal, mechanical, internal gas, and material properties response in the analysis of fuel rod behavior. This code is part of a continuing development program by the Nuclear Regulatory Commission designed to produce analytical tools for accurate prediction of nuclear reactor system behavior during normal and abnormal operating conditions. The code described in this document (FRAP-S-MOD003) is the **third** in a series of fuel rod codes planned for periodic release, with each succeeding version incorporating the most recent advancements that have been made in fuel rod response analysis models. The code is presently programmed and running on the IBM-360/75 and CDC 7600 computers. A transient fuel rod analysis code, FRAP-T, is being developed at the Idaho National Engineering Laboratory to accept history dependent initial conditions from FRAP-S to initiate an off-normal transient. Both codes are being developed with common subcodes and compatible input-output features.

FRAP-S 3 is a modular code. Each type of computation, such as the internal gas pressure computation, is performed by an analytical model programmed in a separate subcode or subroutine. This configuration is designed to allow maximum flexibility in developing and modifying the code with minimum impact on the unmodified portion of the code.

A major subcode of FRAP-S3 is MATPRO. This subcode is composed of modular function subprograms and subroutines which define the material properties required by the computational subcodes of FRAP-S3 Each function subprogram or subroutine defines only one material property.

This document describes the FRAP-S3 code and its input instructions.

CONTENTS

FIGURES

TABLES

FRAP-S3 A COMPUTER CODE FOR THE STEADY-STATE ANALYSIS OF OXIDE FUEL RODS

I. INTRODUCTION

FRAP-S3 (Fuel Rod Analysis Program-Steady State, Version 3) is a FORTRAN IV computer code developed to describe the steady state and long-term burnup response of oxide fuel rods in light water reactors (LWR). In addition, the code is designed to generate parametric data required as initial conditions for transient accident analysis using versions of the transient analysis code -- FRAP-T[1]. This effort is part of a safety analysis code improvement program being sponsored by the Office of Water Reactor Safety Research of the Nuclear Regulatory Commission (NRC).

The code described in this report (FRAP-S MOD 003) is the third of a series of steady state fuel rod codes planned for release at intervals with each succeeding version incorporating the most recent advancements made in fuel rod response analysis models.

FRAP-S3 is a modular code with each type of computation and analytical model, such as internal gas pressure, contained in a separate module or subroutine. This configuration is designed to allow maximum versatility in development and to permit modification of a module without impacting the unmodified portion of the code.

A major subcode of FRAP-S3 is MATPRO[4], see Appendix E. This subcode is comprised of modular function subprograms and subroutines which define the material properties required by the computational subcodes of FRAP-S3. Each function subprogram or subroutine defines a single material property.

The FRAP-S3 developmental process includes two separate verification efforts designed to test the analytical capability of the code - Developmental Verification and Independent Verification. Developmental Verification is an ongoing verification process whereby model additions and changes are checked for both model correctness and for any perturbation of the overall computer code. Independent Verification is a verification process which takes place after a code version has been frozen to future changes and involves comparison with a large amount of fuel rod response data.

This document describes the FRAP-S3 code, the models used in the code, and examples of code input and output. Section II describes the purpose of the code and the general methods by which the objectives are achieved. Sections III and IV cover the analytical and correlative models, respectively. Section V describes the computational flow of the code and presents a detailed flow diagram of the code for clarity. Appendices contain a user input manual (Appendix A), a FRAP-S example problem (Appendix B), a problem illustrating the FRAP-S link to FRAP-T (Appendix C), and a description of the configuration control procedure used at EG&G Idaho, Inc. to document analytical codes (Appendix D).

II. PROGRAM SUMMARY DESCRIPTION

The FRAP-S code is being developed to predict the behavior of fuel rods during long-term irradiation and to calculate initial conditions for transient accident analyses performed using the FRAP-T code. The program calculates the interrelated effects of fuel and cladding temperature, rod internal pressure, fuel and cladding deformation, release of fission product gases, fuel swelling, cladding thermal growth, cladding corrosion, and crud deposition as a function of time and specific power. Calculations can be performed for rods which are expected to experience varying axial power distributions as well as rod power level changes with time and/or burnup or changes in core system conditions. Parametric fuel rod design studies can be performed by varying as-fabricated rod dimensions or specifications. Printout for up to 15 axial rod increments and for 69 power/time steps can be obtained for each case.

1. RESPONSE MODELS

FRAP-S3 contains models which calculate the following quantities as a function of irradiation time:

(1) Coolant bulk and cladding axial temperature distribution

(2) Temperature distribution in the fuel pellets at eleven radial nodes and up to 15 axial increments

(3) Zircaloy cladding corrosion and hydriding at each axial increment in either a boiling water reactor (BWR) or pressurized water reactor (PWR) environment

(4) Fuel swelling, densification, and thermal expansion at each axial increment and radial node

(5) Cladding irradiation-induced growth at each axial increment

(6) Elastic-plastic pellet-cladding interaction and contact pressure at each axial increment

(7) Pellet to cladding gap and fuel crack gas composition and thermal conductivity

(8) Cladding stresses and strains at each axial increment including zircaloy cladding creep

(9) Krypton, xenon, and helium generation at each pellet node

(10) Total fuel rod gas release and internal rod pressure through summation of the release in each axial increment and calculation of the plenum, dish, gap, and crack void volumes and temperatures.

2. PROGRAMMING FEATURES

FRAP-S3 incorporates certain programming features which influence its application to providing transient code initial conditions that are dependent on prior operating history.

(1) Creep rates are applied over the time step after the code has converged on the power of that time step.

(2) With respect to fuel cladding properties, as well as input and output routines, the degree of modularization in FRAP-S3 is equivalent to that exhibited by versions of FRAP-T. The MATPRO material properties subcode is called repeatedly by both codes.

(3) Some of the other submodels in the code representing physical mechanisms such as gas release and void volume calculations

are called by the control program but the interface is currently functional rather than modular in nature. The calling sequence uses a large common block to pass information to and from the subroutines. A similar situation exists for the fuel swelling model which is called from subroutine TEMP. TEMP incorporates the analytical fuel rod temperature calculation, as well as convergence control, and models for corrosion and cladding stress.

(4) Where common mechanisms exist, the same physical models, such as fuel thermal expansion and gap conductance, are used in FRAP-S and FRAP-T.

Current plans are to increase use of modular programming in FRAP-S and improve consistency of physical models between the FRAP-S and FRAP-T.

3. OPERATIONAL FEATURES

As an indication of how FRAP-S3 operated, the input features and calculational procedures are given below.

3.1 Input Data Required

The input required for running the FRAP-S code is that collection of data necessary to describe the fuel rod geometry, core thermal and hydraulic conditions, and the expected irradiation history, namely:

(1) Fuel rod geometry (initial cold dimensions):

(a) Cladding material

(b) Cladding outside diameter

(c) Cladding inside diameter

(d) Pellet diameter

(e) Percent of UO_2 theoretical density

(f) UO_2 enrichment

(g) Fuel stack length

(h) Cold pellet height

(i) Dish depth

(j) Dish spherical radius

(k) Cold plenum length

(l) Hold-down spring (coil) diameter

(m) Hold-down spring wire diameter

(n) Total number of spring turns.

(2) Core thermal and hydraulic conditions:

(a) Primary loop system pressure

(b) Coolant mass flow rate

(c) Hydraulic diameter

(d) Core inlet water temperature.

(3) Rod power:

(a) Axial power distribution as a function of time

(b) Rod average heat flux or power as a function of time.

3.2 Calculation Procedure

The FRAP-S3 code iteratively calculates the interrelated effects of fuel and cladding temperature, rod internal pressure, fuel and cladding elastic-plastic deformation, release of fission product gases, fuel swelling and densification, cladding thermal expansion and irradiation-induced growth, cladding corrosion, and crud deposition as functions of time and specific power.

The fuel rod power history is approximated by a series of steady state power levels with instantaneous jumps from one power level to another. The length of the rod is divided into a number of axial segments, each assumed to operate at an average set of conditions over its length. The axial flux (power) shape is input and may be varied as a function of time. Fuel and cladding temperatures, fuel swelling, densification, thermal expansion, cladding thermal and irradiation induced growth, cladding stresses and strains, and fission gas releases are calculated separately for each axial segment. The fission gas release and fuel and cladding deformations are then integrated over the length of the fuel rod and added to previous power step values to obtain the rod internal pressure. This pressure is fed back into the fuel and cladding elastic and plastic deflection calculations in subsequent iterations. For purposes of evaluating thermal expansion, fuel swelling, densification, and fission gas release, within each axial increment, the fuel pellet is divided into ten equal-volume concentric rings with each ring assumed to be at its average temperature.

A detailed coverage of the numerical solution procedure is presented in Section V with program flow diagrams and subroutine interactions.

4. FRAP-S/FRAP-T LINK

One of the primary reasons for developing FRAP-S is to provide a computational tool which is compatible with the transient accident

analysis code FRAP-T[1]. For realistic evaluation of fuel rod response during a reactor accident transient such as a loss-of-coolant accident (LOCA), a realistic set of initial conditions, based on a real or hypothetical reactor history, is required to initiate the transient analysis. Consistent computational models in the two codes are required for a smooth transition between the predictions of the two codes at initiation of the transient. The sample problem described in Appendix C shows the result of small discrepancies between similar models in FRAP-S and FRAP-T. These discrepancies presently are being removed in the development process.

The link between FRAP-S3 and FRAP-T is accomplished by having FRAP-S3 generate a magnetic tape containing FRAP-S2 calculated information in the format of a FRAP-T restart tape.

The following data are stored on tape and passed to FRAP-T as initial conditions for each axial node specified:

(1) Gap pressure (vector)

(2) Fuel rod outside diameter (vector)

(3) Radial gap thickness (vector)

(4) Crack volume per unit length (vector)

(5) Interfacial pressure (vector)

(6) Rod surface heat flux (vector)

(7) Fuel outside radius (vector)

(8) Axial cladding strain (vector)

(9) Radial cladding strain (vector)

(10) Length change of fuel stack

(11) Area of the top pellet

(12) Length change of the cladding

(13) Total moles of gas in the rod

(14) Temperature distribution (vector)

(15) Node location (vector)

(16) Fuel displacement due only to swelling (vector)

(17) Cladding creep strain (vector)

(18) Cold gap thickness

(19) Mole fractions of fuel rod gases.

III. DESCRIPTION OF ANALYTICAL MODELS

The major analytical models of FRAP-S3 describe fuel rod behavior in the following response regimes:

(1) Fuel rod temperature

(2) Fuel rod internal gas pressure

(3) Cladding deformation

(4) Fuel deformation

(5) Fuel-cladding interaction.

The equations and models used to describe these response regimes are covered in this section. Each subsection first lists the assumptions and then describes the models. Asterisks (*) mark those assumptions representing known model simplifications for which tasks presently are under way to develop more advanced models.

1. FUEL ROD TEMPERATURE

The fuel rod temperature distribution calculation involves models which yield film, crud, and cladding oxide temperature drops; gap temperature drop; coolant temperature; cladding temperature; and the fuel temperature.

1.1 Assumptions

The calculation of the fuel rod temperature distribution is based on the following assumptions:

(1) No axial heat conduction

(2) No circumferential heat conduction *

(3) Steady state boundary conditions during each time step

(4) Gamma heating effects are negligible.

1.2 Fuel Rod Surface Temperature

The fuel rod surface temperature is calculated by first finding the coolant temperature and then summing the temperature drops due to film and crud.

1.2.1 Coolant Conditions. FRAP-S3 performs a single, closed channel coolant temperature calculation at each axial node along the rod. Bulk temperatures at these positions are determined according to the following expression:

$$T_b(z) = T_{in} + \int_0^z \left[4\dot{q}''(z) / (C_p G D_e)\right] dz \qquad (1)$$

where

$T_b(z)$ = bulk coolant temperature at axial position (F)

T_{in} = inlet coolant temperature (F)

$\dot{q}''(z)$ = rod surface heat flux at axial position (Btu/hr - ft^2 - F)

C_p = heat capacity of the coolant (Btu/lbm - F)

G = coolant mass flux (lbm/hr - ft^2)

D_e = unit flow channel heated diameter (ft).

The rod surface temperature at axial elevation z is taken as the minimum value between the following expressions:

$$T_w(z) = T_b(z) + \Delta T_f(z) + \Delta T_c(z) \quad (2)$$

$$T_w(z) = T_{sat} + \Delta T_{J.L.} \quad (3)$$

where

$T_w(z)$ = rod surface temperature at z (°F)

$\Delta T_f(z)$ = forced convection film temperature drop at z (°F)

$\Delta T_c(z)$ = crud temperature drop (°F)

T_{sat} = coolant saturation temperature (°F)

$\Delta T_{J.L.}$ = nucleate boiling temperature drop (°F).

The forced convection temperature drop across the coolant film layer at the surface of the rod is based on the expression

$$\Delta T_f(z) = q''(z)/h_f \quad (4)$$

where h_f is the Dittus-Boelter[5] film conductance; and

$$h_f = (0.023k/D_e)\ R_e^{0.8} p_r^{0.4} \quad (5)$$

where

K = conductivity of the water

D_e = equivalent diameter of the coolant channel

and

$$\Delta T_c = q''(z) \frac{\delta_c}{k_c}$$

where

δ_c = crud thickness

k_c = crud thermal conductivity (0.5 Btu/hr-ft-°F)

R_e = Reynolds number

P_r = Prandtl number.

The nucleate boiling temperature drop is based on the Jens-Lottes[6] formulation:

$$\Delta T_{J.L.}(z) = 60 \, [q''(z)/10^6]^{0.25}/e^{(P/900)} \qquad (6)$$

where

P = system pressure (psia).

No additional temperature rise occurs due to crud deposition because the coolant is assumed to boil through the crud blanket.

In the case of zircaloy clad rods, the rod surface temperature applies to the ZrO_2 surface temperature.

1.2.2 ZrO_2 Temperature Drop. For zircaloy clad rods, the temperature drop across the zirconium oxide layer at axial station z is determined by the expression

$$\Delta T_{ZrO_2}(z) = \dot{q}''(z)\ \delta_{ZrO_2}(z)/k_{ZrO_2} \qquad (7)$$

where

$\delta_{ZrO_2}(z)$ = oxide thickness at axial position (ft)

k_{ZrO_2} = oxide thermal conductivity (Btu/hr-ft-°F)

1.3 Cladding Temperature Drop

The cladding temperature drop for an axial location is calculated according to the expression

$$\Delta T_{clad} = q''(z)\ R_o\ \ell n\ (R_o/R_i)/k_{clad} \qquad (8)$$

where

R_o = cladding outside radius (ft)

R_i = cladding inside radius (ft)

k_{clad} = temperature and material dependent thermal conductivity of the cladding (Btu/hr-ft-°F).

1.4 Gas Gap Temperature Drop

FRAP-S3 contains two different gap conductance models. The first is based on a cracked pellet geometry[7] and the second is a modification of the Ross and Stoute[8] model.

1.4.1 Cracked Pellet Model.

Assumptions:

(1) Nonuniform geometry of the open gap between the fuel and cladding

(2) Both plastic and elastic deformation occur at the fuel and cladding contact points when the gap is closed.

A gap conductance model was developed for use in the FRAP codes which models the cracked pellet geometry of the open gap between the fuel and cladding as well as the contact conductance when the gap is closed. The model has been compared with experimental data to determine the correct value of the various constants. This section presents an abridged treatment of the cracked pellet gap conductance model (see Reference 4 for more detail).

(1) Open Gap. If the fuel and cladding are not in contact an eccentric cladding-fuel geometry is assumed. The fraction of the pellet circumference in contact with the cladding is considered to be governed by the equations

$$F = \frac{1}{a_1 \left[\frac{100\ \Delta D}{D_F}\right]^{a_2} + a_3} + a_4 \qquad (9)$$

and

$$\frac{1}{a_3} + a_4 = 1 \qquad (10)$$

where

F = fraction of pellet in contact with the cladding

ΔD = diametral gap (in.)

D_F = hot diameter of the fuel pellet (in.)

a_1, a_2, a_3, and a_4 = empirical constants determined from data.

The constant a_4 represents the minimum fraction of pellet-cladding contact for large diametral gaps. The form of Equations (9) and (10) permits a very large fraction of pellet-cladding contact for a small calculated diametral gap. The justification for this form of the equations is that the cracks (radial and circumferential) that form in the fuel pellets will not close appreciably until the gas gap is closed. Thus the actual gas gap will close before the calculated gap. The calculated gap is the equivalent annular gap.

Heat transfer across the gas gap is considered to occur by conduction through the gas in the open gap plus zero pressure contact conductance times that fraction of the gap circumference with pellet-cladding contact. Radiation heat transfer across the open gap is assumed negligible, since reasonable gaps are always small and thus sufficiently large temperature differences between the fuel and cladding do not exist. Heat transfer across the gas gap is therefore calculated from the equation

$$h_{gap} = (1 - F)\, h_1 + F\, h_2 \qquad (11)$$

where

h_{gap} = net gap conductance (Btu/hr-ft^2-°F)

h_1 = open gap conductance (Btu/hr-ft^2-°F)

h_2 = zero pressure contact conductance (Btu/hr-ft^2-°F).

The open gap conductance is determined from equations

$$h_1 = \frac{k_{mix}}{\Delta r' + \delta} \tag{12}$$

and

$$\Delta r' = (r_1 + r_2) / 2 \tag{13}$$

where

k_{mix} = thermal conductivity of gas mixture (Btu/hr-ft-°F)

$\Delta r'$ = average radial gap thickness of eccentric gas gap (ft)

δ = root mean square of the fuel cladding surface roughness

A value of 14.4×10^{-6} ft is normally used

r_1 = hot calculated inside radius of cladding (ft)

r_2 = hot calculated radius of fuel (ft).

(2) Closed Gap. When the fuel and cladding are in contact, the theory of thermal contact conductance for ceramic fuel elements developed by Jacobs and Todreas[9], is used. The governing equation for contact conductance is

$$h_{gap} = C_1 p^n + \frac{k_{mix}}{\delta} \tag{14}$$

where

h_{gap} = net gap conductance (Btu/hr-ft^2-°F)

C_1 = 0.475 for stainless steel cladding and 0.600 for zircaloy-2 and zircaloy-4 cladding

p = pellet-cladding contact pressure (psi)

n = 1 for $0 \leq P \leq 1000$ (psi) and 0.5 for $p \geq 1000$ (psi).

The value of the exponent, n, is governed by the material behavior at the interface of the fuel and cladding contact points. An exponent of 1 is consistent with the Ross and Stoute[8] theory of contact conductance only if the surface peaks of one of the materials are flowing plastically. If the contact points of both materials are behaving elastically the correct value for the exponent, n, is approximately 0.5. The experimental results of Fenech and Rohsenow[10] support this value and also indicate that for metal-ceramic pairs the transition pressure from elastic to plastic flow is approximately 1000 psi. The parameter k_{mix}/δ accounts for the heat conduction through the gas in the gaps between contact points.

1.4.2 Ross and Stoute Model.

Assumptions:

(1) Uniform geometry of the open gap between the fuel and cladding

(2) Elastic cladding deformation at the points of fuel and cladding contact after the gap is closed.

(1) Open Gap. If the fuel and cladding are not in contact, heat is transferred across the gas gap by conduction through the gas and radiation. Heat transfer across the gas gap is considered to be governed by the equation

$$h_g = \frac{K_g}{t_g + c(R_f + R_c) + (g_1 + g_2)} + h_r \qquad (15)$$

where

h_g = gap conductance

K_g = conductivity of gas in gas gap

t_g = gap thickness

g_1 = temperature jump distance at cladding inside surface

g_2 = temperature jump distance at fuel outside surface

c = 1.98

R_c = arithmetic mean roughness height of the cladding (cm)

R_f = arithmetic mean roughness and height of the fuel (cm)

h_r = radiant heat transfer conductance.

Radiant heat transfer conductance is computed using the following equation:

$$h_r = \sigma F_e (T_f^2 + T_c^2)(T_f + T_c) \qquad (16)$$

where

h_r = radiant heat transfer conductance

σ = Stefan-Boltzman constant

F_e = emissivity factor

T_f = temperature of outside surface of fuel

T_c = temperature of inside surface of cladding.

The emissivity factor is computed by the equation

$$F_e = \left[\frac{1}{e_f} + \frac{r_f}{r_c}\left(\frac{1}{e_c} - 1\right)\right]^{-1} \qquad (17)$$

where

F_e = emissivity factor

e_f = emissivity of fuel surface

e_c = emissivity of cladding inside surface

r_f = outside radius of fuel

r_c = inside radius of cladding.

The temperature jump distance is computed by an empirically derived equation presented in the GAPCON code report[3]. The equation is

$$g_1 + g_2 = 5.448\left[\frac{\mu}{p}\left(\frac{T}{M}\right)^{1/2}\right] \qquad (18)$$

where

$g_1 + g_2$ = jump distance (cm)

μ = viscosity of gas (gm/cm-sec)

P = pressure of gas (psi)

T = temperature of gas (K)

M = molecular weight of gas.

(2) Closed Gap. If the fuel and cladding are in contact, the GAPCON code equation for contact conductance is used. This equation agrees with gap conductance data presented by Ross and Stoute[8]. The equation is

$$h_g = \frac{K_m P_i}{a_o R^{0.5} H} + \frac{K_g}{c(R_f+R_c) + (g_1 + g_2)} + h_r \qquad (19)$$

where

h_g = gap conductance (cal/sec-cm^2-°C)

K_m = $\frac{2k_f k_c}{k_f+k_c}$

k_f = fuel conductivity (cal/sec-cm-°C)

k_c = cladding conductivity (cal/sec-cm-°C)

P_i = interfacial pressure between fuel and cladding (psi)

a_o = a constant -- 0.5 cm$^{1/2}$

R = $\frac{(R_f^2 + R_c^2)^{1/2}}{2}$

R_c = arithmetic mean roughness height of cladding (cm)

R_f = arithmetic mean roughness height of fuel (cm)

H = Meyer-Hardness of cladding (psi).

The coefficient c in Equation (19) is computed by the empirical equation

$$c = 1.98\ e^{-0.00125\ P_i} \qquad (20)$$

where

P_i = interfacial pressure between fuel and cladding (kg/cm^2).

1.5 Pellet Heat Conduction

The pellet temperature distribution is calculated using one of two models. The first relies on results generated by the depletion code LASER, whereas the second makes use of flux depression.

1.5.1 Pellet Temperature Distribution with LASER. The heat transfer formulation in FRAP-S2 is based on a nonlinear least squares fit of LASER[11] generated radial power distribution data. The model accounts for the spatial effects of isotopic production on pellet self-shielding characteristics at any burnup and power level for both PWR and BWR plutonium or uranium enriched spectrums. The radial power depression has been obtained for typical commercial fuel enrichments by making use of the results from the depletion code LASER.

From a heat balance across a differential annular ring

$$\theta\left(k + \frac{dk}{dr}\,dr\right)(r + dr)\left.\frac{dT}{dr}\right|_{r + dr} - \theta kr\left.\frac{dT}{dr}\right|_{r} + q'''(r)rdr = 0 \quad (21)$$

where the terms are defined in Figure 1. After rearrangement of Equation (21), omission of higher order terms, and integration we obtain:

$$kr\frac{dT}{dr} = -\int_0^r rq'''(r)dr. \quad (22)$$

A second integration, from the pellet surface, a, to some point, r, gives:

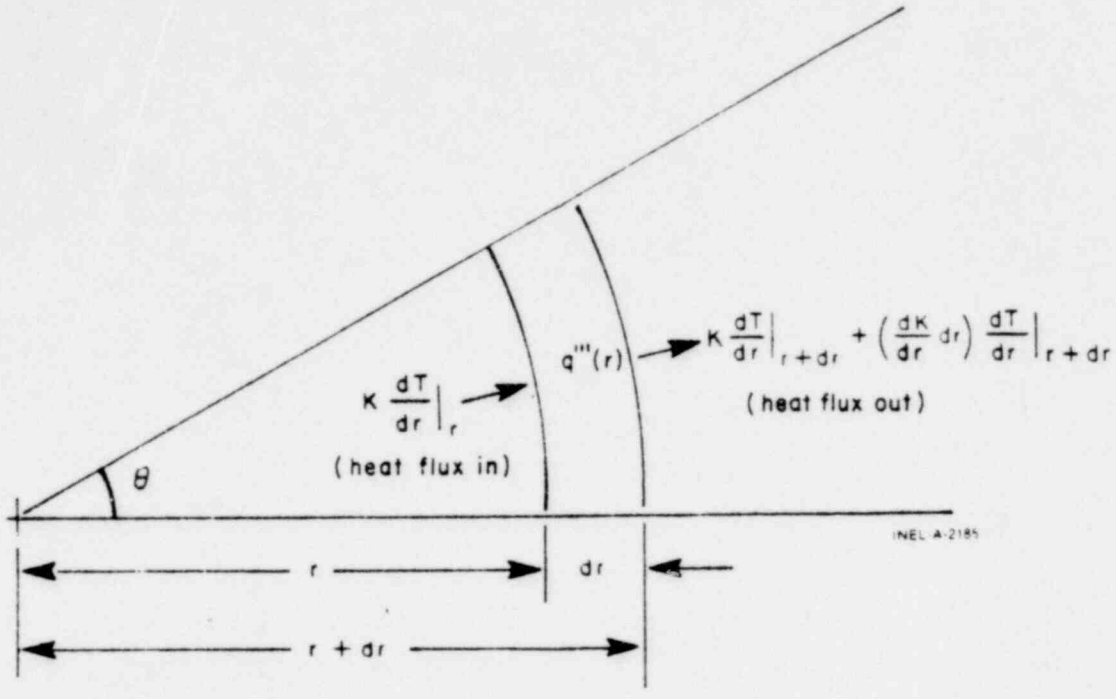

Fig. 1 Heat conduction in fuel rod.

$$\int_{T_a}^{T_r} k(T)dT = \int_{r}^{a} \left[\int_{o}^{r} q'''(r)rdr \right] dr/r. \tag{23}$$

From a least square surface fit of the LASER code output we obtain values of P_1, P_2, and P_3.

$$q'''(r) = P_1 R^{P_2} + P_3 \tag{24}$$

where the P's are some function of time and enrichment and R is a fractional radius.

The heat generation distribution of Equation (24) can be normalized as follows:

$$q'''(r) = \frac{q'}{12\pi a^2 q_L'''} \left[P_1 \left(\frac{r}{a}\right)^{P_2} + P_3 \right] \tag{25}$$

where

$q'''(r)$ = radially dependent energy generation ($kW/in.^3$)

q' = average local power (kW/ft)

a = pellet radius (in.)

q'''_L = LASER average heat generation rate ($kW/in.^3$)

= 7.7316069 for PWR
= 4.4353724 for BWR

} for typical commercial rods

P_1, P_2, and P_3 = factors generated from LASER output which vary with time and enrichment.

Then substitution of Equation (25) into Equation (23) results in

$$\int_{T_a}^{T_r} k(t)dt = \frac{q'}{12\pi a q_L'''} \int_r^a \left\{ \int_0^r \left[P_1 (r/a)^{P_2} + P_3 \right] r dr \right\} dr/r \quad (26)$$

and integrating twice,

$$\int_{T_a}^{T_r} k(t)dt = \frac{q'}{12\pi a q_L'''} \int_r^a \left[\frac{P_1 r^{P_2+2}}{(P_2+2)a^{P_2}} + \frac{1}{2} P_3 r^2 \right] dr/r \quad (27)$$

$$\int_{T_a}^{T_r} k(t)dt = \frac{q'}{\pi a^2 q_L'''} \left[\frac{P_1 a^{P_2+2}}{(P_2+2)^2 a^{P_2}} + \frac{1}{4} P_3 a^2 - \frac{P_1 r^{P_2+2}}{(P_2+2)^2 a^{P_2}} - \frac{1}{4} P_3 r^2 \right]. \quad (28)$$

The FRAP-S3 code divides the pellet into ten equal area rings, with boundaries numbered 1 at the surface and 11 at the center. The fractional radius R can, therefore, be written as

$$R_L = \sqrt{(12 - L)/10} \tag{29}$$

$$R_{L+1} = \sqrt{(11 - L)/10} \tag{30}$$

where L is the ring boundary number.

To determine the integral of the thermal conductivity across any one FRAP-S pellet ring, Equation (28) is written as

$$\int_{T_L}^{T_{L+1}} k(t)dt = \frac{q'}{\pi q_L'''} \left[\frac{P_1 R_L^{P_2+2}}{(P_2+2)^2} + \frac{1}{4} P_3 R_L^2 - \frac{P_1 R_{L+1}^{P_2+2}}{(P_2+2)^2} - \frac{1}{4} P_3 R_{L+1}^2 \right] \tag{31}$$

where R_L and R_{L+1} are defined in Equations (29) and (30). Note that $r_L = a \quad R_L$.

The value of $\int kdT$ to any point r in the pellet is calculated by summing each ring $\int kdT$ calculation of Equation (31), starting from the surface. Then, from an empirical correlation of temperature as a function of $\int kdT$ (polynominal fit of data) the temperature of ring R_L is calculated.

1.5.2 Pellet Temperature Distribution with Flux Depression.

(1) Basic Relationships. The equation for the radial conduction of heat across a circular boundary within a solid cylindrical pellet may be written

$$\int_0^r P(r)\, 2\pi r dr + 2\pi r k(dT/dr) = 0 \tag{32}$$

where

r = the radius of the circle

P(r) = the volumetric heat generation rate at radius r

T = the temperature

k = the pellet thermal conductivity, a function of T.

The average value of P(r) is given by the equation

$$\bar{P} = \int_0^a P(r)\, 2\pi r dr / \int_0^a 2\pi r dr = (2/a^2)\int_0^a P(r) r dr \qquad (33)$$

where a is the pellet radius.

The relationship between the thermal heat rating q', the surface heat flux q'', and $\bar{P}$ is given by the equation

$$q' = \pi a^2 \bar{P} = 2\pi a q''. \qquad (34)$$

The value of P(r) at the center of the pellet is designated P_o, i.e.

$$P_o = P(r)\Big|_{r=0}. \qquad (35)$$

The surface and center temperatures of the pellet are T_s and T_c, respectively.

(2) Uniform Heat Generation. Consider the case of uniform heat generation. For this case Equations (33) and (35) give

$$P(r) = \bar{P} = P_o. \qquad (36)$$

Substituting Equation (36) in Equation (32) and carrying out the integration gives

$$P_o r^2/2 + rk(dT/dr) = 0. \tag{37}$$

Separating variables and integrating from r = r to r = a gives

$$(P_o/4)(a^2-r^2) = \int_{T_s}^{T} k\,dT. \tag{38}$$

Using Equations (34) and (37), Equation (39) becomes

$$(q'/4\pi)(1-\rho^2) = \int_{T_s}^{T} k\,dT \tag{39}$$

where ρ is the dimensionless radius given by the equation

$$\rho = r/a. \tag{40}$$

At the center of the pellet, $\rho = 0$ and $T = T_c$ in which case Equation (39) becomes

$$q'/4\pi = \int_{T_s}^{T_c} k\,dT. \tag{41}$$

An expression for radius as a function of temperature within the pellet may be found by solving Equation (39) for ρ:

$$\rho = [1 - (4\pi/q')\int_{T_s}^{T} k\,dT]^{1/2}. \tag{42}$$

(3) Nonuniform Heat Generation (Diffusion Theory). Due to self-shielding effects, the power generation within an enriched fuel pellet will not be uniform. The following equation is obtained from simple diffusion theory.

$$P(r) = AI_o(\kappa r) \tag{43}$$

where

A = a constant

I_o = the zero order modified Bessel function of the first kind

κ = the reciprocal of the thermal diffusion length in the fuel.

The value of κ depends upon the fuel density and enrichment. A plot[36] indicates that for UO_2 of 95% theoretical density, κ varies from 2 to 3 cm^{-1} for enrichment values of 2.5 to 6% U-235. Substituting Equation (43) in Equation (35) leads to $A = P_o$ since $I_o(0) = 1$. Equation (43) can thus be written

$$P(r) = P_o I_o(\kappa r). \tag{44}$$

Substituting Equation (44) in Equation (33) gives

$$\bar{P} = 2P_o[I_1(\kappa a)]/(\kappa a) \tag{45}$$

where I_1 is the first order modified Bessel function of the first kind. Substituting Equation (44) in Equation (32) and carrying out the integration gives

$$P_o r[I_1(\kappa r)]/\kappa + rk(dT/dr) = 0. \tag{46}$$

Separating variables and integrating from $r = r$ to $r = a$ gives

$$(P_o/\kappa^2)[I_o(\kappa a)-I_o(\kappa r)] = \int_{T_s}^{T} k\,dT. \qquad (47)$$

Using Equations (34) and (45), Equation (47) becomes

$$(q'/4\pi)\ \left\{2[I_o(\kappa a)-I_o(\kappa r)]\right\} / \left\{\kappa a[I_1(\kappa a)]\right\} = \int_{T_s}^{T_c} k\,dT. \qquad (48)$$

At the center of the pellet $r = 0$ and $T = T_c$ in which case Equation (48) becomes

$$(q'/4\pi)\ \left(2[I_o(\kappa a)-1]/\left\{\kappa a[I_1(\kappa a)]\right\}\right) = \int_{T_s}^{T_c} k\,dT. \qquad (49)$$

The expression multiplying $q'/4\pi$ in this equation is called f. Since f is less than 1, a comparison of Equations (41) and (49) indicates that the thermal heat rating associated with given fuel surface and center temperatures is greater for nonuniform heat generation given by Equation (44) than for uniform heat generation given by Equation (36), the ratio of the two heat ratings being f. Thus, nonuniform heat generation decreases the effect of the thermal heat rating on fuel temperature and consequently f is termed the flux depression factor.

(4) Nonuniform Heat Generation (Parabolic Approximation). As was shown above, a tedious calculation procedure is required to obtain the radial temperature distribution for the nonuniform heat generation relationship given by Equation (44). Equation (44) can be approximated very well by the relation

$$P(r) = P_o[1 + 0.27(\kappa r)^2]. \qquad (50)$$

In order to obtain a better fit for any particular problem, the following equation is proposed:

$$P(r) = P_o[1 + B(r/a)^2] \tag{51}$$

where B will be determined as a function of f only.

Equation (51) is in agreement with the results of a fission distribution analysis obtained using several digital computer programs. Substituting Equation (51) in Equation (33) gives

$$\bar{P} = P_o(1+B/2). \tag{52}$$

Substituting Equation (51) in Equation (32) and carrying out the integration gives

$$(p_o r^2/2)[1 + (B/2)(r/a)^2] + rk(dT/dr) = 0.$$

Separating variables and integrating from r = r to r = a gives

$$(P_o/4)(a^2-r^2)[1 + B(a^2+r^2)/(4a^2)] = \int_{T_s}^{T} k\,dT. \tag{53}$$

Using Equations (34), (40), and (52), Equation (53) becomes

$$(q'/4\pi)(1-\rho^2)[B(1+\rho^2) + 4]/(2B+4) = \int_{T_s}^{T} k\,dT. \tag{54}$$

At the center of the pellet, $\rho = 0$ and $T = T_c$, in which case Equation (54) becomes

$$(q'/4\pi)[(B+4)/(2B+4)] = \int_{T_s}^{T_c} k\,dT. \tag{55}$$

Solving for B gives

$$B = 4(1-f)(2f-1). \tag{56}$$

Substituting in Equation (54) gives

$$(q'/4\pi)(1-\rho^2)[f + (1-f)\rho^2] = \int_{T_s}^{T} k dT. \qquad (57)$$

Equation (57) is a quadratic equation in ρ^2 which when solved for ρ gives

$$\rho = 1-2f + \left\{[q' - 16\pi(1-f) \int_{T_s}^{T} k dT]/q'\right\}^{1/2} /[2(1-f)]^{1/2}. \qquad (58)$$

Equation (58) enables solving for ρ in terms of T directly. Note that for f = 1, Equation (58) reduces to $\rho = [0/0]^{1/2}$. Applying L'Hospital's rule to Equation (58) results in Equation (42).

1.6 Stored Energy

The stored energy in the fuel rod is calculated by summing the energy of each pellet ring calculated at that ring temperature in the same manner as one of the methods used in GAPCON-THERMAL-1[3].

$$E = \frac{\sum_{i=1}^{N} m_i \int_{298°C}^{T_i} C_p(T) dT}{m} \qquad (59)$$

where

E = stored energy (Btu/lbm)

m_i = mass of ring segment i (lbm)

T_i = temperature of ring segment i (^oF)

$C_p(T)$ = specific heat (Btu/lbm - ^oF)

m = mass of the axial segment (lbm)

N = number of annular rings (10 maximum).

2. FUEL ROD INTERNAL GAS PRESSURE

2.1 Assumptions

The static fuel rod internal pressure model is based on the following assumptions:

(1) Perfect gas law holds (PV = NRT)

(2) Gas pressure is constant throughout the fuel rod

(3) Gas in the fuel rod cracks is at the fuel average temperature.

2.2 Static Fuel Rod Internal Pressure

Fuel rod internal gas pressure is computed by the equation:

$$P_g = \frac{M_g R}{\frac{V_p}{T_p} + \sum_{n=1}^{N} \left(\pi \frac{(r_{cn}^2 - r_{fn}^2)\Delta z_n}{T_{G_n}} + \frac{V_c \Delta z_n}{T_c} \right)} \qquad (60)$$

where

P_g = internal fuel rod pressure

M_g = moles of gas in fuel rod

R = universal gas constant

V_p = plenum volume

n = axial node number

T_p = temperature of gas in plenum

N = number of axial nodes into which fuel rod is divided for numerical solution

r_{cn} = radius of inside surface of fuel at axial node n

r_{fn} = radius of outside surface of fuel at axial node n

T_{G_n} = temperature of gas in gas gap at axial node n

Δz_n = fuel rod length associated with axial node n

V_c = fuel crack volume per unit length

T_c = temperature of the crack volume.

2.3 Plenum Gas Temperature

The plenum gas temperature is calculated based on energy transfer between the top of the pellet stack and the plenum gas, between the coolant channel and the plenum gas, and between the spring and the plenum gas. The three contributions are discussed in the following.

Natural convection from the top of the fuel stack is calculated based on heat transfer coefficients from McAdams[12] for laminar or turbulent natural convection from flat plates.

$$Nu = C(GrPr)^m \tag{61}$$

where

Nu = the Nusselt number

Gr_f = the Grashof number

Pr_f = the Prandtl number

and for

$$GrPr \leq 2.0 \times 10^7 \quad C = 0.54 \text{ and } m = 0.25$$

or

$$GrPr > 2.0 \times 10^7 \quad C = 0.14 \text{ and } m = 0.33.$$

The heat transfer coefficient is calculated from

$$h_p = \frac{k\ Nu}{D} \tag{62}$$

where

h_p = the heat transfer coefficient from the top of the pellet stack to the plenum gas (Btu/hr-ft-°F)

Nu = Nusselt number as found above

D = inside diameter of the cladding of the top node (ft)

k = conductivity of the plenum gas (Btu/hr-ft^2-°F).

The overall effective conductivity from the coolant to the plenum is found as follows:

$$U_c = \frac{1.0}{\frac{1}{\frac{D\ h_f}{2}} + \frac{\ln\left(\frac{D_o}{D_I}\right)}{k_{clad}} + \frac{1.0}{D_o\ (1.0 + \alpha\Delta T)\ h_{DB}}} \tag{63}$$

where

U_c = overall effective conductivity from the coolant to the plenum gas (Btu/hr-ft-°F)

D = hot state inside cladding diameter (ft)

h_f = cladding inside surface film coefficient (Btu/hr-ft-°F)

D_o = cold state outside cladding diameter (ft)

D_I = cold state inside cladding diameter (ft)

k_{clad} = cladding thermal conductivity (Btu/hr-ft^2-°F)

α = coefficient of thermal expansion of the cladding (ft/ft-°F)

ΔT = temperature difference between cladding average temperature and datum temperature (°F)

h_{DB} = heat transfer coefficient between the coolant and the cladding (Btu/hr-ft-°F).

Gamma heating in the hold-down spring is calculated at a volumetric rate of 1.146 Btu/hr-ft^3 for every Btu/hr-ft^2 of rod average heat flux

$$Q_{sp} = 1.146\ \dot{q}''\ V_s \qquad (64)$$

where

Q_{sp} = energy generated in the spring (Btu/hr)

$\dot{q}''$ = average heat flux of the rod (Btu/hr-ft)

V_s = volume of the spring (ft^3).

The plenum temperature is then approximated from the following equation:

1568 353

$$T_{plen} = \frac{Q_{sp} + U_c \frac{V_p}{D^2} T_{BLK} + T_{pa}\, h_p\, \pi\, D^2/4}{U_c \frac{V_p}{D^2} + \frac{h_p\, \pi\, D^2}{4}} \qquad (65)$$

where

Q_{sp}, U_c, D, and h_p are previously described

and

T_{plen} = plenum temperature (°F)

V_p = volume of the plenum (ft^3)

T_{BLK} = bulk coolant temperature at the top axial increment (°F)

T_{pa} = temperature associated with the insulator or top pellet (°F).

2.4 Pellet Dish Volume

The volume between pellets is calculated and included as part of the overall volume in the internal pressure model. The interpellet volume is calculated at each time step as the difference between the cold pellet geometry and the hot pellet operating geometry.

Figure 2 shows: (A) a cold pellet interface configuration; and (B) an exaggerated hot pellet interface configuration. The volume available for expansion of internal fill gas is defined by the cross hatched areas (A and B) in the figure.

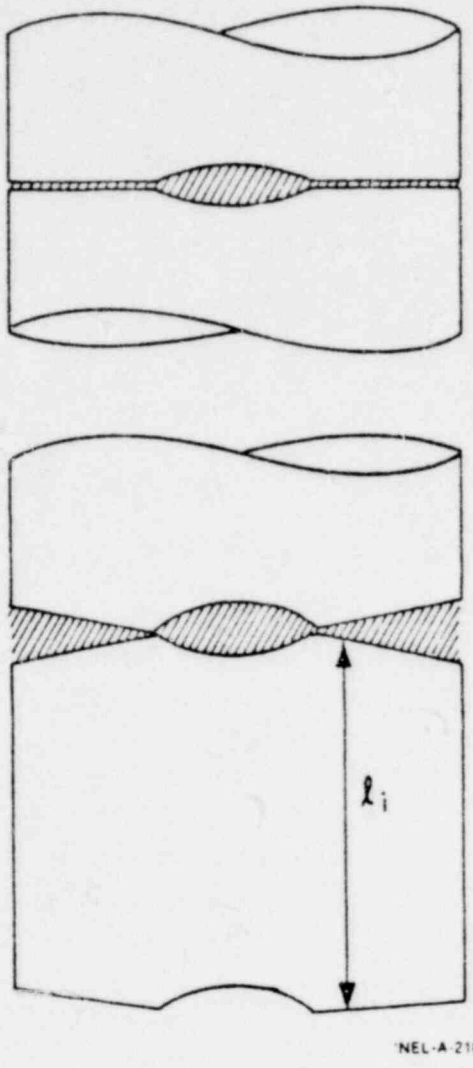

Fig. 2 Pellet expansion.

3. CLADDING DEFORMATION

3.1 Assumptions

The cladding deformation model is based upon the following assumptions:

(1) Incremental theory of plasticity

(2) Prandtl-Reuss flow rule

(3) Isotropic work-hardening

(4) Thin wall cladding (stress, strain, and temperature are uniform through cladding thickness)

(5) If fuel and cladding are in contact, no slippage occurs at fuel-cladding interface

(6) Bending strains and stresses in cladding are insignificant

(7) Axisymmetric loading and deformation of cladding

(8) Incompressible fuel.*

This section describes the models which perform the mechanical analysis of the cladding. The models analyze the elastic and plastic deformation of the cladding due to thermal and pressure loadings, as well as loads due to mechanical interaction between the cladding and the fuel pellets.

Fuel Rod and Cladding Analysis Subcode (FRACAS) consists of a set of individual subroutines, each of which is independent of the others. Hence, the model contained in each subroutine can be modified or replaced without requiring changes in any other part of the subcode.

Deformation and stresses in the cladding in the open gap regime are computed in subroutine CLADF. The model considered is that of a thin cylindrical shell with specified internal and external pressures and a prescribed uniform temperature.

Calculations for the closed gap regime are made in subroutine COUPLE. The model considered is a thin cylindrical shell with prescribed external pressure and a prescribed radial displacement of its inside surface. The prescribed displacement is obtained from the fuel displacement models contained in FRAP-S. Further, since no slip is assumed to take place when the fuel and cladding are in contact, the axial expansion of the fuel is transmitted directly to the cladding, and hence, the change in axial strain in the shell is also prescribed.

Calculations for the trapped stack regime are made in subroutine STACK. The model considered is a thin cylindrical shell with prescribed internal and external pressures and a prescribed total change in length of the cylinder. In contrast to CLADF and COUPLE, which solve for the stresses and strains at only one axial location at a time, subroutine STACK simultaneously solves for the stresses and strains in all axial nodes which are being strained axially by the trapped stack of fuel pellets.

The decision as to whether or not the gap is open or closed, and whether to call COUPLE, STACK or CLADF is made in the executive subroutine, FCMI, (Fuel-Clad Mechanical Interaction). This is the only subroutine which must be called to initiate the fuel-clad interaction analysis. At the completion of this analysis, FCMI returns either a new gap size or a new interface pressure between fuel and clad for use in the next iteration of the thermal calculations.

In each of COUPLE, STACK, and CLADF, either an elastic-plastic (time-independent) solution or a creep-stress relaxation (time-dependent) solution is obtained, depending on the value of an input flag.

For the plasticity calculations, two additional subroutines, STRAIN and STRESS, compute changes in yield stress with work-hardening, given a uniaxial stress-strain curve. This stress-strain curve will be obtained from the material properties package subcode, MATPRO[4]. Subroutine STRAIN computes the effective total strain and new effective plastic strain given a value of effective stress and the effective plastic strain at the end of the last loading increment. Subroutine STRESS computes the effective stress given an increment of plastic strain and the effective plastic strain at the end of the last loading increment. Depending on the work-hardened value of yield stress, loading can be either elastic or plastic, while unloading is constrained to occur elastically. (Isotropic work-hardening is assumed in these calculations.)

For the creep and stress relaxation analysis, the creep rate (at the appropriate stress and temperature) is obtained from subroutine CREPR, while the creep-stress corresponding to a given creep rate is obtained from subroutine CREEP. The creep calculations are based on the so-called "equation of state" approach in which the numerical calculations closely parallel those in the incremental plasticity calculations.

Section 3.2 of this report presents a discussion of the general problem of elastic-plastic analysis in biaxial stress fields. It will be indicated there how the formulation of the problem naturally leads to the Method of Successive Substitutions as a means of obtaining a solution to the coupled, nonlinear elastic-plastic continuum equations. Section 3.3 describes the general multiaxial creep-stress relaxation problem, and describes the method of extending an elastic-plastic incremental solution to consider creep deformation. Section 3.4 describes the individual subroutines and specific equations which are solved.

3.2 General Considerations in Elasto-Plastic Analysis

Problems involving elastic-plastic deformation and multiaxial states of stress involve a number of questions which do not need to be considered in a uniaxial problem. In the following, an attempt is made to briefly outline the structure of incremental plasticity, and to outline the Method of Successive Substitutions (also called the Method of Successive Elastic Solutions) which has been used so successfully in treating multiaxial elastic-plastic problems[7].

In a problem involving only uniaxial stress σ_1, the strain ε_1 is related to the stress by an experimentally determined stress-strain curve as shown in Figure 3, and Hooke's law is taken as

$$\varepsilon_1 = \frac{\sigma_1}{E} + \varepsilon_1^P + \int \alpha \, dT$$

where ε_1^P is the plastic strain. The onset of yielding occurs at the yield stress, which can be determined directly from Figure 3. Given a load (stress) history, the resulting deformation can be determined in a

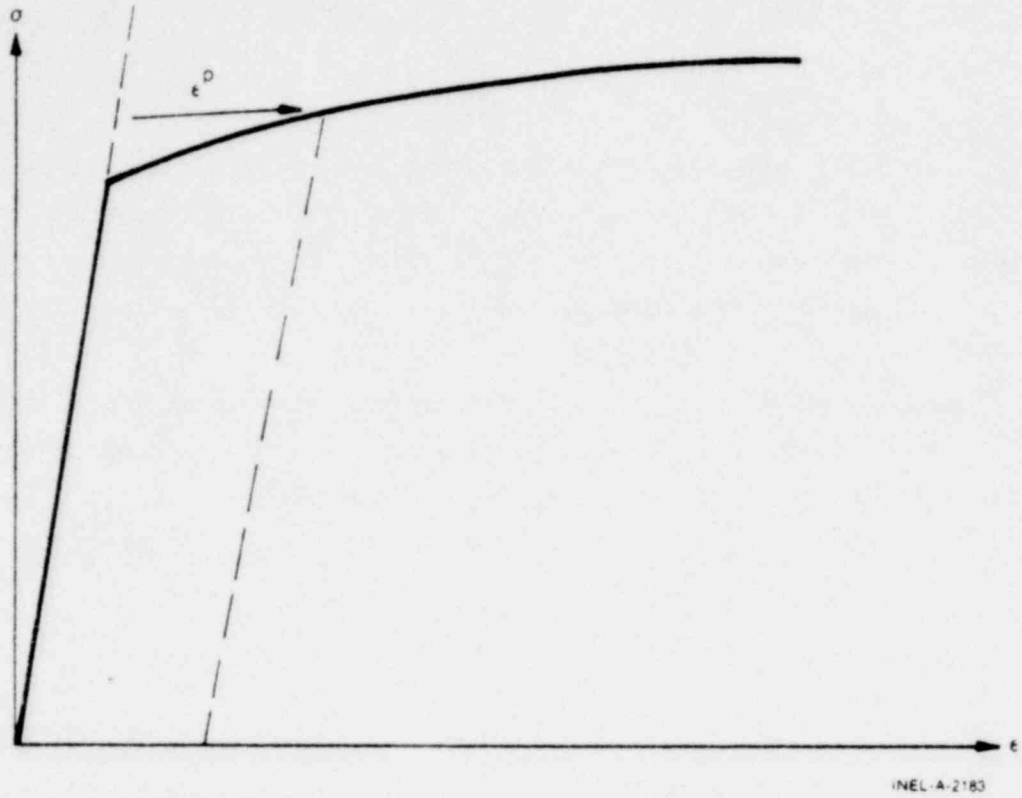

Fig. 3 Typical isothermal stress-strain curve.

simple fashion. Increase of yield stress with work-hardening is easily computed directly from Figure 3.

In a problem involving multiaxial states of stress, however, the situation is not so clear cut. Here one must have a method of relating the onset of plastic deformation to the results of a uniaxial test, and further, when plastic deformation occurs, one must have some means of determining how much plastic deformation has occurred, and how it is distributed among the individual components of strain. These two complications are taken into account by use of the so-called "Yield Function" and "Flow Rule", respectively.

A considerable wealth of experimental evidence exists on the onset of yielding in a multiaxial stress state. The bulk of this evidence supports the von Mises yield criteria, which assert that yielding occurs when the stress state is such that:

$$0.5\left[(\sigma_1 - \sigma_2)^2 + (\sigma_2 - \sigma_3)^2 + (\sigma_3 - \sigma_1)^2\right] = \sigma_y^2 \qquad (66)$$

where σ_i are the principal stresses, and σ_y is the yield stress as determined in a uniaxial stress-strain test. The square root of the left-hand side of this equation is referred to as the effective stress, σ_e, and this effective stress is one commonly used type of yield function.

To determine how the yield stress changes with permanent deformation, it is hypothesized that the yield stress is a function of the effective plastic strain, ε^P. An increment of effective plastic strain is determined at each loadstep and ε^P is defined as the sum of all increments incurred:

$$\varepsilon^P \triangleq \int d\varepsilon^P. \qquad (67)$$

Each increment of effective plastic strain is related to the individual plastic strain components by

$$d\varepsilon^P = \sqrt{\frac{2}{3}}\left[(d\varepsilon_1^P - d\varepsilon_2^P)^2 + (d\varepsilon_2^P - d\varepsilon_3^P)^2 + (d\varepsilon_3^P - d\varepsilon_1^P)^2\right]^{1/2} \qquad (68)$$

where the $d\varepsilon_i^P$ are the plastic strain components in principal coordinates. It is a well known experimental result that at pressures on the order of the yield stress, plastic deformation occurs with no change in volume. This implies that

$$d\varepsilon_1^P + d\varepsilon_2^P + d\varepsilon_3^P = 0 \qquad (69)$$

and hence in a uniaxial test with $\sigma_1 = \sigma$, $\sigma_2 = \sigma_3 = 0$, the plastic strain increments are

$$d\varepsilon_2^P = d\varepsilon_3^P = -1/2\, d\varepsilon_1^P$$

so that in a uniaxial test, Equations (66) and (68) reduce to

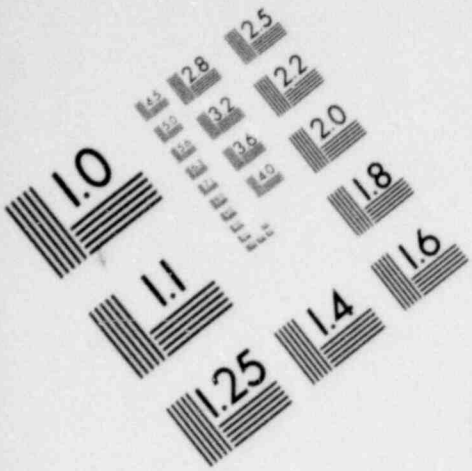

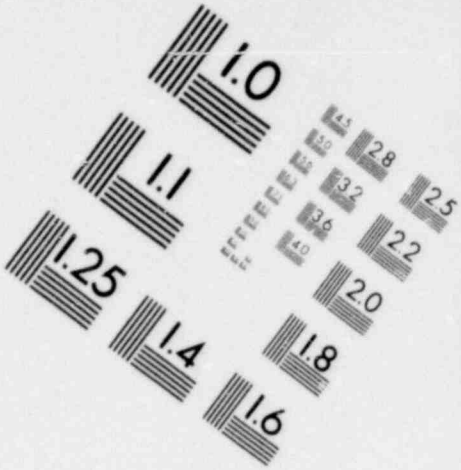

IMAGE EVALUATION TEST TARGET (MT-3)

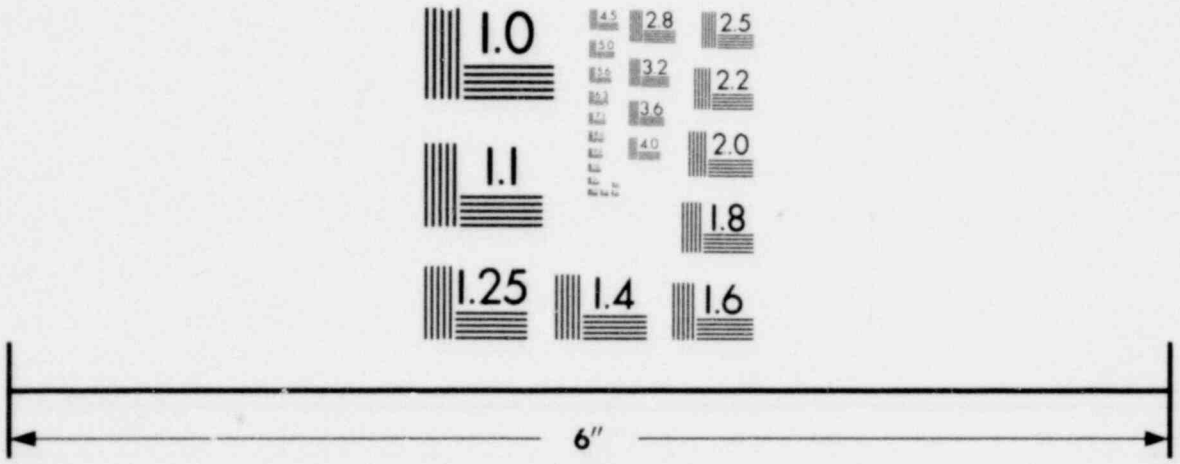

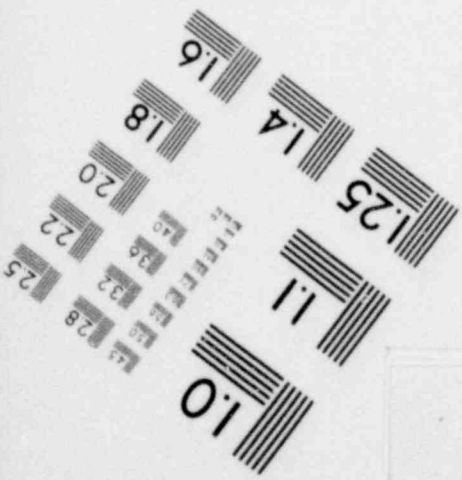

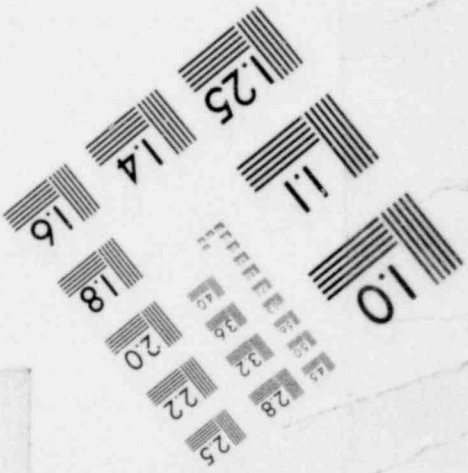

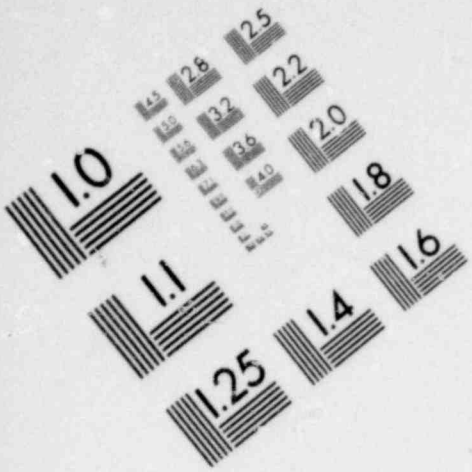

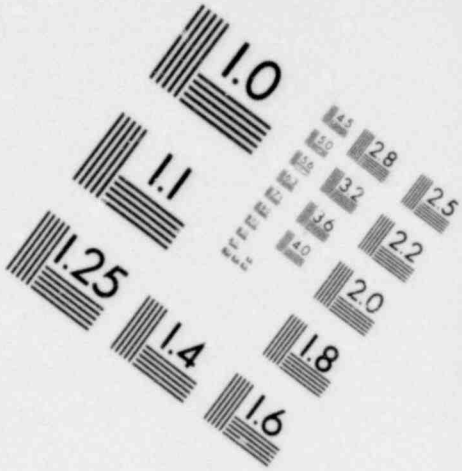

IMAGE EVALUATION TEST TARGET (MT-3)

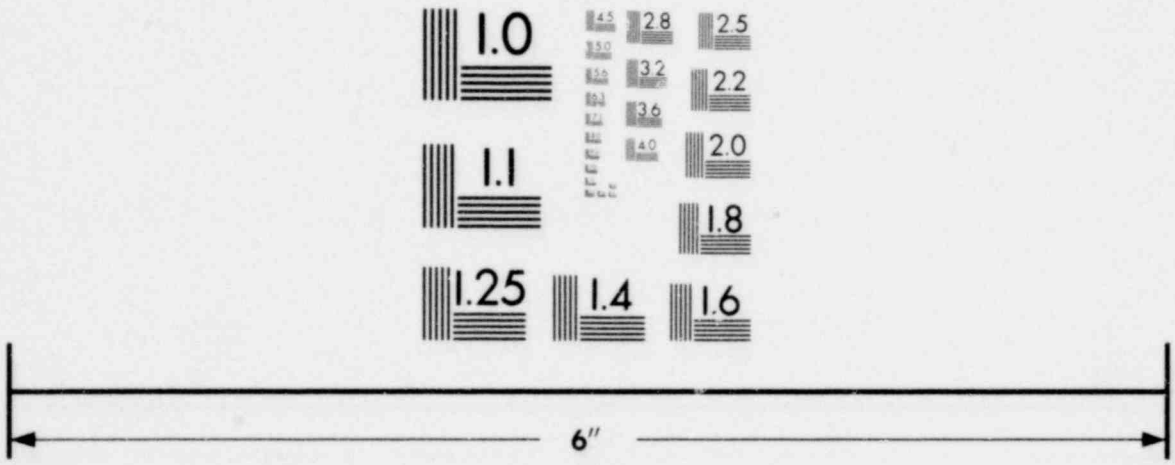

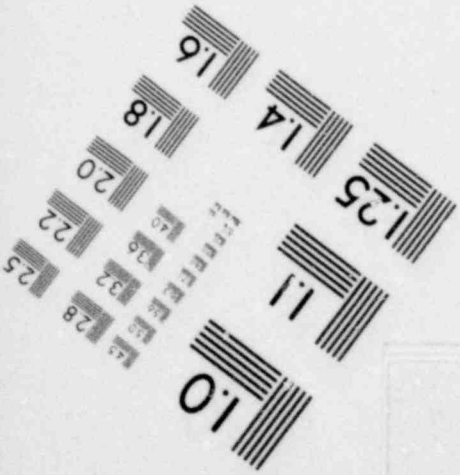

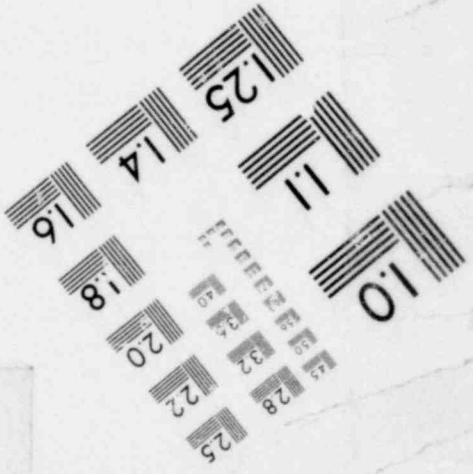

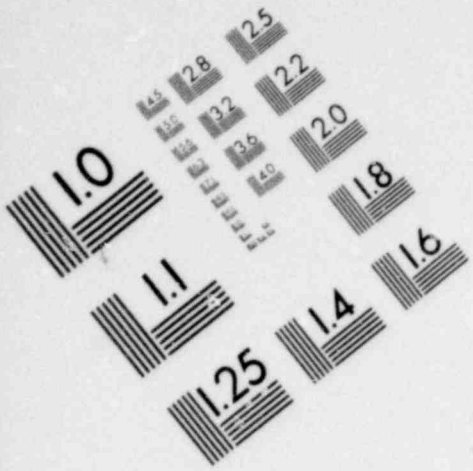

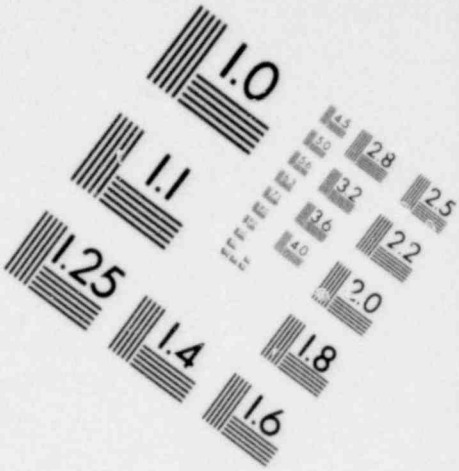

IMAGE EVALUATION
TEST TARGET (MT-3)

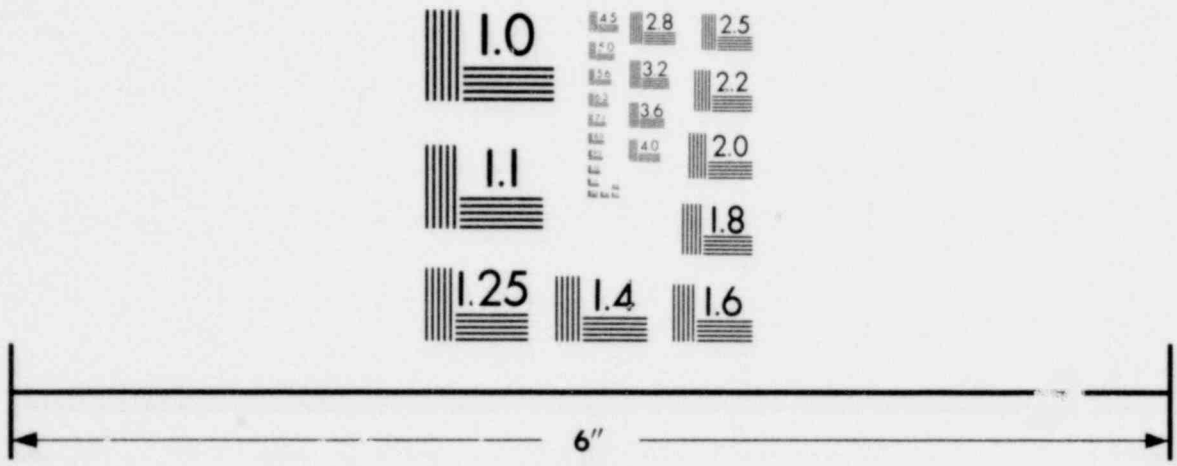

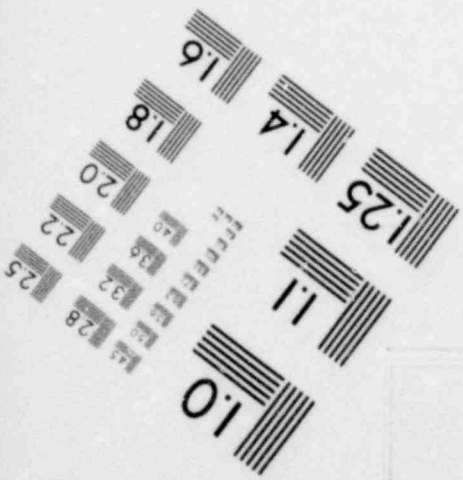

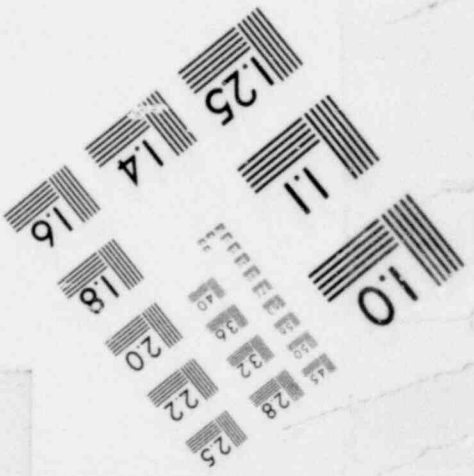

$$\sigma_e = \sigma$$

$$d\varepsilon^p = d\varepsilon_1^p. \tag{70}$$

Thus, when it is assumed that the yield stress is a function of the total effective plastic strain (called the Strain-Hardening Hypothesis), the functional relationship between yield stress and plastic strain can be taken directly from a uniaxial stress-strain curve by virtue of Equation (70).

The relationship between the magnitudes of the plastic strain increments and the effective plastic strain increment is provided by the Prandtl-Reuss Flow Rule:

$$d\varepsilon_i^p = \frac{3\, d\varepsilon^p}{2\, \sigma_e} S_i \qquad i = 1, 3 \tag{71}$$

where S_i are the deviatoric stress components (in principal coordinates) defined by

$$S_i = \sigma_i - \frac{1}{3}(\sigma_1 + \sigma_2 + \sigma_3) \qquad i = 1, 3. \tag{72}$$

Equation (71) embodies the fundamental observation of plastic deformation that the plastic strain increments are proportional to the deviatoric stresses. It may be shown[13] that the constant of proportionality is determined by the choice of the yield function. Direct substitution shows that Equations (67), (69), (70), (71), and (72) are consistent with one another.

Once the plastic strain increments have been determined for a given loadstep, the total strains are determined from a generalized form of Hooke's law given by:

$$\varepsilon_1 = \frac{1}{E}\left[\sigma_1 - \nu(\sigma_2 + \sigma_3)\right] + \varepsilon_1^P + d\varepsilon_1^P + \int \alpha_1 dT$$

$$\varepsilon_2 = \frac{1}{E}\left[\sigma_2 - \nu(\sigma_1 + \sigma_3)\right] + \varepsilon_2^P + d\varepsilon_2^P + \int \alpha_2 dT \qquad (73)$$

$$\varepsilon_3 = \frac{1}{E}\left[\sigma_3 - \nu(\sigma_2 + \sigma_1)\right] + \varepsilon_3^P + d\varepsilon_3^P + \int \alpha_3 dT$$

in which ε_1^P, ε_2^P, and ε_3^P are the total plastic strain components at the end of the previous load increment and ν is Poisson's ratio.

The remaining continuum field equations of equilibrium, strain displacement, and strain compatibility are unchanged. The complete set of governing equations is presented in Table I, written in terms of rectangular Cartesian coordinates and employing the usual indicial notation in which a repeated Latin index implies summation. This set of equations is augmented by an experimentally determined uniaxial stress-strain relation.

3.2.1 Method of Solution. When the problem under consideration is statically determinate, so that the stresses can be found from equilibrium conditions alone, the resulting plastic deformation can easily be determined. However, when the problem is statically indeterminate, and the stresses and deformation must be found simultaneously, then the full set of plasticity equations proves to be quite formidable even in the case of simple loadings and geometries.

One numerical procedure which as been used with considerable success is the Method of Successive Substitutions. This can be applied to any problem for which an elastic solution can be obtained, either in closed form or numerically. A full discussion of this technique including a number of technologically useful examples is contained in Reference 13.

TABLE I

SUMMARY OF GOVERNING EQUATIONS

Equilibrium

$$\sigma_{ji,j} + \rho f_i = 0$$

where

σ = stress tensor

ρ = mass density

f_i = components of body force per unit mass

Stress-Strain

$$\varepsilon_{ij} = \frac{1+\nu}{E} \sigma_{ij} - \delta_{ij} \left(\frac{\nu}{E} \sigma_{kk} - \int \alpha dT\right) + \varepsilon^P_{ij} + d\varepsilon^P_{ij}$$

Strain Displacement

$$\varepsilon_{ij} = \frac{1}{2} (u_{i,j} + u_{j,i})$$

Compatibility

$$\varepsilon_{ij,k\ell} + \varepsilon_{k\ell,ij} - \varepsilon_{ik,j\ell} - \varepsilon_{j\ell,ik} = 0$$

Definitions used in Plasicity

$$\sigma_e \triangleq \sqrt{\frac{3}{2} S_{ij} S_{ij}}$$

$$S_{ij} \triangleq \sigma_{ij} - \frac{1}{3} \sigma_{kk}$$

$$d\varepsilon^P \triangleq \sqrt{\frac{2}{3} d\varepsilon^P_{ij} d\varepsilon^P_{ij}}$$

Prandtl-Reuss Flow Rule

$$d\varepsilon^P_{ij} = \frac{3}{2} \frac{d\varepsilon^P}{\sigma_e} S_{ij}$$

Briefly, the method involves breaking the loading path up into a number of small increments. (For example, in the present application, the loads are external pressure, temperature, and either internal pressure of prescribed displacement or the inside surface of the cladding. These loads all vary during the operating history of the fuel rod.) For each new increment of the loading, the solution to all the plasticity equations listed in Table I is obtained as follows:

First, an initial estimate of the plastic strain increments $d\varepsilon^P_{ij}$ is made. Based on these values, the equations of Equilibrium, Hooke's law, Strain-Displacement and compatibility are solved as for any elastic problem. From the stresses so obtained, the deviatoric stresses S_{ij} may be computed. This represents one path in the computational scheme.

Independently, using the assumed $d\varepsilon^P_{ij}$ values, the increment of effective plastic strain $d\varepsilon^P$ may be computed, and from this and the stress-strain curve, a value of the effective stress σ_e is obtained.

Finally, a new estimate of the plastic strain increments is obtained from the Prandtl-Reuss Flow Rule:

$$d\varepsilon^P_{ij} = \frac{3}{2}\frac{d\varepsilon^P}{\sigma_e} S_{ij}$$

and the entire process is continued until the $d\varepsilon^P_{ij}$ converge. A schematic of the iteration scheme is shown in Figure 4.

The mechanism by which improved estimates of $d\varepsilon^P_{ij}$ are obtained results from the fact that the effective stress obtained from $d\varepsilon^P$ and the stress-strain curve will not be equal to the effective stress which would be obtained from the stresses from the elastic solution. They will only agree when convergence is obtained.

The question of convergence is one that cannot, in general, be answered a priori. However, it can be shown[13] that convergence will be obtained for sufficiently small load increments. Furthermore, lack

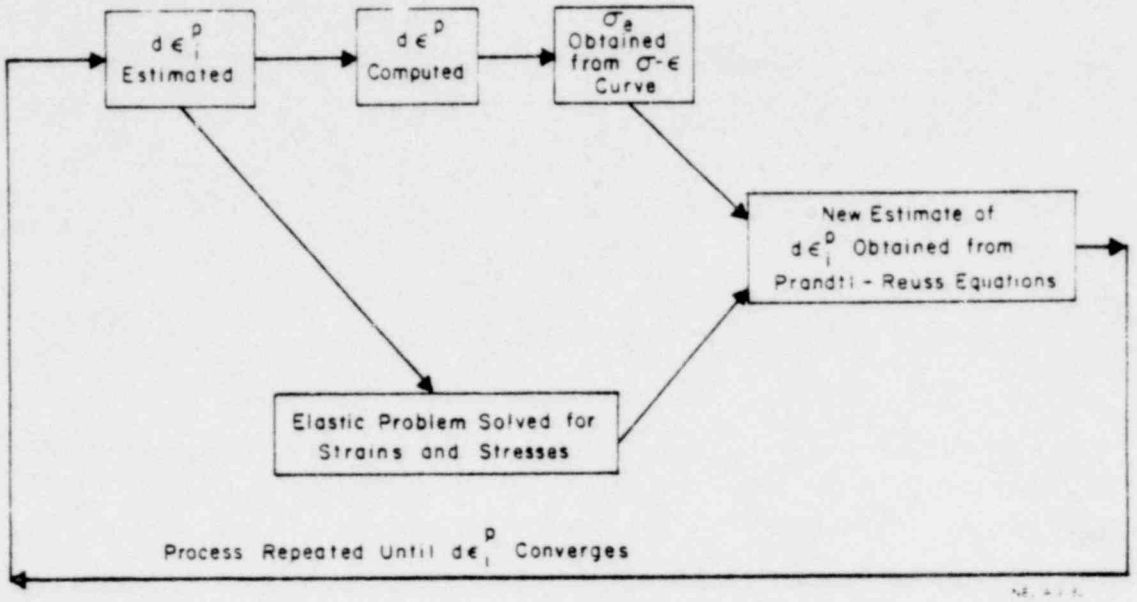

Fig. 4 Schematic of the method of successive elastic routines.

of convergence can usually be traced to the flatness of the stress-strain curve in the plastic region. Problems with convergence are accentuated when the material is at high temperatures (approximately 1200°F and above for zircaloy), due to the fact that work-hardening effects decrease with temperature.

3.2.2 Modified Iteration Scheme. To avoid (or at least minimize) such convergence problems, an alternate iteration scheme was devised by Mendelson and his co-workers. This scheme is based on the von Mises yield function and the Prandtl-Reuss flow rule, so no new hypotheses or assumptions are involved. The iteration scheme is essentially the same as the Prandtl-Reuss iteration scheme described above, except that the iterated variables σ_e and $d\varepsilon_{ij}^p$ (which are related by the highly nonlinear stress-strain law) are replaced by a new pair of variables which are related to $d\varepsilon^p$ in a more nearly linear fashion. The new variables are ε_{et}, the equivalent modified total strain, and ε'_{ij}, the modified deviator strains, and in terms of these new variables, the Prandtl-Reuss flow rule becomes

$$d\varepsilon_{ij}^p = \frac{d\varepsilon^p}{\varepsilon_{et}} e'_{ij}. \qquad (74)$$

Thus, ε_{et} plays the role of σ_e, and ε'_{ij} replaces the deviator stresses S_{ij}. At each step in the iteration, ε_{et} is calculated from the strains obtained from the pseudoelastic solution based on the previous values of the plastic strain increments, and then $d\varepsilon^P$ is related to ε_{et} via the uniaxial stress-strain curve by the expression

$$d\varepsilon^P = \frac{\varepsilon_{et} - \frac{2}{3}\left(\frac{1+\nu}{E}\right)\sigma_e^{old}}{1 + \frac{2}{3}\left(\frac{1+\nu}{E}\right)\left(\frac{d\sigma_e}{d\varepsilon^P}\right)_{old}} \tag{75}$$

in which σ_e^{old} is the value of the effective stress at the end of the last converged loadstep, and $\left(\frac{d\sigma_e}{d\varepsilon^P}\right)_{old}$ is the slope of the stress-plastic strain curve at the end of the last converged loadstep. Since $\left(\frac{d\sigma_e}{d\varepsilon^P}\right)_{old}$ is usually at least an order of magnitude smaller than the elastic modulus E, it can be seen that the denominator in Equation (75) is nearly unity, and thus $d\varepsilon^P$ is very nearly linearly related to ε_{et}. Thus, the convergence difficulties associated with the nonlinearity of the stress-strain curve can be avoided.

Only the appropriate equations which are used in this Plastic Strain-Total Strain iteration scheme will be given here. The full derivation is presented in Mendelson's book[13], Sections 7-9 and 9-1. The modified strains are obtained from

$$\varepsilon'_{ij} = \varepsilon^e_{ij} + d\varepsilon^P_{ij} \tag{76}$$

in which ε^e_{ij} are the elastic strains defined by

$$\varepsilon^e_{ij} = \frac{1+\nu}{E}\sigma_{ij} - \frac{\nu}{E}\sigma_{kk}\delta_{ij}. \tag{77}$$

The modified deviator strains are then obtained from Equation (76) as

$$e'_{ij} = e^e_{ij} + d\varepsilon^P_{ij} \tag{78}$$

where e^e_{ij} are the elastic deviator strains, and the fact that $d\varepsilon^p_{ii} = 0$ has been used. The equivalent modified total strain is defined as

$$\varepsilon_{et} \triangleq \sqrt{\frac{2}{3}} \left[(\varepsilon'_{11} - \varepsilon'_{22})^2 + (\varepsilon'_{22} - \varepsilon'_{33})^2 + (\varepsilon'_{33} - \varepsilon'_{11})^2 + 6(\varepsilon'_{12})^2 + 6(\varepsilon'_{23})^2 + 6(\varepsilon'_{31})^2 \right]^{1/2}. \quad (79)$$

A schematic outline of the Plastic Strain-Total Strain iteration scheme is shown in Figure 5. The similarity with the previous iteration scheme based directly on the Prandtl-Reuss flow relations is evident.

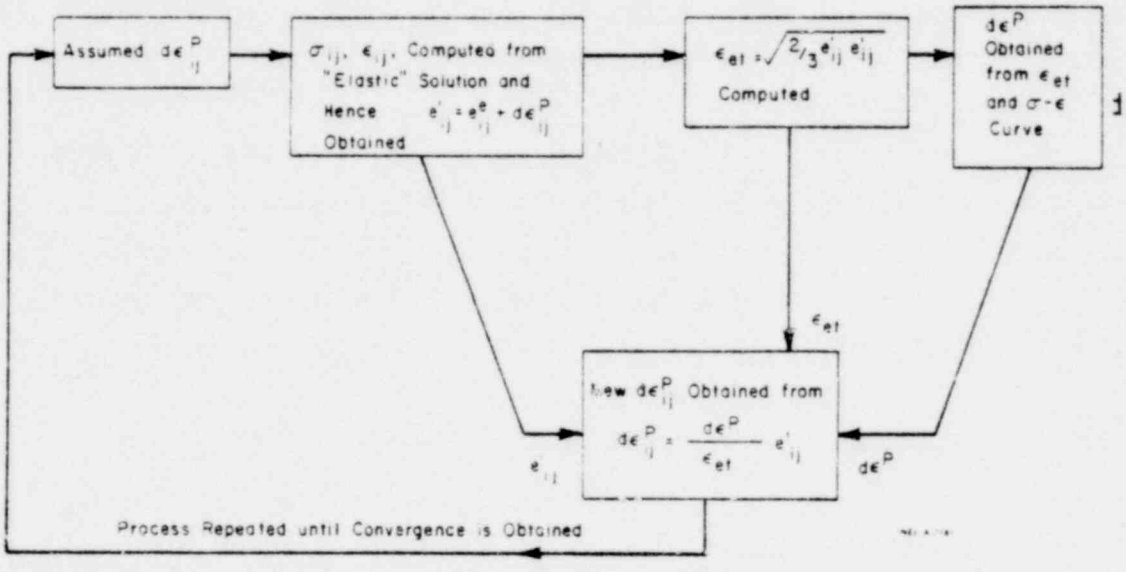

Fig. 5 Flow chart for plastic strain-total strain iteration scheme.

At the start of each loadstep calculation, initial values of $d\varepsilon^p_{ij}$ are assumed. Using these values, the pseudoelastic equations are solved for new stresses and strains. From the strains so calculated ε_{et} and ε'_{ij} are obtained. Then, using the uniaxial stress-strain curve, a value of $d\varepsilon^p$ corresponding to ε_{et} is obtained using Equation (75). Finally, new estimates of $d\varepsilon^p_{ij}$ are obtained from the modified flow rule

$$d\varepsilon^p_{ij} = \frac{d\varepsilon^p}{\varepsilon_{et}} e'_{ij}$$

and the process is repeated until convergence is obtained.

This modified iteration procedure differs from the previous iteration scheme in one important aspect. In the previous scheme, if one of the nodes at which the plastic strains are being sought is actually only strained elastically, then in the course of the iteration process, the plastic strain increments will approach zero, and the correct elastic solution will be obtained automatically. In the modified iteration scheme, however, the iteration process will not converge to the appropriate elastic solution, but will, in fact, generally diverge in this case. Thus, at each step in the iteration process it is necessary to compute the effective stress and compare it with the current, work-hardened yield stress. If the yield stress has not been exceeded, then the plastic strain increments are set to zero.

Not only will the modified iteration scheme described above permit convergent plasticity calculations for higher temperatures and larger loadsteps, it also converges much more rapidly than the previous iteration scheme. Hence, the modified iteration scheme is utilized in all the (time-dependent) plasticity calculations.

3.3 General Considerations in Creep-Stress Relaxation Analysis

3.3.1 Uniaxial Behavior. Creep can broadly be defined as the inelastic time-dependent change in stress and strain in a body under constant load. For most common structural metals, high temperatures are required. Shown in Figure 6 are typical creep curves taken on a uniaxial specimen at constant stress for zircaloy-2 at 300°C taken from a correlation by Ibrahim[14].

Two features are notable. First, doubling the stress more than doubles the strain. Second, the strain rate decreases as time goes on. A typical uniaxial creep test taken to failure is shown in Figure 7. From time $t = 0$ to $t = t_1$, the creep rate (slope of ε versus t) is continually decreasing. This is called the period of primary, or transient creep. From time t_1 to t_2, the creep rate is approximately constant (although it does depend on the stress level, temperature, radiation

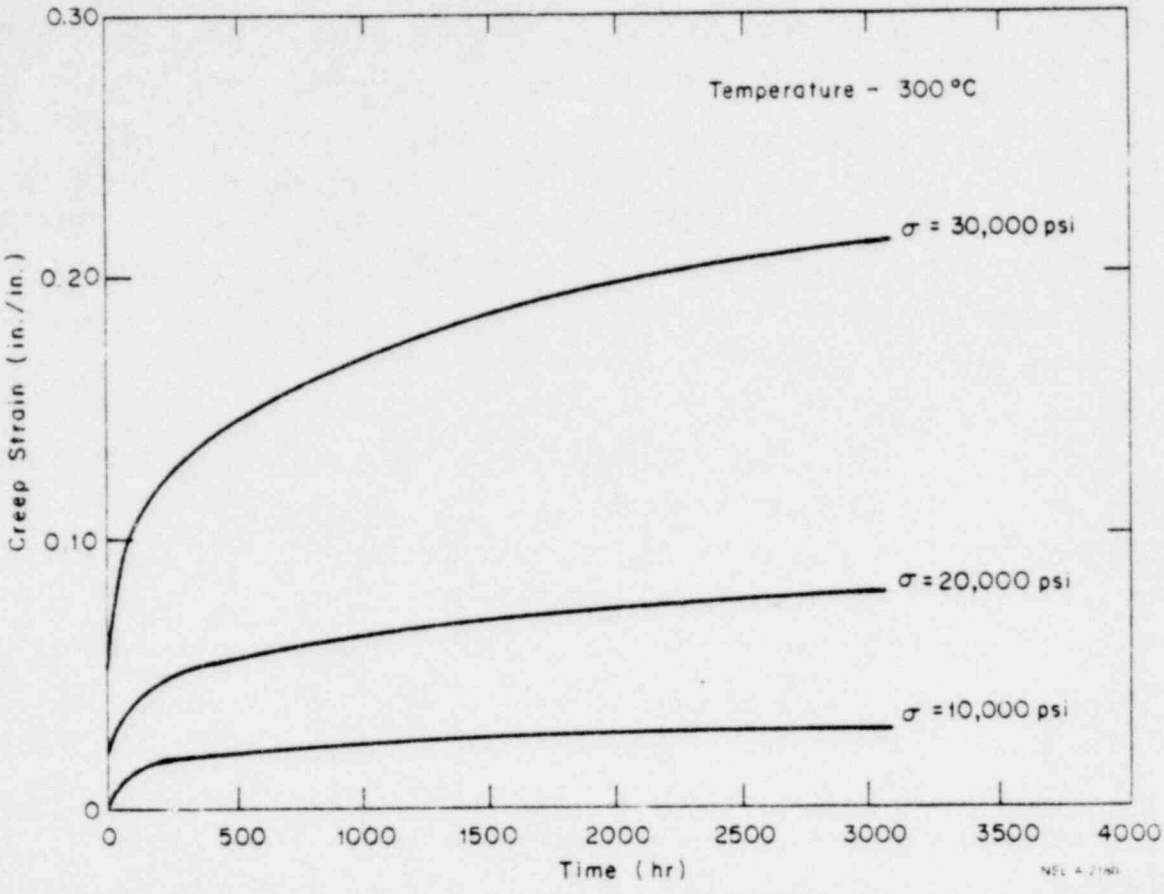

Fig. 6 Creep curves for zircaloy-2 at 300 C (572°F) (correlations from Ibrahim, Reference 14).

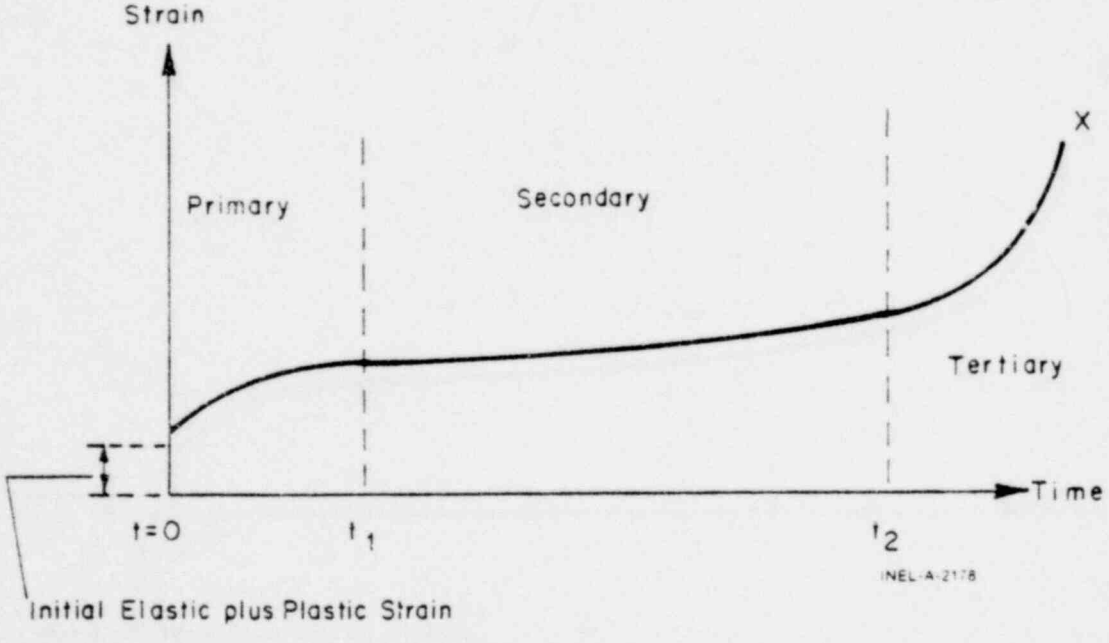

Fig. 7 Typical creep test taken to failure.

flux, etc.). The region of constant creep rate is called the region of secondary or steady state creep.

The final region is one in which the creep rate begins increasing and is called the region of tertiary creep. In this region, the specimen usually exhibits cracks or other nonuniform deformation, and hence, the usual continuum theory is not applicable. Thus, in a structural analysis, attention is restricted to the primary and secondary stages of creep.

One approximation that is often used in creep analysis is to consider only the steady state portion of creep, so that the creep rate is independent of time. This considerably simplifies any such analysis. However, as can be seen from Figure 6, the creep strain incurred during the period of transient creep cannot be neglected in comparison to the creep incurred during the period of steady state creep (at least for hold times of less than 3000 hours) so that both transient and secondary creep must be included. This consideration is especially important when comparisons are to be made between code predictions and laboratory experiments which are usually of limited duration compared to anticipated service life.

The strains induced during creep are permanent, and it is a basic assumption of creep analysis that the constitutive law can be written:

$$\varepsilon_1 = \frac{1}{E}\left[\sigma_1 - \nu(\sigma_2 + \sigma_3)\right] + \varepsilon_1^P + \varepsilon_1^C + d\varepsilon_1^C \qquad (80)$$

where

ε_1^P = accumulated plastic strain

ε_1^C = accumulated creep strain

$d\varepsilon_1^C$ = increment of creep strain.

Although both plastic strains and creep strains are permanent, there is a fundamental difference between plasticity, which does not depend on

time, and creep which is explicitly time-dependent. That is, the magnitude of the plastic strains resulting from the application of a sequence of loads to a body does not depend on the time intervals between the applications of the individual loads. The magnitude of the resulting creep strain, however, is greatly affected by the time history of the application of the loads.

Since creep is explicitly a time-dependent process, it would be most appropriate to use a theory in which the time rates of strain are related to the rates of stress, i.e., a visco-elastic theory. And, in fact, there are simple, linear rheological models available which can qualitatively reproduce all the effects observed in a uniaxial creep test. However, as pointed out in regard to Figure 6, the creep response of metals is a nonlinear function of stress. Hence, a nonlinear theory of visco-elasticity would have to be used to accurately predict creep strains. While such a nonlinear theory does exist (in the Frechet Expansion Theorem), its implementation is currently beyond the scope of present day computers. Further, the theory requires experimental data which do not exist to date, and which would be relatively difficult to obtain. Thus, the use of a nonlinear visco-elastic theory is not within the current state of the art. For a further discussion of this, reference is made to C. E. Pugh et al[15].

3.3.2 The Equation of State Approach. A workable alternative to a visco-elastic creep analysis is to use the so-called "equation of state" approach. Here, analytical expressions are fit to the experimental uniaxial creep strain versus time curves measured at constant applied stress, giving the functional relation:

$$\varepsilon = f(\sigma,t,T,R) \qquad (81)$$

where

σ = applied constant stress

t = time

T = temperature

R = irradiation flux parameter.

The creep strain rate is obtained analytically by differentiating Equation (81) to obtain

$$\dot{\varepsilon} = \alpha'(\sigma, t, T, R). \tag{82}$$

Now it must be kept in mind that Equations (81) and (82) are strictly valid for constant stress only. To extend their use to problems involving continuously varying stress, certain assumptions must be made. Consider the two creep curves in Figure 8 obtained at two different stress levels. Suppose that creep strain has been accumulating at stress σ_1 until time t_1, and then the stress is changed to σ_2. The question to be answered is: at what point on the $\sigma = \sigma_2$ creep curve do we start our calculations for further creep analysis? One of two hypotheses is commonly made:

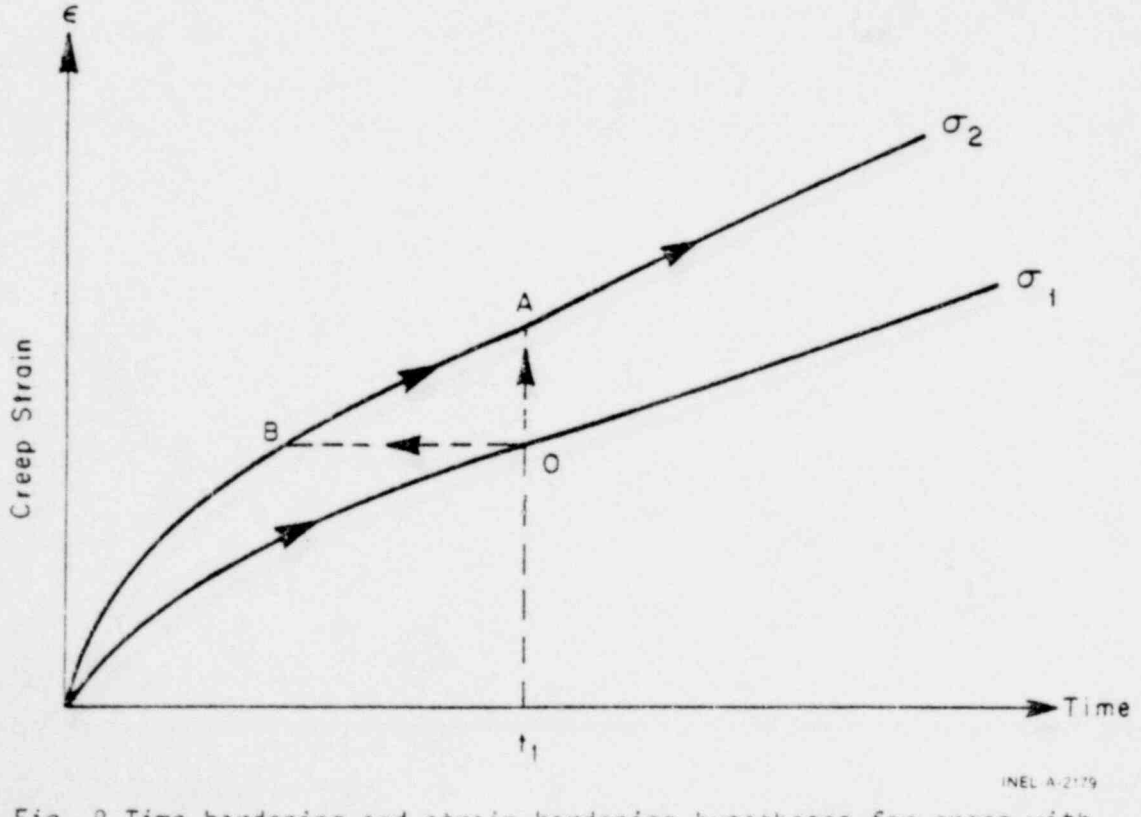

Fig. 8 Time hardening and strain hardening hypotheses for creep with varying stress.

(1) Time-hardening Hypothesis: Here it is assumed that it is the elapsed time which is the determining factor, so that in making the transition from stress σ_1 to σ_2, one moves from point O to point A in Figure 8. Hence, creep strain rates are determined directly from Equation (82).

(2) The Strain-hardening Hypothesis: Here it is assumed that it is the accumulated creep strain which is the determining factor. Thus, one moves from point O to point B in Figure 8. Analytically, this is accomplished by eliminating time, t, from Equation (82) by use of Equation (81) to obtain

$$\dot{\varepsilon} = h(\sigma,\varepsilon,T,R) \tag{83}$$

and thus the subsequent creep strain rates are determined by the accumulated creep strain.

In general, experimental data agree better with analytical predictions based on the strain-hardening assumption, so this is the assumption which is incorporated into the FRACAS subcode. This is in accordance with the recommendations of Reference 15.

When the creep function, Equation (81), is a complicated function of its arguments, it is often not possible to eliminate time analytically between Equations (81) and (82). In these cases it is necessary to perform the elimination of time numerically. This can be done for arbitrary functional forms of Equations (81) and (82) and thus, complete generality can be maintained. However, this is achieved at the cost of having to solve a pair of highly nonlinear, coupled algebraic equations at each step of the creep iteration scheme, which is a time consuming procedure.

In order to optimize the computation time for creep calculations in FRACAS, the following procedure is utilized. It is assumed that the creep law, Equation (81), is such that time can be explicitly evaluated so as to obtain Equation (83), and that Equation (83) is available to

FRACAS from a subroutine denoted CREPR. Secondly, it is assumed that Equation (83) can be written in the form

$$\sigma = \sigma\ (\dot{\varepsilon}, \varepsilon, T) \tag{84}$$

and that this equation is available to FRACAS from a subroutine denoted CREEP. In the majority of cases, subroutine CREEP will use an iteration scheme to obtain σ given $\dot{\varepsilon}$ and ε, but this can usually be done very efficiently. For use in the FRAP codes, subroutine CREPR is obtained from the material properties subcode MATPRO. Subroutine CREEP uses the analytic expression for creep rate from MATPRO and the method of successive substitutions. This results in minimizing the creep calculation time.

3.3.3 Extension to Multiaxial Creep Problems. All of the foregoing discussion is applied to uniaxial loading behavior only. To extend this to creep and stress relaxation in multiaxial states of stress, we proceed in a fashion similar to that used in plasticity, and introduce an effective creep strain increment defined by

$$d\varepsilon^c \triangleq \sqrt{\frac{2}{3}\, d\varepsilon^c_{ij}\, d\varepsilon^c_{ij}} \tag{85}$$

which is, of course, directly analogous to the effective plastic strain defined for the plasticity calculations. Then the effective creep strain rate is computed from

$$\dot{\varepsilon}^c = \frac{d\varepsilon^c}{dt} = \frac{1}{\Delta t}\ \sqrt{\frac{2}{3}\, d\varepsilon^c_{ij}\, d\varepsilon^c_{ij}}. \tag{86}$$

The same effective stress is utilized:

$$\sigma_e \triangleq \sqrt{\frac{3}{2}\, \sigma_{ij}\sigma_{ij}}.$$

It is then assumed that the effective stress, σ_e, and the effective creep strain rate, $\dot{\varepsilon}^c$, are related by the uniaxial creep strain function, Equation (83). For any given problem, the equilibrium and kinematic equations are identical with those used in the plasticity calculations.

The external loading (temperatures, pressures, displacements etc.,) are assumed to be applied stepwise. At each time that these loads are

incremented, a (time-independent) plasticity solution is obtained as described in the previous sections. The time periods in between (at constant load) are subdivided into a number of small time increments, Δt, and a creep analysis is performed. For each time increment, Δt, the Method of Successive Elastic Solutions is applied in the usual fashion, except that the effective stress, σ_e, is obtained from the uniaxial creep curve at the iterated value of the effective creep rate, $\dot{\varepsilon}^c$, instead of from the uniaxial stress-strain curve. Thus, for each time increment, Δt, the creep solution is obtained as follows:

(1) Assume the creep strain increments, $d\varepsilon^c_{ij}$

(2) Compute the effective creep strain rate

$$\dot{\varepsilon}^c = \frac{1}{\Delta t} \sqrt{\frac{2}{3} d\varepsilon^c_{ij} d\varepsilon^c_{ij}}$$

(3) Obtain the effective stress from the uniaxial creep curve, using the strain-hardening hypothesis

$$\sigma_e = h(\dot{\varepsilon}^c, \varepsilon^c, T, R)$$

where ε^c is the total accumulated effective creep strain, including $d\varepsilon^c = \dot{\varepsilon}^c \Delta t$ incurred during the current time increment

(4) Obtain the deviator stresses from the elastic solution, with Hooke's law taken as

$$\varepsilon_{11} = \frac{1}{E}\left[\sigma_{11} - \nu(\sigma_{22} + \sigma_{33})\right] + \varepsilon^p_{11} + \varepsilon^c_{11} + d\varepsilon^c_{11}$$

$$\varepsilon_{12} = \frac{1+\nu}{E}\sigma_{12} + \varepsilon^p_{12} + \varepsilon^c_{12} + d\varepsilon^c_{12}$$

where etc.

ε^p_{ij} = accumulated plastic strains at end of last load step

ε^c_{ij} = accumulated creep strains at end of last Δt time increment

$d\varepsilon^c_{ij}$ = increments of creep strain durin
Δt time increment

(5) Obtain new estimates of the creep strain increments from the Prandtl-Reuss flow rule:

$$d\varepsilon^c_{ij} = \frac{3}{2}\frac{\dot{\varepsilon}^c \Delta t}{\sigma_e} S_{ij}.$$

(6) Repeat until convergence.

3.4 Description of Individual Subroutines

The package of subroutines which perform the Fuel-Clad Mechanical Interaction analysis consists of four main subroutines. FCMI is the executive subroutine, and it calls either COUPLE, STACK, or CLADF as appropriate. STRESS and STRAIN are called by either CLADF, STACK, or COUPLE to obtain the necessary mechanical properties. Subroutine CLOSE is an interpolation routine called by FCMI to locate the point at which the gap closes for each node. These subroutines are described in detail below.

3.4.1 Subroutine FCMI. Subroutine FCMI performs the basic function of determining whether or not the fuel pellets and the cladding are in contact. The radial expansion of the fuel is obtained from models contained externally to the fuel-clad interaction subroutines, and is passed to FCMI in the calling sequence. Stress effects on the fuel expansion are known to be small relative to thermal expansion and swelling, and so the fuel expansion is uncoupled from the cladding deformation. (Stress induced creep is important, however, and is being considered separately.)

The decision as to whether or not the fuel is in contact with the cladding is made by comparing the radial displacement of the fuel with the radial displacement which would occur in the cladding due to the prescribed external (coolant) pressure and the prescribed internal (fission gas) pressure. Both of these values are passed to FCMI through the calling sequence. This free cladding radial displacement is obtained in CLADF. Then, if

$$u_r^{fuel} \geq u_r^{clad} + \delta \tag{87}$$

where δ is the initial (as-fabricated) gap between the fuel and the cladding, the fuel is determined to be in contact with the cladding. The as-fabricated gap δ is a constant which does not change throughout the loading history of the rod. The loading history enters into this decision by virtue of the permanent plastic cladding strains which are used in the CLADF solution, and which are updated at each call to CLADF or COUPLE. These plastic strains (and total effective plastic strain ε^P) are stored in the main calling program, and are passed to FCMI through the calling sequence.

If the fuel and cladding displacements are such that Equation (87) is not satisfied, the gap has not closed during the current loadstep, and the solution obtained by CLADF is the appropriate solution. The current value of the gap is computed and passed back to the main calling program. The plastic strain values may be changed in the solution obtained by CLADF if additional plastic straining has occurred.

If Equation (87) is satisfied, however, the fuel and cladding are in contact during the current loading step. If the gap was open at the end of the last loadstep, then subroutine CLOSE is called. This routine linearly interpolates between the current load values and the last load values to determine exactly when the gap closed. For that portion of the loadstep in which the gap is open, subroutine CLADF is called. For the remaining portion of the loadstep, in which the cladding and the fuel are in contact, radial continuity at the contact interface requires that

$$u_r^{clad} = u_r^{fuel} - \delta \tag{88}$$

while in the axial direction it is assumed that no-slip occurs between the fuel and the cladding. Since a thin shell theory is used for the cladding, it is assumed that the strain induced in the cladding by the axial expansion of the fuel is taken up entirely by straining of the middle surface of the cladding.

Note that only the additional strain which occurs in the fuel after lock-up has occurred is transferred to the cladding. Thus, if $\varepsilon_{z,o}^{clad}$ is the axial strain in the cladding just prior to contact and $\varepsilon_{z,o}^{fuel}$ is the corresponding axial strain in the fuel, then the no-slip condition in the axial direction becomes

$$\varepsilon_z^{clad} - \varepsilon_{z,o}^{clad} = \varepsilon_z^{fuel} - \varepsilon_{z,o}^{fuel} . \tag{89}$$

The values of the prestrains $\varepsilon_{z,o}^{fuel}$ and $\varepsilon_{z,o}^{clad}$ are set equal to the values of the strains which existed in the fuel and the cladding at the last load increment during which the gap was open. These values are stored in the main calling program, and passed to FCMI in the calling sequence. They are updated at the end of any load increment during which the gap closes.

After u_r^{clad} and ε_z^{clad} have been computed in FCMI, they are passed to subroutine COUPLE, which considers a thin cylindrical shell with prescribed axial strain, external pressure, and prescribed radial displacement of its inside surface. After the solution to this problem is obtained in COUPLE, subroutine FCMI passes a value of the interface pressure back to the main calling program, along with new plastic strains and stresses.

After all the nodes in the fuel rod have been examined for open or closed gaps as described above, all those nodes with open gaps are re-examined to consider axial compatibility. This is necessary because in the course of normal power histories it is possible for gaps to exist between the fuel pellets. The gaps can, in the case of collapsible cladding, give rise to local high strain concentrations. As a means of following the generation and development of such axial gaps, models are included in FCMI to consider the behavior of the cladding in the situations depicted in Figure 9a or Figure 9b. In both of these figures, nodes J* and J-1 are nodes which have been determined to be in firm contact with the cladding. Nodes J to J*-1 are nodes which have been determined not to be in contact with the cladding.

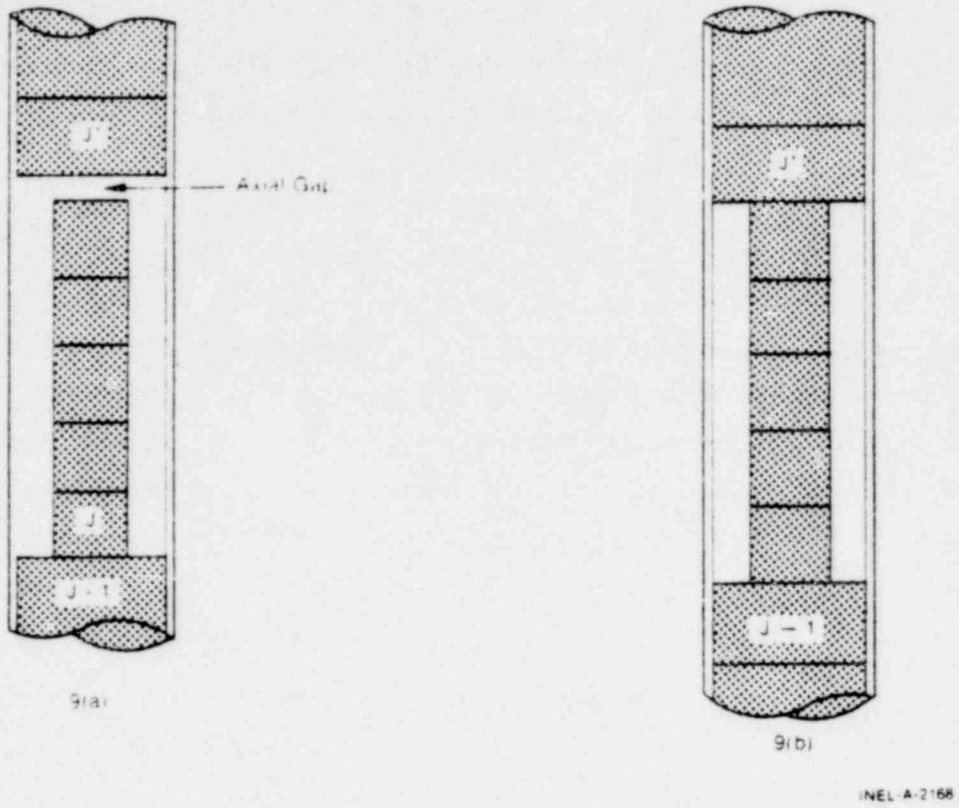

Fig. 9 Axial gap and trapped stack configurations.

Figure 9a depicts the case where, due to the pressure differences and thermal expansion, the length of the enclosed column of pellets is less than the length of the cladding, and hence, an axial gap exists. For the case of vertical fuel rods, the gap will occur at the top of the uppermost pellet. In this situation, the deformation of the cladding is determined by the internal (fission gas) and external (coolant) pressures, and the axial temperature distribution in the cladding.

By contrast, it can happen that the axial expansion of the column of fuel pellets is great enough so that no gap can exist, and in fact, the expansion of the fuel pellets trapped between nodes J-1 and J* actually stretches the cladding axially, as depicted in Figure 9b. This situation is denoted as the "Trapped Stack" regime.

Models for the determination of the elastic-plastic deformation of the cladding for the two regimes discussed above are contained in the two subroutines CLADF and STACK, which are described in detail later in

this report. In the following, the assumptions and logic used to determine which deformation regime is appropriate are discussed.

Consider the situation shown in Figure 9a, wherein nodes J* and J-1 have been determined to be in firm contact. Nodes J through J*-1 are nodes with open radial gaps, and thus, for these nodes, the fuel is not in contact with the cladding. Let $\xi^K(i)$ denote the axial gap between node i and node i + 1 at the end of the loadstep k. (It is assumed that there is never any gap between the lowest pellet and the bottom of the fuel rod.) Then, at the start of loadstep k + 1, it is assumed that all the fuel pellets consolidate at the bottom of the stack, so that all axial gaps are zero except the gap between the top node in the free stack and the next locked node J*, that is

$$\begin{cases} \xi^{k+1}(J^*-1) = \sum_{i=j-1}^{J^*-1} \xi^k(i) \\ \xi^{k+1}(i) = 0 \quad \text{for} \quad i = j-1 \text{ to } J^*-2. \end{cases}$$

The change in length of the stack of fuel pellets is determined from the prescribed axial fuel strains, using

$$\Delta\ell_{fuel}^{k+1} = \sum_{i=j}^{J^*-1} \left(\varepsilon_{z,fuel}^{k+1} - \varepsilon_{z,fuel}^{k} \right) dz(i) \qquad (90)$$

where the summation is taken over all nodes in the stack, and the superscript indicates the loadstep number.

The length of the trapped cladding can now be computed assuming that the fuel and cladding do interact, and that changes in the length of the trapped cladding are determined by changes in the length of the stack of fuel pellets. The trapped cladding length, assuming axial interaction, is given by

$$\ell_{clad}^{(k+1)} = \ell_{clad}^{(k)} + \Delta\ell_{fuel}^{(k+1)} - \xi^{k+1}(J^*-1) \qquad (91)$$

where

$\ell_{clad}^{(k)}$ = length of trapped cladding at the end of the last loadstep

$\Delta\ell_{fuel}^{(k+1)}$ = change in length of column of fuel pellets during current loadstep

$\xi^{k+1}(j^*-1)$ = axial gap between column of fuel pellets and upper end of trapped cladding.

The trapped cladding length computed above is compared with the length that the cladding would assume due to the internal and external pressures and temperature gradients acting alone, as in the absence of axial fuel-cladding interaction. This free length can be obtained from the strains computed by subroutine CLADF, using

$$\ell_{free}^{(k+1)} = \sum_{i=j}^{J^*-1} \left[1 + \varepsilon_{z,CLADF}^{(k+1)}\right] dz(i). \qquad (92)$$

The decision as to whether or not fuel-cladding axial interaction takes place can now be made. If the length that the cladding would assume under the action of pressure and thermal gradients alone is greater than the length the cladding would assume due to axial interaction, then no axial interaction is possible and, in general, an axial gap will exist. Otherwise, axial interaction must have taken place. The two cases are considered separately.

Case A:

If $\ell_{free}^{(k+1)} > \ell_{clad}^{(k+1)}$, then a gap has opened between the fuel pellet stack and the cladding and the stresses and strains are set equal to those computed in CLADF. The new axial gap (at the top of the fuel pellet stack) can be computed from

$$\xi^{k+1}(J^*-1) = \xi^{k}(j^*-1) + \Delta\ell_{clad}^{(k+1)} - \Delta\ell_{fuel}^{(k+1)} \qquad (93)$$

in which $\Delta\ell_{clad}^{(k+1)}$ is the change in length of the trapped cladding during the current loadstep, and is obtained from

$$\Delta\ell_{clad}^{(k+1)} = \ell_{free}^{(k+1)} - \ell^{(k)} \tag{94}$$

where $\ell^{(k)}$ is the length of the trapped cladding at the end of the last loadstep. The axial gaps between all other axial nodes in the stack of fuel pellets (including the gap beneath the lowest pellet in the stack) are set equal to zero.

Case B:

If $\ell_{clad}^{(k+1)} > \ell_{free}^{(k+1)}$, then axial interaction has taken place and no axial gap will exist. The change in length of the trapped cladding is determined by the preexisting axial gap and the change in the fuel pellet stack length via

$$\Delta\ell_{clad}^{(k+1)} = \Delta\ell_{fuel}^{(k+1)} - \xi^{k}(J^{*}-1) \tag{95}$$

This quantity is then passed to subroutine STACK, after which all the axial gaps in the fuel stack are set equal to zero.

Finally, if the stack of pellets with open radial gaps occurs at the top of the fuel rod, then the solution obtained in CLADF is the appropriate solution, and all axial gaps are set to zero. This is done since it is assumed that there is always a plenum volume containing a hold-down spring at the top of the fuel rod, and hence that the uppermost pellet can never contact the top of the fuel rod cladding.

3.4.2 Subroutine CLADF. This subroutine considers a thin cylindrical shell loaded by both internal and external pressures. Axisymmetric loading and deformation are assumed. Loading is also restricted to be uniform in the axial direction, and no bending is considered. The geometry and coordinates are shown in Figure 10. The displacements of the midplane of the shell are u and w in the radial and axial directions respectively.

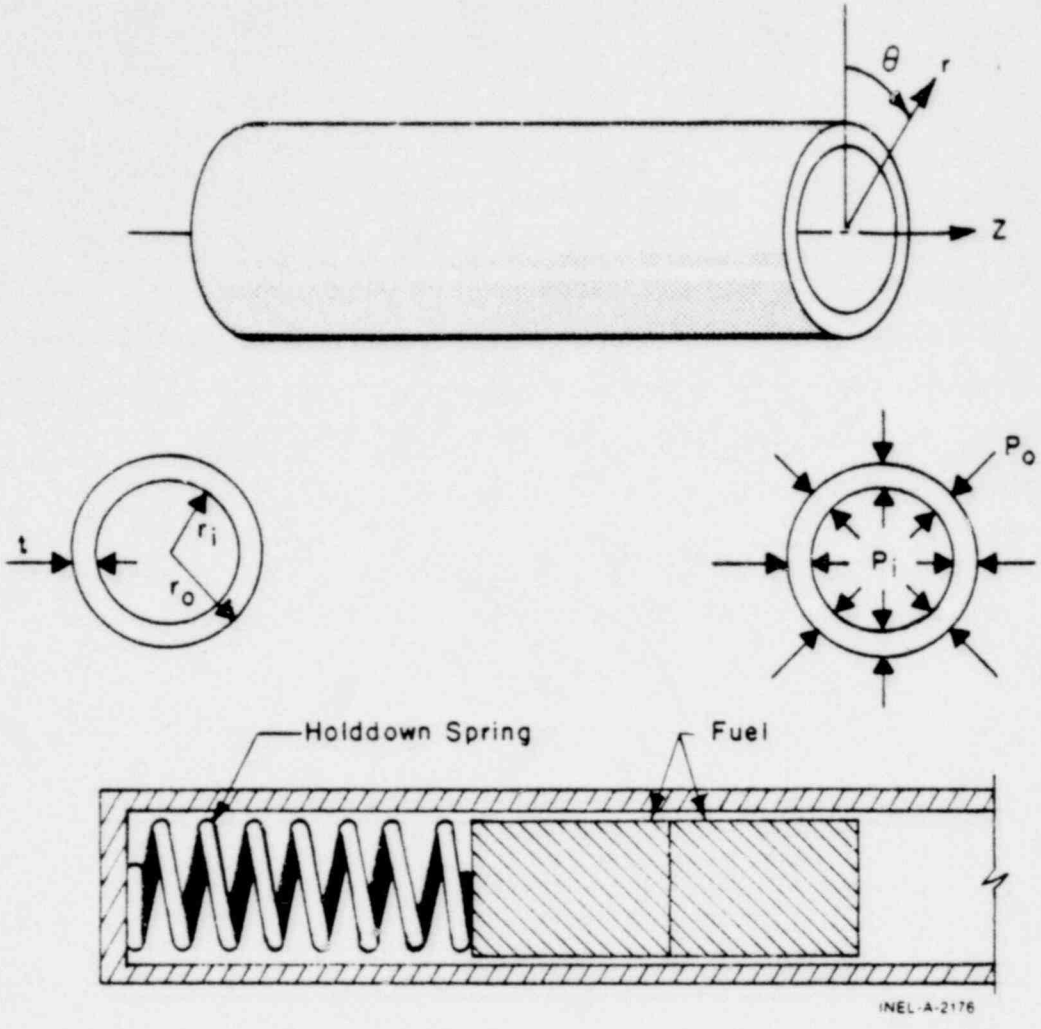

Fig. 10 Fuel rod geometry and coordinates.

Then, as is well known, the equilibrium equations simplify considerably, and are identically satisfied by

$$\sigma_\theta = \frac{r_i P_i - r_o P_o}{t} \tag{96}$$

$$\sigma_z = \frac{r_i^2 P_i - r_o^2 P_o}{r_o^2 - r_i^2}. \tag{97}$$

For membrane shell theory[16], the strains are related to the midplane displacements by

$$\varepsilon_z = \frac{\partial w}{\partial z} \tag{98}$$

$$\varepsilon_\theta = \frac{u}{\bar{r}} \tag{99}$$

where $\bar{r}$ is the radius of the midplane. Strain across the thickness of the shell will be allowed. In shell theory, since the radial stress can be neglected, and since the hoop stress, σ_r, and axial stress, σ_z, are uniform across the thickness when bending is not considered, the radial strain is due only to Poisson's effect, and is uniform across the thickness. (Normally, radial strains are not considered in a shell theory, but when plastic deformations are to be considered, plastic radial strains must be included.)

The stress-strain relations are written in the incremental form:

$$\varepsilon_\theta = \frac{1}{E}\left[\sigma_\theta - \nu\sigma_z\right] + \varepsilon_\theta^P + d\varepsilon_\theta^P + \int_{T_o}^{T} \alpha_\theta dT \tag{100}$$

$$\varepsilon_z = \frac{1}{E}\left[\sigma_z - \nu\sigma_\theta\right] + \varepsilon_z^P + d\varepsilon_z^P + \int_{T_o}^{T} \alpha_z dT \tag{101}$$

$$\varepsilon_r = -\frac{\nu}{E}\left[\sigma_\theta + \sigma_z\right] + \varepsilon_r^P + d\varepsilon_r^P + \int_{T_o}^{T} \alpha_r dT \tag{102}$$

where

T_o = strain-free reference temperature

$\alpha_\theta, \alpha_z, \alpha_r$ = coefficients of thermal expansion

T = current average clad temperature.

The terms ε_θ^P, ε_z^P, and ε_r^P are the plastic strains at the end of the last load increment, and $d\varepsilon_\theta^P$, $d\varepsilon_r^P$, and $d\varepsilon_z^P$ are the additional plastic strain increments which occur due to the new load increment.

As discussed in Section 3.2, the magnitudes of the additional plastic strain increments are determined by the effective stress and the Prandtl-Reuss flow rule, namely:

$$\sigma_e = \frac{1}{\sqrt{2}} \left[(\sigma_\theta - \sigma_z)^2 + (\sigma_z)^2 + (\sigma_\theta)^2 \right]^{1/2} \tag{103}$$

$$\begin{aligned} d\varepsilon_\theta^P &= \frac{3}{2} \frac{S_\theta}{\sigma_e} d\varepsilon^P \\ d\varepsilon_z^P &= \frac{3}{2} \frac{S_z}{\sigma_e} d\varepsilon^P \\ d\varepsilon_r^P &= - d\varepsilon_\theta^P - d\varepsilon_z^P \end{aligned} \tag{104}$$

$$\begin{aligned} S_\theta &= \sigma_\theta - \frac{1}{3} (\sigma_\theta + \sigma_z) \\ S_z &= \sigma_z - \frac{1}{3} (\sigma_\theta + \sigma_z) \\ S_r &= -\frac{1}{3} (\sigma_\theta + \sigma_z). \end{aligned} \tag{105}$$

The solution in CLADF proceeds as follows. At the end of the last load increment the plastic strain components ε_r^P, ε_θ^P, and ε_z^P, are known, and also the total effective plastic strain, ε^P, is known.

The loading is now incremented with new values of P_i, P_o, and T prescribed. The new stresses can be determined immediately from Equations (96) and (97), and a new value of effective stress is obtained from Equation (103).

The increment of effective plastic strain, $d\varepsilon^P$, which results from the current increment of loading can now be determined from the uniaxial stress-strain curve at the new value of σ_e, as shown in Figure 11. (The new elastic loading curve depends on the value of ε^P.) This computation is performed by subroutine STRAIN.

Once $d\varepsilon^P$ is determined, the individual plastic strain components are found from Equations (104), and the total strain components are obtained from Equations (100) through (102).

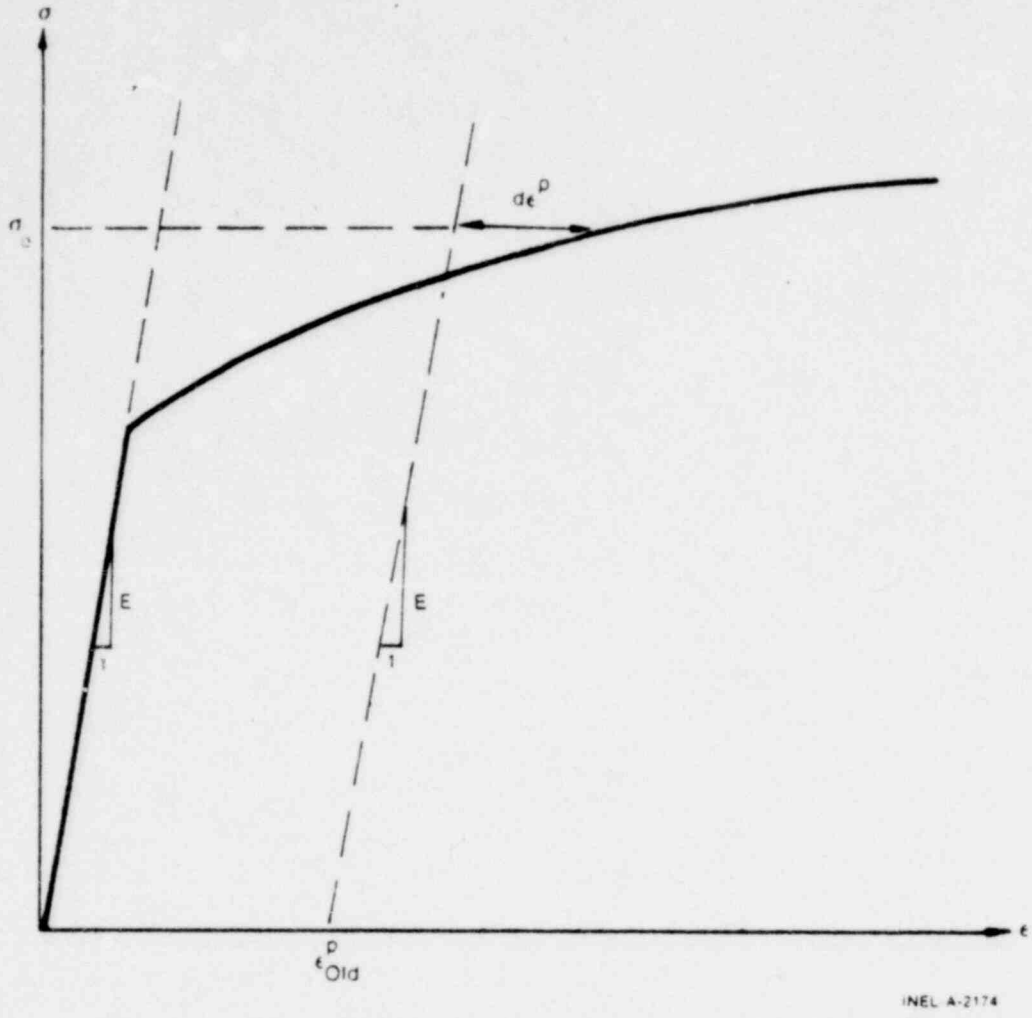

Fig. 11 Calculation of effective stress σ_e from $d\varepsilon^p$.

The displacement of the inside surface of the shell must be determined so that a new gap width can be computed. The radial displacement of the inside surface is given by

$$u(r_i) = \bar{r}\,\varepsilon_\theta - \frac{t}{2}\,\varepsilon_r \qquad (106)$$

where the first term is the radial displacement of midplane [from Equation (99)] and ε_r is the uniform strain across the thickness, t.

The final step performed by CLADF prior to returning control to FCMI is to add the plastic strain increments to the previous plastic strain values as in

Thus, prescribing the displacement of the inside surface of the shell is equivalent to a constraining relation between ε_θ and ε_r. As before, Hooke's law is taken in the form

$$\varepsilon_\theta = \frac{1}{E}\left(\sigma_\theta - \nu\,\sigma_z\right) + \varepsilon_\theta^P + d\varepsilon_\theta^P + \int_{T_o}^{T} \alpha_\theta dT \qquad (108)$$

$$\varepsilon_z = \frac{1}{E}\left(\sigma_z - \nu\,\alpha_\theta\right) + \varepsilon_z^P + d\varepsilon_z^P + \int_{T_o}^{T} \alpha_z dT \qquad (109)$$

$$\varepsilon_r = -\frac{\nu}{E}\left(\sigma_\theta + \sigma_z\right) + \varepsilon_r^P + d\varepsilon_r^P + \int_{T_o}^{T} \alpha_r dT. \qquad (110)$$

Using Equations (107) and (110) in Equation (108) yields a relation between the stresses σ_θ, σ_z, and the prescribed displacement $u(r_i)$:

$$\frac{u(r_i)}{\bar{r}} + \frac{1}{2}\frac{t}{\bar{r}}\left(\varepsilon_r^P + d\varepsilon_r^P + \int_{T_o}^{T} \alpha_r dT\right) - \left(\varepsilon_\theta^P + d\varepsilon_\theta^P + \int_{T_o}^{T} \alpha_\theta dT\right) = \frac{1}{E}\left[\left(1 + \frac{\nu}{2}\frac{t}{\bar{r}}\right)\sigma_\theta + \nu\left(\frac{1}{2}\frac{t}{\bar{r}} - 1\right)\sigma_z\right]. \qquad (111)$$

Equations (109) and (111) are now a pair of simultaneous algebraic equations for the stresses σ_θ and σ_z, which may be written as

$$\begin{bmatrix} A_{11} & A_{12} \\ A_{21} & A_{22} \end{bmatrix} \begin{bmatrix} \sigma_\theta \\ \sigma_z \end{bmatrix} = \begin{bmatrix} B_1 \\ B_2 \end{bmatrix}$$

$$(\varepsilon_\theta^P)_{new} = (\varepsilon_\theta^P)_{old} + d\varepsilon_\theta^P$$

$$(\varepsilon_z^P)_{new} = (\varepsilon_z^P)_{old} + d\varepsilon_z^P$$

$$(\varepsilon_r^P)_{new} = (\varepsilon_r^P)_{old} + d\varepsilon_r^P$$

$$(\varepsilon^P)_{new} = (\varepsilon^P)_{old} + d\varepsilon^P$$

and these values are returned to FCMI for use at the next load increment.

Thus, all the stresses and strains can be computed directly since, in this case, the stresses are determinate. In the case of the driven cladding displacement, the stresses depend on the displacement, and such a straightforward solution is not possible.

3.4.3 Subroutine COUPLE. This subroutine considers the problem of a cylindrical shell for which the radial displacement of the inside surface and axial strain are prescribed. Here the stresses cannot be computed directly since the pressure at the inside surface (the interface pressure) must be determined as part of the solution.

As in CLADF, the displacement at the inside surface is given by

$$u(r_i) = u - \frac{t}{2}\varepsilon_r$$

where u is the radial displacement of the midplane. From Equation (73), $u = \bar{r}\,\varepsilon_\theta$ and hence:

$$u(r_i) = \bar{r}\,\varepsilon_\theta - \frac{t}{2}\varepsilon_r. \qquad (107)$$

where

$$A_{11} = 1 + \frac{\nu}{2}\frac{t}{\bar{r}}$$

$$A_{12} = \nu\left(\frac{1}{2}\frac{t}{\bar{r}} - 1\right)$$

$$A_{21} = -\nu$$

$$A_{22} = 1$$

$$B_1 = E\,\frac{u(r_i)}{i\cdot} + \frac{E}{2}\frac{t}{\bar{r}}\left[\varepsilon_r^P + d\varepsilon_r^P + \int_{T_0}^{T} \alpha_r dT\right]$$

$$- E\left[\varepsilon_\theta^P + d\varepsilon_\theta^P + \int_{T_0}^{T} \alpha_\theta dT\right]$$

$$B_2 = E\,\varepsilon_z - E\left[\varepsilon_z^P + d\varepsilon_z^P + \int_{T_0}^{T} \alpha_z dT\right].$$

Then the stresses can be written explicitly as

$$\sigma_\theta = \frac{B_1 A_{22} - B_2 A_{12}}{A_{11} A_{22} - A_{12} A_{21}} \qquad (112)$$

$$\sigma_z = \frac{B_2 A_{11} - B_1 A_{21}}{A_{11} A_{22} - A_{12} A_{21}}. \qquad (113)$$

These equations relate the stresses to $u(r_i)$ and ε_z which are prescribed and to $d\varepsilon_\theta^P$, $d\varepsilon_z^P$, and $d\varepsilon_r^P$, which are to be determined. The remaining equations which must be satisfied are

$$\varepsilon_{et} = \sqrt{\frac{2}{3}}\left[(\varepsilon_\theta' - \varepsilon_z')^2 + (\varepsilon_z' - \varepsilon_r')^2 + (\varepsilon_r' - \varepsilon_\theta')^2\right]^{1/2}. \qquad (114)$$

The modified Prandtl-Reuss flow equations are

$$d\varepsilon_\theta^p = \frac{d\varepsilon^p}{\varepsilon_{et}} e'_\theta$$

$$d\varepsilon_z^p = \frac{d\varepsilon^p}{\varepsilon_{et}} e'_z \qquad (115)$$

$$d\varepsilon_r^p = -d\varepsilon_\theta^p - d\varepsilon_z^p$$

in which e'_θ and e'_z are the modified deviator strains defined by Equation (78). The equivalent modified total strain ε_{et} is related to the plastic strain increment $d\varepsilon^p$ using Equation (79) and the uniaxial stress-strain law. Equations (112) through (115) must be simultaneously satisfied for each loading increment.

As discussed in Section 3.1, a straightforward numerical solution to these equations can be obtained via the Method of Successive Substitutions. Here, one initially assumes arbitrary values for the increments of plastic strain, and uses Equations (111) through (115) to obtain improved estimates of the plastic strain components. The steps performed by COUPLE for each increment of load are as follows:

(1) Values of $d\varepsilon_\theta^p$, $d\varepsilon_z^p$, and $d\varepsilon_r^p$ are assumed

(2) From Hooke's law, using the assumed plastic strain increments and the prescribed values of $u(r_i)$ and ε_z, values for the stresses can be obtained from Equations (111) and (112)

(3) From the pseudoelastic solution in Step 2, compute the modified strains and modified deviator strains, and hence obtain ε_{et} from Equation (114)

(4) Obtain $d\varepsilon^p$ from ε_{et} and the uniaxial stress-strain curve

(5) Compute new values of the plastic strain increments using the modified Prandtl-Reuss equations

(6) The old and new values of $d\varepsilon_\theta^P$, $d\varepsilon_z^P$, and $d\varepsilon_r^P$ are compared and the process continued until convergence is obtained

(7) Once convergence has been obtained, the interface pressure is computed from Equation (96):

$$P_{int} = \frac{t\,\sigma_\theta + r_o\,P_o}{r_i} . \tag{116}$$

When steps 1 through 7 have been accomplished, the solution is complete, provided that the interface pressure is not less than the local gas pressure.

Due to unequal amounts of plastic straining in the hoop and axial direction, however, it often happens on unloading that the interface pressure as obtained in Step 7 is less than the gas pressure even though the gap has not opened. When this situation occurs, the frictional locking mechanism which is assumed to constrain the cladding axial deformation to equal the fuel axial deformation can no longer act. The axial strain and stress adjust themselves so that the interface pressure just equals the gas pressure, at which point the axial strain is again locked. Thus, on further unloading, the axial strain and the hoop and axial stresses continually readjust themselves so as to maintain the interface pressure equal to the gas pressure until the gap opens. Because the unloading occurs elastically, a solution for this portion of the fuel-cladding interaction problem can be obtained directly as follows.

Since the external pressure and the interface pressure are known, the hoop stress is obtained from Equation (96) as:

$$\sigma_\theta = \frac{r_i\,P_{int} - r_o\,P_o}{t} . \tag{117}$$

From Equation (106) we can write:

$$\varepsilon_\theta = \frac{u_r^{fuel} - \delta + t/2\ \varepsilon_r}{\bar{r}}. \tag{118}$$

Substituting ε_θ and ε_r as given by Equations (108) and (110) into Equation (118) gives an explicit equation for σ_z as:

$$\nu\, r_i\, \sigma_z = (\bar{r} + \nu\, t/2)\, \sigma_\theta + \bar{r}\, E \left[\int \alpha_\theta dT + \varepsilon_\theta^P\right] - \frac{t}{2} E \left[\int \alpha_r dT + \varepsilon_r^P\right] - E\, u(r_i) \tag{119}$$

in which σ_θ is known from Equation (117). With σ_z and σ_θ known, the strains may be computed from Hooke's law, Equations (108) through (110). This set of equations is included in subroutine COUPLE and is automatically invoked when a value of P_{int} less than the local gas pressure is computed.

As in CLADF, the last step performed by COUPLE before returning control to FCMI is to set the plastic strain components and total effective strain ε^P equal to their new values by adding in the computed increments $d\varepsilon_i^P$ and $d\varepsilon^P$.

3.4.4 Subroutine STACK. Subroutine STACK is called when one or more fuel pellet nodes are trapped between the lower end of the cladding and a pellet in firm contact with the cladding, as shown in Figure 12. In this case the axial expansion of the fuel will be imparted to the cladding even though the cladding and fuel are not in radial contact.

The total change in length of the trapped cladding is computed in FCMI, and passed to STACK in the calling sequence. For each axial node in the trapped cladding, the axial strain is given by

$$\varepsilon_z(i) = \frac{1}{E(i)}\left[\sigma_z - \nu(i)\, \sigma_\theta(i)\right] + \varepsilon_z^P(i) + d\varepsilon_z^P(i) + \int_{T_o}^{T(i)} \alpha_z dT \tag{120}$$

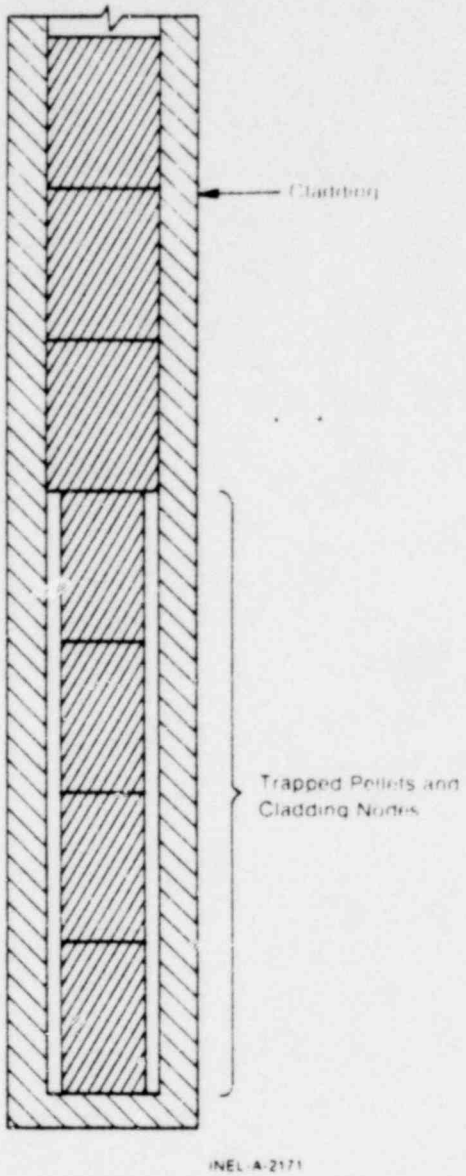

Fig. 12 Schematic of trapped stack.

in which i denotes the axial node number. Axial force equilibrium requires that σ_z be the same in each node. Since the total length change is prescribed, one can write

$$\Delta\ell = \sum_{i=1}^{n} \left[\varepsilon_z(i) - \varepsilon_z^o(i) \right] dz(i)$$

in which dz(i) are the axial cladding node lengths, and $\varepsilon_z^o(i)$ are the axial strains in the cladding at the end of the last loadstep. Inserting Equation (120) in the above equation yields

1569 033

$$\sigma_z = \left[\sum_{i=1}^{N} \frac{E(i)}{dz(i)}\right] \left\{ \Delta\ell + \sum_{i=1}^{N} dz(i) \left[\frac{\nu(i)\,\sigma_\theta(i)}{E(i)} \right.\right.$$

$$\left.\left. + \varepsilon_z^o(i) - \varepsilon_z^p(i) - d\varepsilon_z^p(i) - \int_{T_o}^{T(i)} \alpha_z dT \right]\right\} . \qquad (121)$$

For each node, the plasticity equations are

$$\varepsilon_{et}(i) = \sqrt{\frac{2}{3}} \left\{ \left[\varepsilon_z'(i) - \varepsilon_r'(i)\right]^2 + \left[\varepsilon'_r(i) - \varepsilon_\theta'(i)\right]^2 \right.$$

$$\left. + \left[\varepsilon_\theta'(i) - \varepsilon_z'(i)\right]^2 \right\}^{1/2} \qquad (122)$$

$$e_j'(i) = e_j^e(i) + d\varepsilon_j^p(i) \qquad j = r, \theta, z \qquad (123)$$

and the modified Prandtl-Reuss equations:

$$\begin{cases} d\varepsilon_z^p(i) = \dfrac{d\varepsilon^p(i)}{\varepsilon_{et}(i)}\, e_z'(i) \\ d\varepsilon_\theta^p(i) = \dfrac{d\varepsilon^p(i)}{\varepsilon_{et}(i)}\, e_\theta'(i) \\ d\varepsilon_r^p(i) = -d\varepsilon_\theta^p(i) - d\varepsilon_z^p(i). \end{cases} \qquad (124)$$

Equations (121) through (124) must be simultaneously satisfied for all the trapped axial cladding nodes. And since the nodes may have different temperatures, different stress-strain curves are used at different nodes.

As before, the Method of Successive Elastic Solutions is used. In contrast to subroutine COUPLE, however, the method is applied simultaneously to several axial nodes. Because more than one node is being considered, an additional possibility arises.

This is the possibility that, due to the axial stretching and Poisson's effect, some (or all) of the cladding nodes may come into contact with the fuel pellets, although contact would not occur due to internal and external pressures alone. In this case, the hoop stress in Equation (121) is no longer given by Equation (96), but now depends on σ_z and the radial displacement of the fuel. While contact occurs, however, radial compatibility as expressed in Equation (106) requires that

$$\bar{r}\varepsilon_\theta(i) - 0.5\ t\ \varepsilon_r(i) = u_r^{fuel}(i) - \delta.$$

Substituting for $\varepsilon_\theta(i)$ and $\varepsilon_r(i)$ from Hooke's law, Equations (100) and (102) there results a single equation relating $\sigma_\theta(i)$ at each node to the axial stress σ_z, which can be solved for $\sigma_\theta(i)$ explicitly to obtain

$$\left[\frac{\bar{r}}{E(i)} + \frac{0.5\nu(i)\ t}{E(i)}\right]\ \sigma_\theta(i) = u_r^{fuel}(i) - \delta$$

$$- \bar{r}\left[\frac{-\nu(i)}{E(i)}\ \sigma_z + \varepsilon_\theta^p(i) + d\varepsilon_\theta^p(i) + \int_{T_o}^{T(i)} \alpha_\theta dT\right] \qquad (125)$$

$$+ \frac{t}{2}\left[\frac{-\nu(i)}{E(i)}\ \sigma_z + \varepsilon_r^p(i) + d\varepsilon_r^p(i) + \int_{T_o}^{T(i)} \alpha_r dT\right]$$

which applies at each node where contact has occurred. Finally, Equation (125) is used to eliminate $\sigma_\theta(i)$ from Equation (121) for those nodes at which contact has occurred. Thus, we obtain an equation for σ_z involving summations over all nodes not in contact plus summations over all nodes,

denoted j*, where contact has occurred. This equation, solved explicitly for σ_z, is shown below:

$$\left\{ \sum_i \frac{dz(i)}{E(i)} - \sum_{i-j^*} \frac{dz(i)\,\nu(i)}{E(i)} \left[\frac{(\bar{r}-0.5t)\,\nu(i)}{\bar{r}+0.5t\,\nu(i)} \right] \right\} \sigma_z$$

$$= \delta\ell + \sum_i \varepsilon_z^o(i)\, dz(i)$$

$$- \sum_i \left[\varepsilon_z^p(i) + d\varepsilon_z^p(i) + \int_{T_o}^{T(i)} \alpha_z dT \right] dz(i)$$

$$+ \sum_{i \neq j^*} \frac{\nu(i)}{E(i)} \left[\frac{P_i(i) r_i - P_o(i) r_o}{r_o - r_i} \right] dz(i) \qquad (126)$$

$$+ \sum_{i=j^*} \frac{\nu(i)\,dz(i)}{\bar{r}+0.5t\,\nu(i)} \left\{ \upsilon_r^{fuel}(i) - \delta \cdot \bar{r} \left[\varepsilon_\theta^p(i) + d\varepsilon_\theta^p(i) + \int_{T_o}^{T(i)} \alpha_\theta dT \right] + 0.5t \left[\varepsilon_r^p(i) + d\varepsilon_r^p(i) + \int_{T_o}^{T(i)} \alpha_r dT \right] \right\}.$$

This modified equation for σ_z allows for an arbitrary number of contacting nodes, and is solved for σ_z at each step in the iteration for the plastic strain increments. Of course, it is not known a priori which nodes may be in contact.

However, for given values of the plastic strain increments (the iterates in the Method of Successive Elastic Solutions) the governing

equations are all linear. Thus, one can solve for σ_z assuming no pellets are in contact, then compute the gaps, and if any negative gaps are found, recompute σ_z with those nodes now assumed to be in contact. This process is repeated until all calculated gaps are either positive or zero. At most, N steps are required since the equations are linear, where N is the number of nodes in the stack.

Thus, in this application, the Method of Successive Elastic Solutions becomes an iteration within an iteration, and one in which the set of variables iterated upon is determined as the solution progresses.

3.4.5 Subroutines STRAIN and STRESS. These two subroutines are called by COUPLE and CLADF to relate stress and plastic strain, taking into consideration the direction of loading and the previous plastic deformation. A typical stress-strain curve is shown in Figure 13. This curve represents the results of a uniaxial stress-strain experiment, and may be interpreted (beyond initial yield) as the locus of work-hardened yield stresses. The equation of the curve is provided by MATPRO[4] at each temperature.

To utilize this information, the usual idealizations of the mechanical behavior of metals are made. Thus, we assume linear elastic behavior until a sharply defined yield stress is reached, after which plastic (irrecoverable) deformation occurs. Unloading from a state of stress beyond the initial yield stress, σ_y^o, is assumed to occur along a straight line having the elastic modulus for its slope. When the (uniaxial) stress is removed completely, a residual plastic strain remains, and this plastic strain completely determines the subsequent yield stress. That is, it is assumed that when the specimen is loaded again, loading will occur along line BA, and no additional plastic deformation will occur until Point A is again reached. Point A is the subsequent yield stress. If $\sigma = f(\varepsilon)$ is the equation of the plastic portion of the stress-strain curve (YAC), then for a given value of plastic strain, the subsequent yield stress is found by solving simultaneously the pair of equations:

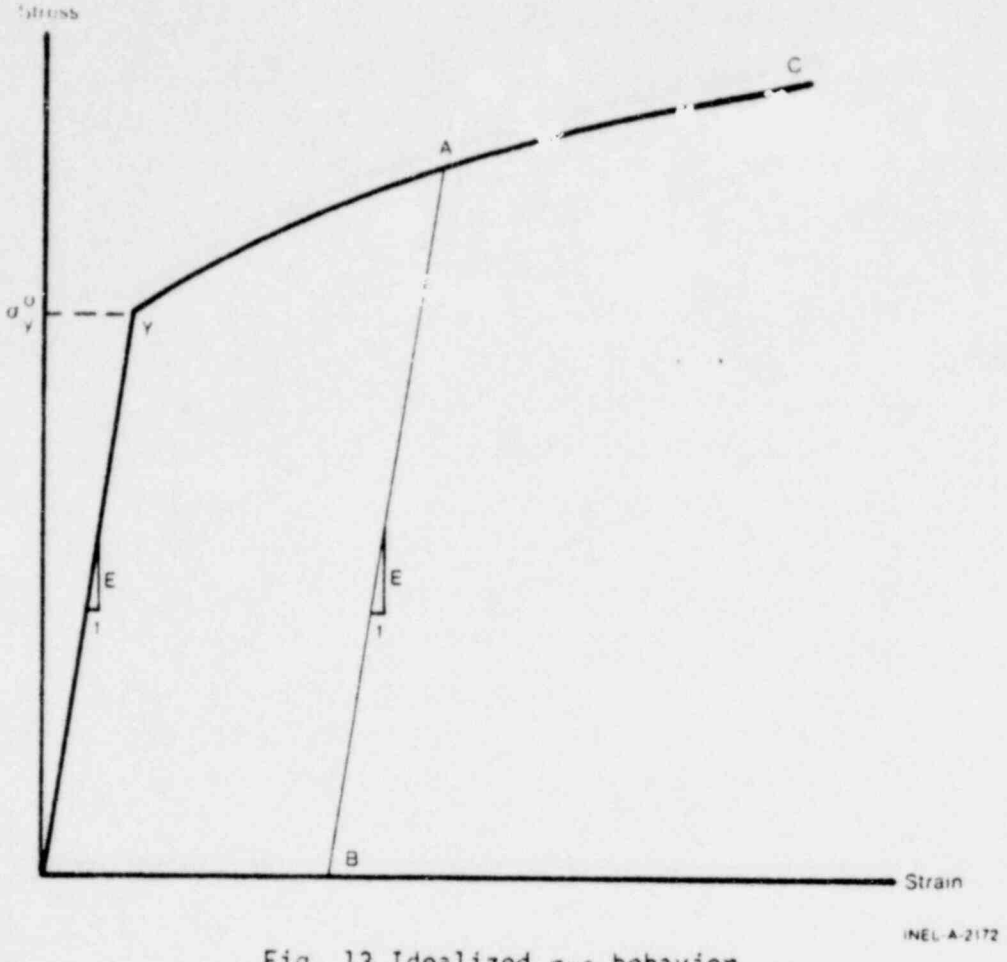

Fig. 13 Idealized σ-ϵ behavior.

$$\begin{cases} \sigma = f(\epsilon) \\ \\ \sigma = E(\epsilon - \epsilon^P) \end{cases}$$

which may be written as

$$\sigma = f(\frac{\sigma}{E} + \epsilon^P).$$

The solution to this nonlinear equation may be computed very efficiently by Newton's Iteration Scheme:

$$\sigma^{(m+1)} = f(\frac{\sigma^{(m)}}{E} + \epsilon^P) \qquad m = 0, 1, 2, \ldots \qquad (127)$$

The initial iterate $\sigma^{(o)}$ is arbitrary, and without loss of generality, is taken as 5000 psi. It can be proven that, for any monotonically increasing stress-plastic strain relation, the iteration scheme in Equation (127) converges uniformly and absolutely. Furthermore, it converges so rapidly that it is sufficient to perform the iteration no more than 30 times to obtain 8 decimal accuracy. Thus, no convergence or error criteria are necessary in utilizing this scheme.

The computations in STRAIN and STRESS are described below. It is to be noted that STRESS is only called when additional plastic deformation has occurred.

(1) Subroutine STRAIN. Values of plastic strain, ε^P, temperature and stress are passed to STRAIN through the calling sequence.

(a) For given temperature, obtain $\sigma = f(\varepsilon)$ from MATPRO

(b) Obtain yield stress σ_y for given ε^P from Equation (127)

(c) For given value of stress, σ,

(i) if $\sigma \leq \sigma_y$, $\quad \varepsilon = \frac{\sigma}{E} + \varepsilon^P$

$$\varepsilon^P_{new} = \varepsilon^P_{old}$$

$$d\varepsilon^P = 0$$

(ii) if $\sigma > \sigma_y$, $\quad \varepsilon = f(\sigma)$

$$\varepsilon^P_{new} = \varepsilon - \sigma/E$$

$$d\varepsilon^P = \varepsilon^P_{new} - \varepsilon^P_{old}$$

(d) Return.

(2) Subroutine STRESS. Values of plastic strain, ε^P, temperature and plastic strain increment $d\varepsilon^P$ are passed to STRESS through the calling sequence.

(a) For given temperature, obtain $\sigma = f(\varepsilon)$ from MATPRO

(b) Obtain yield stress σ_y for given ε^P from Equation (127)

(c) Given $d\varepsilon^P$ (see Figure 14)

$$\varepsilon^P_{new} = \varepsilon^P_{old} + d\varepsilon^P$$

Since $d\varepsilon^P > 0$, the new value of stress and strain must lie on the plastic portion of the stress-strain curve $\sigma = f(\varepsilon)$. So σ, ε are obtained by simultaneously solving, as before,

$$\begin{cases} \sigma = f(\varepsilon) \\ \sigma = E(\varepsilon - \varepsilon^P_{new}) \end{cases}$$

(d) Return.

3.4.6 Subroutines CLOSE and GAPT. These two subroutines are called by FCMI when one of the node gaps has been found to be closed between two successive power changes. It is assumed that all the applied loads vary linearly between the two loadsteps, so that

$$\begin{aligned} P_c(\lambda) &= P_c(i-1) + \lambda \left[P_c(i) - P_c(i-1)\right] \\ P_g(\lambda) &= P_g(i-1) + \lambda \left[P_g(i) - P_g(i-1)\right] \\ T(\lambda) &= T(i-1) + \lambda \left[T(i) - T(i-1)\right] \\ u_r^{fuel}(\lambda) &= u_r^{fuel}(i-1) + \lambda \left[u_r^{fuel}(i) - u_r^{fuel}(i-1)\right] \end{aligned} \tag{128}$$

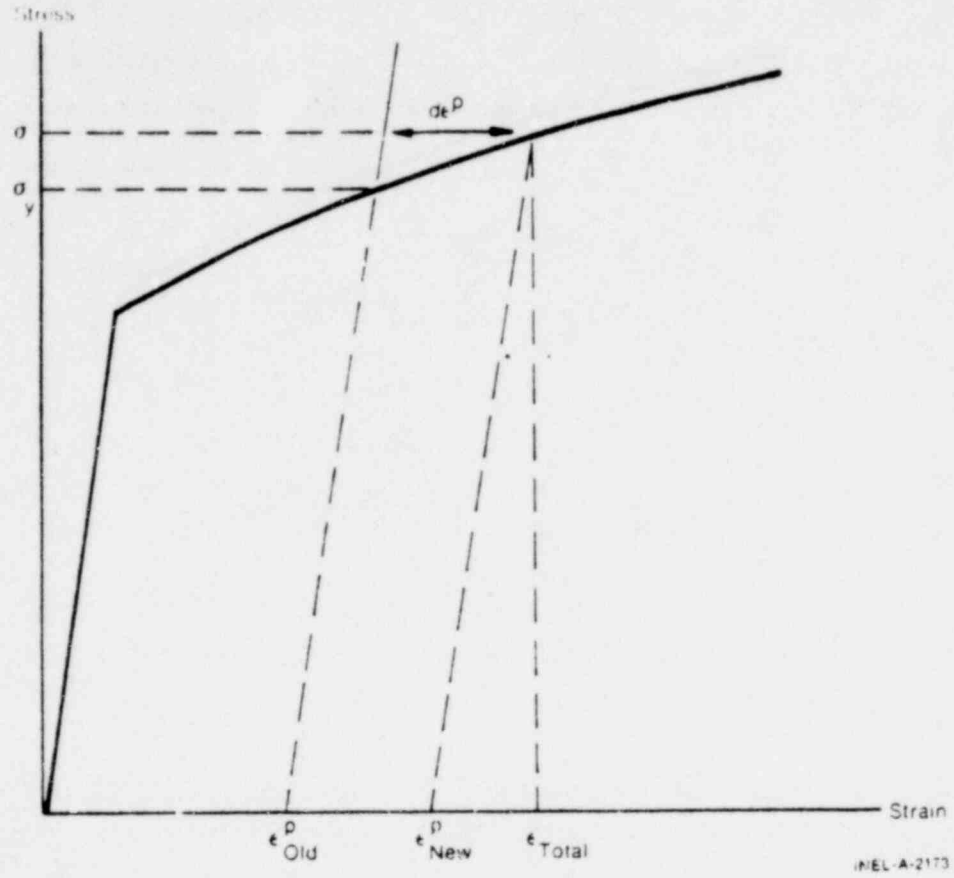

Fig. 14 Computations in subroutine STRESS.

---

where the index i-1 denotes the loads as the last power step, i denotes the current load values and λ varies between zero and unity. Subroutine CLOSE iterates on λ to find the exact value of λ at which the radial gap closes. Given the old and new load values for any given value of λ, subroutine GAPT computes the size of the radial gap by calling subroutine CLADF, and passing to it the linearly interpolated values computed from Equation (128). The method used is the Modified Newton-Raphson iteration scheme which solves for the roots of the equation:

$$\text{Radial gap} = f(\lambda) = 0$$

by use of the recurrence relation:

$$\lambda^{(m+1)} = \lambda^{(m)} - \frac{f[\lambda^{(m)}]}{g[\lambda^{(m)}, \lambda^{(m-1)}]} \tag{129}$$

$$g\left[\lambda^{(m)}, \lambda^{(m-1)}\right] = \frac{f[\lambda^{(m)}] - f[\lambda^{(m-1)}]}{\lambda^{(m)} - \lambda^{(m-1)}} \tag{130}$$

in which $f(\lambda)$ is the gap thickness as a function of the interpolating parameter λ as given by subroutine GAPT. The iteration procedure is performed until

$$|f(\lambda)| < \text{CUT} \tag{131}$$

where CUT is the tolerance value which is currently set (internally) to the value 1.0×10^{-8} inches. If, for any reason, the iteration scheme cannot converge to a gap value less than CUT, an error message is printed out, and the last computed value of λ is returned. However, experience has shown that convergence has always occurred for values of CUT greater than 10^{-10}.

4. FUEL MECHANICAL RESPONSE

Deformation of the fuel is calculated as a function of thermal expansion, irradiation swelling, and densification. The deformation model is described here with irradiation swelling calculations described in Section IV.

4.1 Assumptions

(1) No pellet deformation from stresses induced by fuel-cladding contact or thermal stresses*

*Note again. Asterisks (*) mark those assumptions for which tasks are presently under way to develop more advanced models.

(2) No pellet creep under induced stresses*

(3) Free ring thermal expansion.

4.2 Radial Expansion

Radial expansion of the pellet due to temperature, irradiation swelling, and densification is calculated by a free ring expansion model. The governing equation for this model is

$$R_H = \sum_{i-1}^{N} \Delta r_i \left(1+\alpha_{T_i} T_i + \frac{\Delta L}{L} s_i + \frac{\Delta L}{L} d_i\right) \qquad (132)$$

where

R_H = hot pellet radius

α_{T_i} = coefficient of thermal expansion of i^{th} radial ring for temperature T_i

T_i = average temperature of i^{th} radial ring

Δr_i = width of i^{th} radial ring

N = number of radial rings

$\frac{\Delta L}{L} s_i$ = swelling strain

$\frac{\Delta L}{L} d_i$ = densification strain.

4.3 Axial Expansion

Axial expansion of the fuel stack is calculated by summing the maximum ring axial expansions of each pellet. Maximum ring axial expansion of each pellet is calculated as the difference between the length

of the ring with the maximum overall hot length and the cold length of the pellet.

The calculation of overall ring height includes consideration of the depression of a central dish. The fuel stack length is thus calculated by

$$L_f = \sum_{j=1}^{M} (1 + \alpha_{T_i} T_i + \frac{\Delta L}{L} s_i + \frac{\Delta L}{L} d_i) \ell_i \qquad (133)$$

where

i is the ring with the maximum axial length of the j^{th} node

and

L_f = hot length of fuel stack

M = number of axial nodes

ℓ_i = length of i^{th} radial ring

T_i, α_{T_i}, N, $\frac{\Delta L}{L} s_i$, and $\frac{\Delta L}{L} d_i$ are defined as above.

4.4 Fuel Crack Volume

As the fuel expands, extensive cracking occurs due to the high thermally-induced stresses. This crack volume is computed as

$$V_c = V_{eg} - V_{TX}$$

where

V_c = crack volume

V_{eg} = volume defined by expanded radial nodes

V_{TX} = volume of thermally expanded fuel

with

$$V_{eg} = \sum_{i=1}^{N} \pi (r_i^2 - r_{i-1}^2) \ell_i \qquad (134)$$

and

$$V_{TX} = \sum_{i=1}^{N} \pi (r_{ic}^2 - r_{ic-1}^2) \ell_{ic} (1 + 3\alpha_i T_i) \qquad (135)$$

where

ℓ_{ic} = cold length of i^{th} radial ring

r_{ic} = cold radius of i^{th} node.

5. FUEL ROD FAILURE MODELS

A subcode has been developed for the FRAP codes to predict failure of the zircaloy cladding of light water reactor fuels. This subcode, FRAIL (FRAP Integrity Limits), is a modular routine that predicts the probability of failure of fuel cladding under a variety of steady state and transient conditions.

The FRAIL subcode is composed of several subroutines, each of which has the capability of predicting zircaloy fuel rod cladding failure. The subroutines are distinguished from one another by mode of failure. A probability of failure is calculated for each mode, and these probabilities are then appropriately combined to yield a general probability of failure of the fuel rod cladding. The cladding failure models that are currently operable in FRAIL include:

(1) cladding melt
(2) oxide layer wall thinning
(3) ballooning (without rupture)
(4) eutectic melt
(5) collapse
(6) overstress failure
(7) cumulative stress damage
(8) overstrain failure

IV. CORRELATION MODELS

This section on correlation models deals with those fuel rod models which fall somewhere between an analytical model such as cladding deformation and a material property such as thermal conductivity.

These models are usually defined by a mathematical model which reflects a theory of behavior but are quite heavily weighted by experimental data.

Models which require substantial material property data such as cladding creep are covered in greater detail in the material property documentation of MATPRO[4].

1. FISSION GAS PRODUCTION

Given production rates for the major diffusing gases, the burnup dependent total fission gas generated at axial station z is calculated as follows:

$$GPT(z) = \frac{BU(z)\,VF(z)}{100\,A_v}\left(PR_{krypton} + PR_{helium} + PR_{xenon}\right) \quad (136)$$

where

GPT(z) = total fission gas produced at z (gm-moles)

BU(z) = burnup at z (fiss/cc)

VF(z) = fuel volume (cc)

A_v = Avogadro's Number

PR_e = Fission gas production rate (atoms/100 fissions) for krypton, xenon, and helium, respectively, 30, 30, and 0.3.

2. FISSION GAS RELEASE

The fission gas release model used in FRAP-S3 considers the release to be determined by escape of gas from the fuel matrix and release of trapped gas from grain boundaries or dislocations. If k^1 represents the portion of fission gas that escapes without being trapped, then

$$dn_1 = k^1 p dt$$

where

dn_i = the moles of gas released directly in time dt

dt = the time increment

and

p = the gas production rate.

If the probability of trapped particle release per unit time is k and the number of moles trapped is C, then the trapped moles released in dt is $dn_2 = k\ C\ dt$. Only a fraction, k, of the gas released from traps reaches the surface, thus the total gas released is $dn = k^1\ k\ c\ dt + k^1\ p\ dt$.

If C is replaced by $(p\ t - n)$ and integration is performed:

$$n = p \left\{ t - \frac{1 - k^1}{k^1 k} \left[1 - \exp-(k^1 k t) \right] \right\} . \qquad (137)$$

At constant power, the total fractional release is

$$F = n/(pt) = 1 - (1 - k^1) \frac{1 - e^{-Kt}}{Kt} \qquad (138)$$

where $K = k^1 k$. The constants, K and k^1, have been evaluated from the available data as functions of fuel temperature and density only in the form

$$K, k^1 = Ae^{(-B/T - Cd + D)} \qquad (139)$$

where

T = fuel temperature (°R)

d = fuel density

and for K and k^1 respectively:

A = 0.25, 1

B = 21,410, 12,450

C = 0, 0.333

D = 0, 33.95.

The preceding formulation [Equation (137)] is extended to variable power time histories by assuming reactor operation is described by a series of constant power steps. The number of moles released, Δn_i, during the i^{th} interval is then

$$\Delta n_i = n_i - n_{i-1} = P_i \left\{ \Delta t_i - \frac{1 - k_i^1}{K_i} \left[1 - \exp(-K_i \Delta t_i) \right] \right\} + C_{i-1} \left[1 - \exp(-K_i \Delta t_i) \right] . \qquad (140)$$

The first two terms, identical with Equation (137) represent the release during Δt_i, had the initial concentration been zero. The last term is additional release due to previously produced gas. Since the total release from time zero is $\Sigma \Delta n_i$, the fraction of total gas produced which is released is

$$F = \left(\sum_{i-1}^{m} \Delta n_i \right) / \left(\sum_{i-1}^{m} P_i \Delta t_i \right) . \qquad (141)$$

3. NITROGEN RELEASE

The release of nitrogen initially present in fuel material from fabrication occurs as a result of a diffusion transport mechanism. From the model proposed by Booth[18], given the assumptions that

(1) The initial concentration of diffusing substance C_o is assumed to be uniform throughout a sphere of radius a

(2) Transport of material does not occur from the external phase (gaseous nitrogen) back into the initial carrier medium, the following diffusion expression holds:

$$r \frac{\partial C}{\partial t} = D \frac{\partial^2 (Cr)}{\partial r^2} \qquad (142)$$

where

r = radial location

C = concentration of diffusing substance

t = time

D = diffusion coefficient

and

$C = 0$ when $r = a$

$C = C_o$ when $t = 0$.

By applying a series solution method, the fractional release of the diffusing substance (nitrogen) can be approximated by the following, based on the value of B.

If

$$B = \pi^2 D_{N_2}(T)t \tag{143}$$

where

D_{N_2} = temperature dependent diffusion coefficient for nitrogen

t = time (sec) from the start of diffusion

then, when $B > 1$, the fraction of nitrogen released as of time t, equals:

$$F_{N_2} = 1 - 6\, e^{-B/\pi^2} \tag{144}$$

and when $B \leq 1$

$$F_{N_2} = 6 \left[D_{N_2}(T)t/\pi\right]^{0.5} - 3D_{N_2}(T)t. \tag{145}$$

From the experimental data of Ferrari:[19, 20]

$$D_{N_2}(t) = (1 \times 10^{-12})\, e^{G} \tag{146}$$

where

$$G = 20202\ (1/1673 - 1/T) \qquad (147)$$

and

T is in degrees kelvin

4. FUEL RELOCATION

Two closely related models are used to compute the effect of relocation. The fuel surface relocation model results in an effective pellet-cladding gap which is used in computing the gap conductance. The space made available for cracks based on this model is distributed inside the pellet. This leads to the second relocation model which calculates the effective thermal conductivity across the cracked pellet. The effective conductivity model accounts for variable composition of fission gas in the cracks, as well as a simplified treatment of crack width. The model considers that relocation effects are moderated as cracks are calculated to close due to structural gap closure occurring as a result of changes in fuel or cladding deformation conditions. The operative assumption here is that open cracks have less strength than fuel or cladding. Crack healing is used to restrict relocation effects on thermal conductivity to the outer, unrestructured fuel regions. Instantaneous crack healing occurs whenever local pellet temperatures reach or exceed a restructuring threshold temperature. The two models are presented below.

4.1 Fuel Surface Relocation

The amount of fuel surface relocation necessary to result in the proper gap closure versus power was studied by Coleman using FRAP-T3. These results are presented in Reference 35. The model which was developed from these results provides FRAP with an effective fuel strain which is a function of cold state geometry. This strain is treated as any of the other fuel radial strains (thermal expansion, swelling, and densification).

$$\left(\frac{\Delta r}{r}\right)_{rel} = 0.0 \quad \text{when,} \quad \frac{\delta}{r_p} \leq 0.005$$

$$\frac{\delta}{r_p} - 0.005 \quad \text{when,} \quad \frac{\delta}{r_p} > 0.005$$

where, $\left(\frac{\Delta r}{r}\right)_{rel}$ = relocation strain (m/m)

δ = cold state radial gap (m)

r_p = cold state pellet radius (m)

This model is shown graphically in Figure 16.

4.2 Relocated Fuel Thermal Conductivity

The thermal conductivity of cracked fuel cannot be the same as that of uncracked fuel. In order to compute the correct effective thermal conductivity, a relocation factor, R, is used.

$$k_{eff} = R\, k_{lab}$$

where, k_{eff} - effective relocated thermal conductivity $\left(\frac{W}{m - K}\right)$

k_{lab} - lab measured fuel thermal conductivity a function of temperature $\left(\frac{W}{m - K}\right)$

The relocation factor equation contains factors which account for the above mentioned available initial gap space $\left(\frac{\delta}{r_p}\right)$, the gas composition of the cracks $\left(1.0 - \frac{k_g}{k_{lab}}\right)$, and the strain dependent space available for cracks $\left(\frac{\delta_S - \delta_T}{\delta - 0.005\, r_p}\right)$.

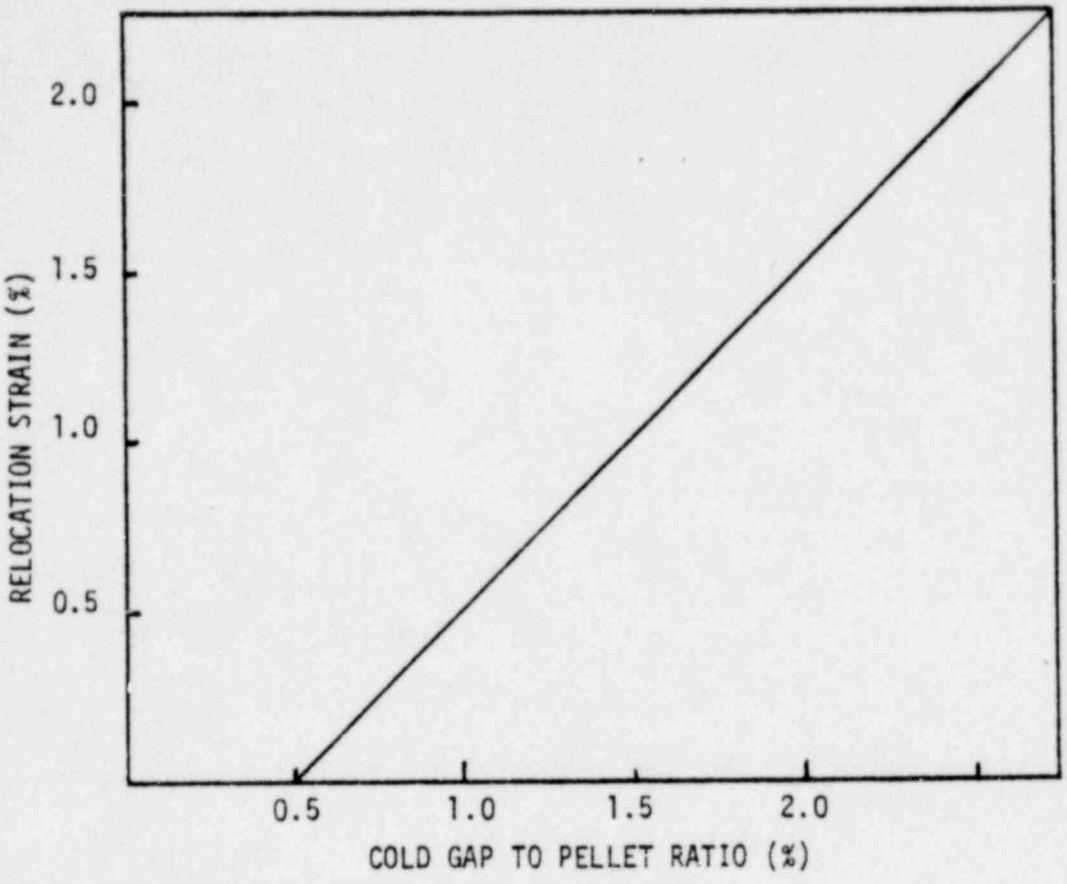

Fig. 16 Fuel surface relocation

$$R = 1.0 - C \left(\frac{\delta_s - \delta_T}{\delta - 0.005\ r_p}\right) \left(\frac{\delta}{r_p}\right) \left(1.0 - \frac{k_g}{k_{lab}}\right) \qquad (148)$$

C = constant (8π)

k_g = gas thermal conductivity ($\frac{w}{m - K}$)

δ_s = gap assuming no fuel surface relocation (m)

δ_T = gap assuming fuel surface relocation (m)

δ, r_p and k_{lab} as defined above.

Crack healing is modeled by enforcing the following:

$$R = 1.0 \text{ when } T_r \geq T_{trans}$$

where T_r = local fuel temperature (K)

T_{trans} = fuel transition temperature (K)

Re-evaluation of the FRAP-T3 verification (Reference 35) results with respect to gap closure indicated that a limit exists on how much gap space can be redistributed. No more than 80% is assumed to redistribute, therefore, the factor R is never less than 0.45.

One assumption made is that cracks instantaneously heal and re-crack when fuel regions are above or below the transition temperature respectively. Another assumption is that the relative gas and fuel conductivities are lab values not relocated values. These assumptions will be assessed by the verification effort.

5. CRUD BUILDUP

Crud thickness is assumed to be one mil unless a value is specified in the input. Flags in the input also determine whether the crud thickness remains constant or varies. If a variable crud thickness is specified, a crud buildup rate of 2.283×10^4 mils/hr is assumed. Crud thermal conductivity of 6000 Btu-mils/hr-ft^2-^{o}F is used. This model was obtained as part of the FUEL[2] code.

V. NUMERICAL SOLUTION PROCEDURE

This section describes the program numerical sequence and the convergence checks made at various points in FRAP-S3. A flow diagram of the code is given in Table II.

Figure 17 presents a summary of the major interactions dealt with by the FRAP-S code (an arrow from A to B means A affects B). Due to the large number of interaction and feedback between the thermal conditions and the physical behavior of a fuel rod, several iterative processes are nested in the core calculations. The major iterative loops are

(1) At each axial increment the gap and fuel temperatures, the fuel thermal expansion, and the cladding strain, are iterated on until convergence is obtained

(2) At each specified time step the entire rod conditions are recalculated with iterations continued until gas release and rod internal pressure are unchanged.

The code calculations begin with bulk coolant temperatures determined by a one-channel enthalpy rise evaluation. Then, for each given axial segment of the rod, the cladding outside surface temperature is calculated by the Dittus-Boelter[5] formula for subcooled heat transfer or the Jens-Lottes[6] correlation if nucleate boiling is present; a crud temperature rise which is a function of the crud density and thickness, (not considered when nucleate boiling occurs); and an oxide temperature rise. The cladding corrosion rate (oxide thickness) is calculated as an exponential function of the cladding-to-oxide interface temperature, proportional to time at temperature and dependent on material and system conditions (BWR or PWR). The temperature rise across the cladding is calculated as a function of power level and cladding dimensions. The gap conductivity between the pellet surface and the cladding inside diameter is calculated as a function of the composition and pressure of the internal gas mixture and the contact pressure between the fuel and

TABLE II

FRAP-S FLOW DIAGRAM

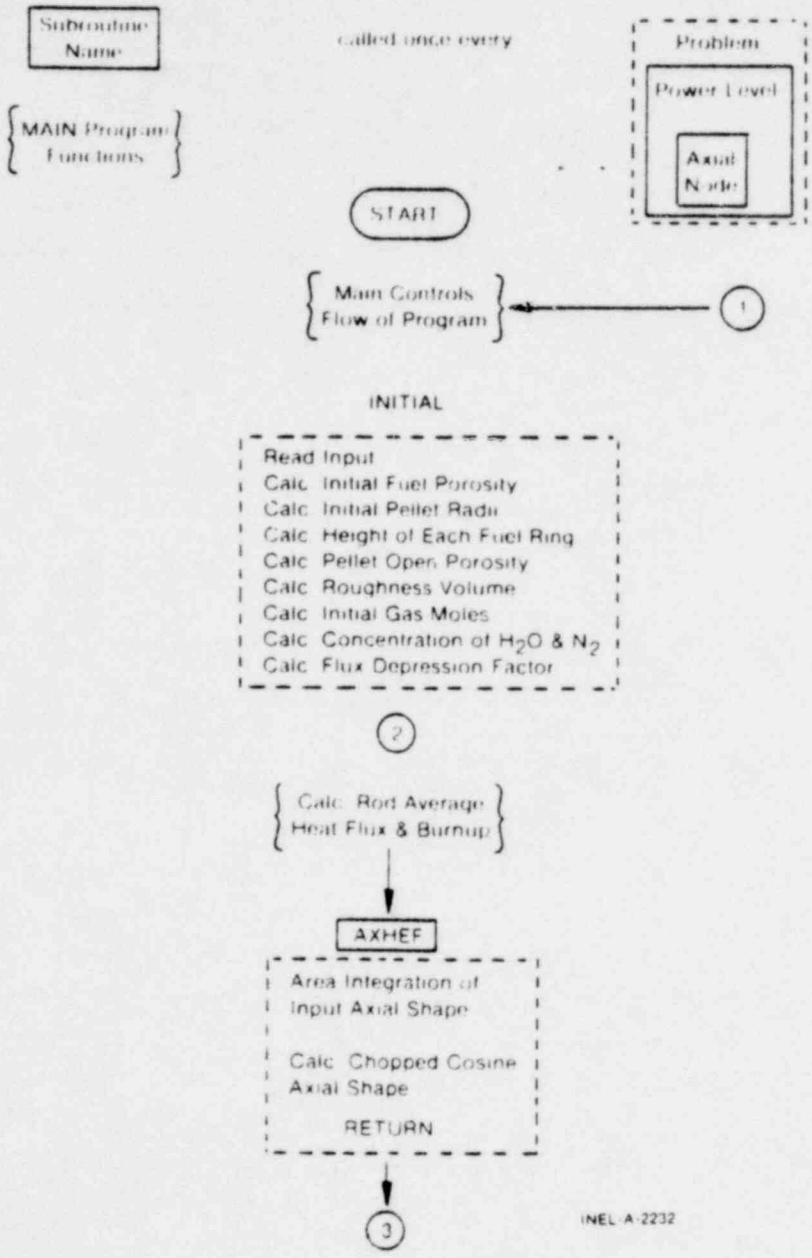

TABLE II (continued)

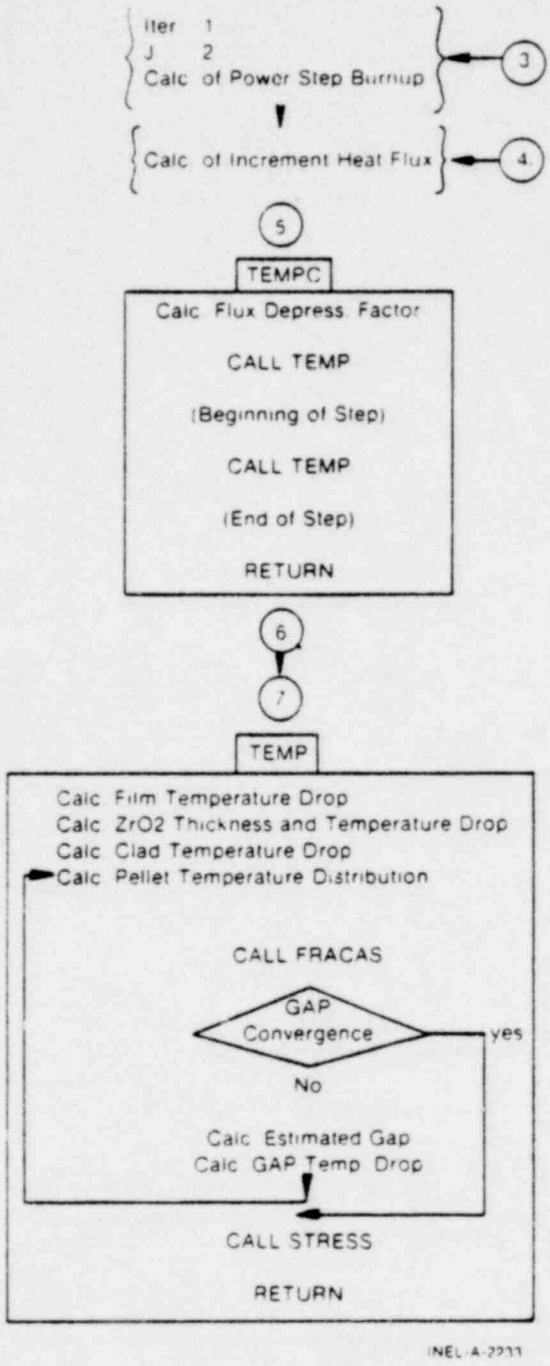

INEL-A-2211

TABLE II (continued)

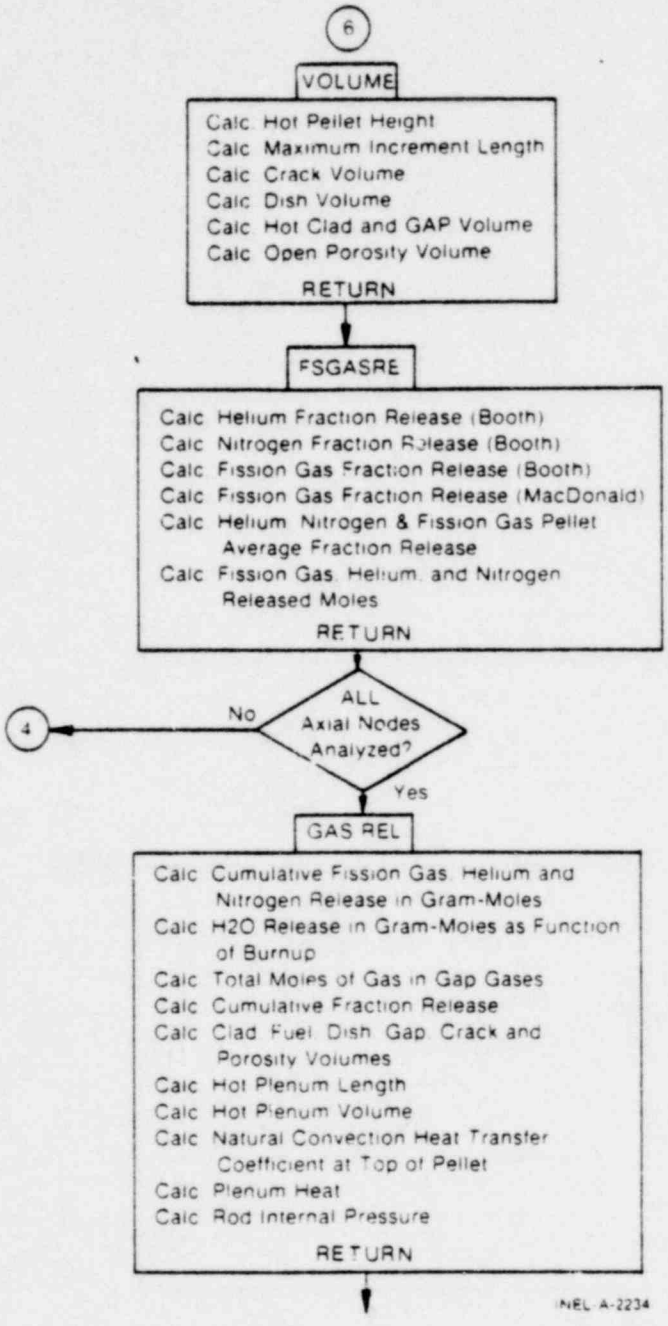

TABLE II (continued)

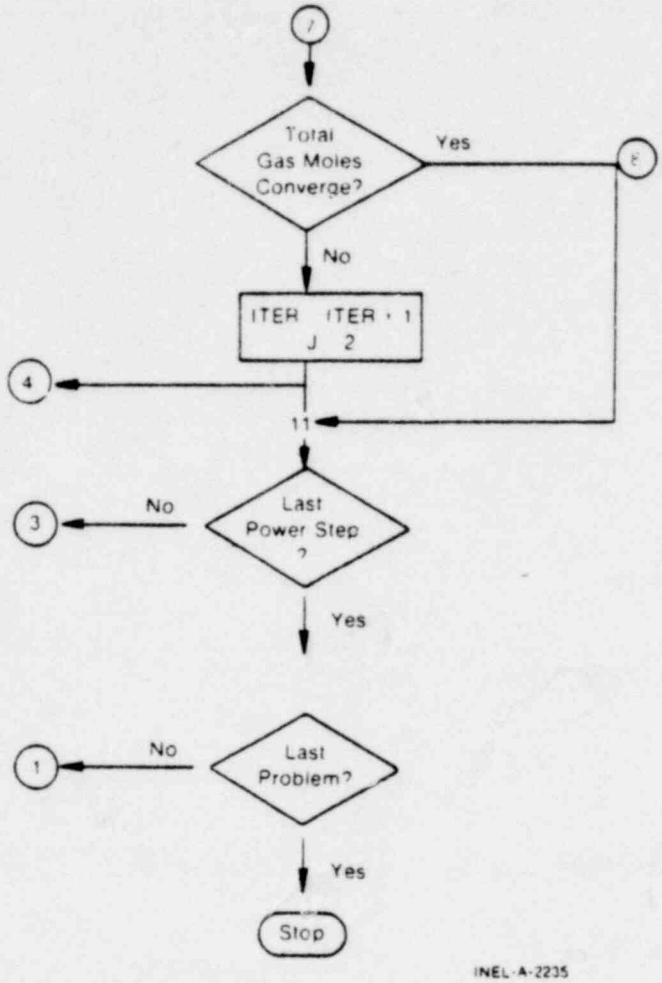

INEL-A-2235

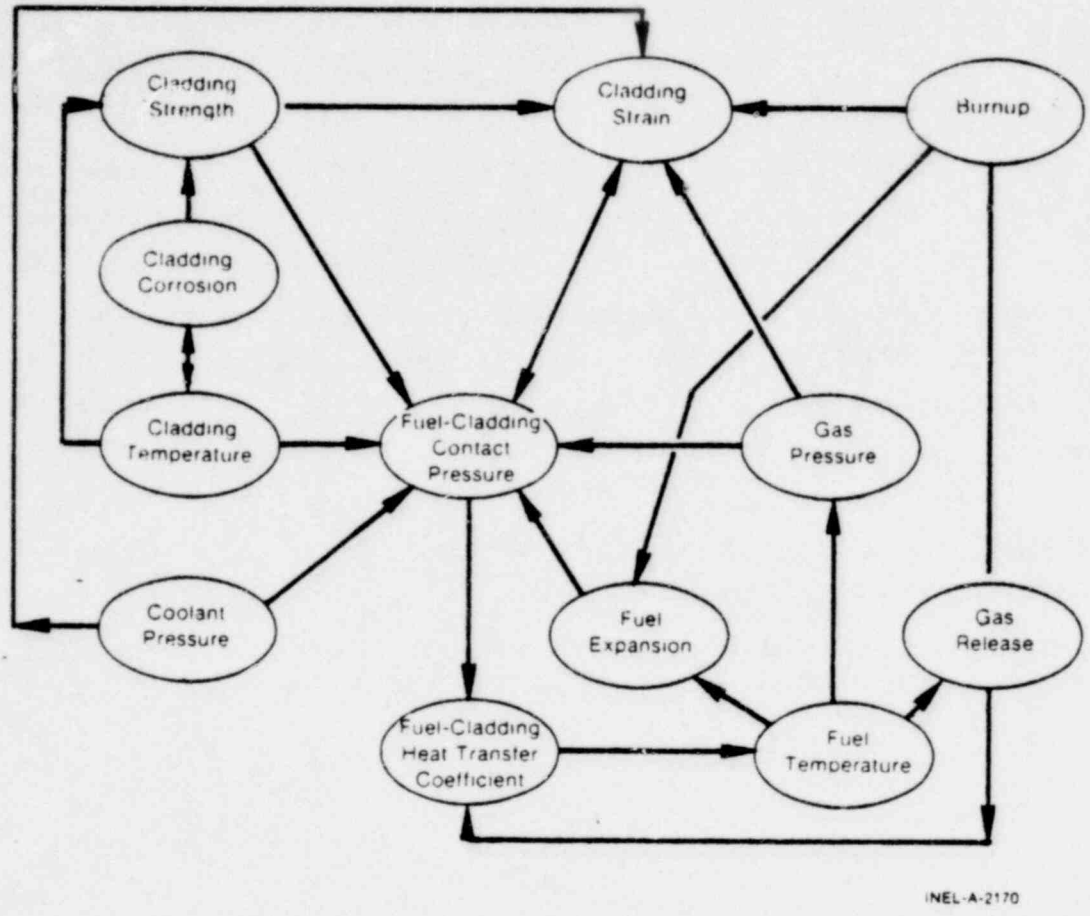

Fig. 17 FRAP-S computational interactions.

cladding. The radial temperature distribution through the pellet is calculated for the 10 rings by the $\int k\,dT$ method described by Robertson et al[30], and is corrected to account for relocation of the cracks.

Burnup dependent pellet radial power distributions, fit to the output of the lattice depletion code LASER[11] can be used in calculating the fuel temperature distribution. Also radial power profiles can be input.

After the temperatures in each fuel subvolume are calculated, the fission gas fractional release is calculated using the diffusion-trapping model of Weisman and MacDonald[17]. The quantity of generated fission gases in each fuel subvolume is calculated as a function of fuel burnup (the burnup is calculated for each subvolume from the input power/time

and axial flux shapes and from the burnup dependent pellet radial flux depression). The dish, pellet-to-cladding gap, fuel crack, fuel open porosity, and plenum volumes are calculated considering the various fuel and cladding thermal, stress induced, and fission product induced deformation and then, the total fission product gas release and the rod internal pressure is calculated using the ideal gas law by summing the individual axial segment calculated gas releases and void volumes. The plenum temperature calculation considers heat flow from the top of the fuel stack, from the coolant channel, and gamma heating in the hold-down spring.

The new pressure and gas composition are used in the next iteration to recalculate the heat transfer across the pellet to cladding gap. The cladding stresses, strains, and interface pressures or gaps are computed by FRACAS[31]. **And, the zircaloy cladding creep is calculated as described in Section 3.**

VI. SUMMARY AND DIFFERENCE BETWEEN FRAP-S VERSIONS

FRAP-S3 contains improvements over FRAP-S2 in areas such as fuel surface relocation and effective conductivity. These and other improvements are summarized in Table III. Improvements of FRAP-S3 are continuing as errors are discovered and corrected. If programming errors are detected in the use of this version of FRAP-S, notification of the authors would be greatly appreciated.

TABLE III

DIFFERENCES IN VERSIONS OF FRAP-S

Phenomenon	FRAP-S1	FRAP-S2	FRAP-S3
Heat conduction	Stacked 1-D radial with $\int k dt$	Stacked 1-D radial with $\int k dt$, 2D r - θ	Stacked 1-D radial with $\int k dt$ and effective thermal conductivity
Gap conductance	Cracked pellet	Modified Ross and Cracked pellet	Modified Ross and Stoute, Cracked pellet
Internal pressure	Ideal gas law	Ideal gas law	Ideal gas law, Improved initial fill gas
Cladding deformation		Triaxial coupled plastic stress-strain equations, fuel-cladding interaction, creep considered	Triaxial coupled plastic stress-strain equations, fuel-cladding interaction, strain-rate effects, cold-work and fast neutron flux effects
Rod internal gas	MacDonald-Weisman fission gas and helium release, Booth diffusion of nitrogen and water vapor	MacDonald-Weisman fission gas and helium release, Booth diffusion of nitrogen and water vapor	Mac-Donald-Weisman fission gas and helium release, Booth diffusion of nitrogen (H_2O assumed to react with cladding)
Cladding failure	No model	FRAIL-1	FRAIL-2
Fuel deformation	Swelling (Bettis data) free thermal expansion model	Swelling (Bettis data) densification, free thermal expansion model	Swelling (MATPRO) densification, free thermal expansion model
Fuel relocation	No model	Bulking factor relocation	Coleman relocation model
Fuel, cladding and gas properties	MATPRO-3	MATPRO-7	MATPRO-9
S to T links	S1/T2	S2/T2, T3	S3/T2, T3, T4

VII. REFERENCES

1. J. A. Dearien et al, FRAP-T3: A Computer Code for the Transient Analysis of Oxide Fuel Rods, TFBP-TR-194 (August 1977).

2. Personal Communication with W. I. Schindler, ANC, (June 1974).

3. C. R. Hann, C. E. Beyer, and L. J. Parchen, GAPCON-THERMAL-1: A Computer Program for Calculating the Gap Conductance in Oxide Fuel Pins, BNWL-1778 (September 1973).

4. P. E. MacDonald et al, MATPRO: A Handbook of Materials Properties For Use in the Analysis of Light Water Reactor Fuel Rod Behavior. ANCR-1263, NRC-3 (February 1976).

5. F. W. Dittus and L. M. K. Boelter, "Heat Transfer in Automobile Radiators of the Tubular Type," University of California Publications in Engineering, 2, 13 (1930) pp 443-461.

6. W. H. Jens and P. A. Lottes, Analysis of Heat Transfer, Burnout, Pressure Drop, and Density Data for High-Pressure Water, ANL-4627 (1951).

7. P. E. MacDonald et al, MATPRO-Version 09 - A Handbook of Materials Properties for Use in the Analysis of Light Water Reactor Fuel Rod Behavior, TREE-NUREG-1005, (December 1976).

8. A. M. Ross and R. L. Stoute, Heat Transfer Coefficient Between UO_2 and Zircaloy-2, AECL-1552 (June 1962).

9. C. Jacobs and N. Todreas, "Thermal Contact Conductance in Reactor Fuel Elements," Nuclear Science and Engineering, 50, 3 (March 1973) pp 283-290.

10. H. Fenech and W. M. Rohsenow, "A Prediction of Thermal Conductance of Metallic Surfaces in Contact," Transactions of the ASME, Series C, Journal of Heat Transfer, 85, 1 (February 1963) pp 15-24 (ASME paper 62-HT-32).

11. C. G. Poncelet, LASER - A Depletion Program for Lattice Calculations Based on MUFT and THERMOS, WCAP-6073 (April 1966).

12. W. H. McAdams, Heat Transmission, 3rd ed., New York: McGraw-Hill Book Company, Inc., 1954.

13. A. Mendelson, Plasticity: Theory and Applications, New York: The MacMillan Company, 1968.

14. E. F. Ibrahim, An Equation for Creep of Cold-Worked Zircaloy Pressure Tube Material, AECL-2928 (1965).

15. C. E. Pugh et al, Currently Recommended Constitutive Equations for Inelastic Design Analysis of FFTF Components, ORNL-TM-3602 (September 1973).

16. R. E. Skardahl et al, U.S. Experience on Irradiation Performance of UO_2-PuO_2 Fast Reactor Fuel, CONF 671005 (1970).

17. J. Weisman et al, "Fission Gas Release from UO_2 Fuel Rods with Time Varying Power Histories," ANS Transactions, 12, 2 (November 1969).

18. A. H. Booth, A Method of Calculating Fission Gas Diffusion from UO_2 Fuel and Its Application to the X-2 Loop Test, AECL-496 (CRDC-721), (1957).

19. H. M. Ferrari, "Nitrogen Release from UO_2 Pellets at Elevated Temperatures," Nuclear Science and Engineering, 17, 4 (December 1963).

20. H. M. Ferrari, "Diffusion of Nitrogen in Uranium Dioxide," Journal of Nuclear Materials, 12, 2 (1964).

21. R. C. Daniel et al, Effects of High Burnup on Zircaloy Clad Bulk UO_2 Plate Fuel Element Samples, WAPD-263, (September 1963).

22. C. M. Cox, "The Irradiation Performance of Uranium-Plutonium Oxide Fuel Pins," Nuclear Safety, 10, 5 (October 1969) pp 380-391.

23. F. Anselin and W. F. Baily, "The Role of Fission Products in the Swelling of Irradiated UO_2 and $(U, Pu)O_2$ Fuels," Transactions of the American Nuclear Society, 10, 1 (1967) pp 103-104.

24. A. van der Linde, Calculation of the Safe Lifetime Expectancy of Zirconium Alloy Canning in the Fuel Elements of the NERO Reactor, RCN-41 (1965).

25. R. C. Nelson, The Corrosion of Zircaloy-2 Fuel Element Cladding in a Boiling Water Reactor Environment, GEAP-4089 (1969).

26. H. E. Williamson et al, AEC Fuel Cycle Program Examination of UO_2 Fuel Rods Operated in the VBNR to 10,000 MWd/tU, GEAP-4597 (1965).

27. L. S. Tong and J. Weisman, Thermal Analysis of Pressurized Water Reactors, TID-25635 (1970).

28. W. R. Smalley, Saxton Plutonium Program Semi-Annual Progress Report for the Period Ending June 30, 1969, WCAP 3385-20 (October 1969).

29. W. R. Smalley, Saxton Plutonium Program Semi-Annual Progress Report for the Period Ending December 31, 1969, WCAP 3385-22 (March 1970).

30. J. A. L. Robertson, ∫kdt in Fuel Irradiations, CRFD-832 (April 1959).

31. M. P. Bohn, FRACAS -- A Subcode for the Analysis of Fuel Pellet-Cladding Mechanical Interaction, TREE-NUREG-1028 (April 1977).

32. R. S. Brokaw, Alignment Charts for Transport Properties, Viscosity, Thermal Conductivity and Diffusion Coefficients for Nonpolar Gases and Gas Mixtures at Low Density, NASA TR R-81, (1961).

33. J. M. Gandhi and S. C. Saxena, "Correlated Thermal Conductivity Data of Rare Gases and Their Binary Mixtures at Ordinary Pressures," Journal of Chemical and Engineering Data, 13, 3 (1968).

34. H. H. Klepfer and A. S. Melner, Specific Zirconium Alloy Design Program - Final Summary Report, GEAP-10044 (1969).

35. D. R. Coleman and E. T. Laats, FRAP-T3: A Computer Code for Transient Analysis of Oxide Fuel Rods, Volume II - Model Verification Report, TFBP-TR-180 (1977).

36. R. G. Rose and M. Balfour, Materials and Processes Engineering Quarterly Report, April - June 1964, WCAP, p. 58.

APPENDIX A

FRAP-S3 INPUT INSTRUCTIONS

APPENDIX A

FRAP-S3 INPUT INSTRUCTIONS

The required input to FRAP-S3 is presented in this appendix. Section I describes the use of NAMELIST[a], the free form input used by FRAP-S3. Section II presents the standard and optional input with a listing of each mnemonic variable, a description of the variable, and any restrictions or options associated with the variable. Section III presents the job control language (JCL) required to run FRAP-S3 and the plot code on the Idaho National Engineering Laboratory (INEL) 360/75. This is followed by the plot subcode input data.

1. NAMELIST INPUT SPECIFICATION

Input data must be in a special form in order to be read using a NAMELIST list. The first character in each record (card) to be read must be blank. The second character in the first record of a group of data records must be a $, immediately followed by the NAMELIST name. For any FRAP-S version this is FRAPS. The NAMELIST name must be followed by a blank and must not contain any embedded blanks. This name is followed by data items separated by commas. (A comma after the last item is optional.) The end of a data group is signaled by $END.

The form of the data items in an input record is:

symbolic name = constant

The symbolic name may be an array element name or a variable name. Subscripts must be integer constants. The constant may be an

---

[a] IBM System/360 and System/370 FORTRAN IV Language, IBM System Reference Library.

069

integer, real, literal, complex, or logical. (If the constants are logical, they may be in the form T or .TRUE. and F or .FALSE.)
array name - set of constants (separated by commas)
The set of constants consists of constants of the type integer, real, literal, complex, or logical. The number of constants must be less than or equal to the number of elements in the array. Successive occurrences of the same constant can be represented in the form k*constant, where k is a nonzero integer constant specifying the number of times the constant is to occur.

The variable names and array names specified in the input data set must appear in the NAMELIST list, but the order is not significant. A name that has been made equivalent to a name in the input data cannot be substituted for that name in the NAMELIST list. The list can contain names of items in COMMON but must not contain dummy argument names.

Each data record (card) must begin with a blank followed by a complete variable or array name or constant. Embedded blanks are not permitted in names or constants. Trailing blanks after integers and exponents are treated as zeros.

2. INPUT DATA

2.1 Standard Input

The first card which must be included is a job title card. The first 72 columns are available for the title. Each standard input card must be supplied unless an optional input card replaces it.

Variable	Description	Restrictions and Options
CPL	Cold plenum length (in., m)	none

Variable	Description	Restrictions and Options
DCI	Diameter of cladding, inside (in., m)	none
DCØ	Diameter of cladding, outside (in., m)	none
DE	Equivalent hydraulic diameter (in., m)	none
DEN	Pellet true density (% theoretical density - 10.97 gm/cc)	none
DISHSD	Dish shoulder width (pellet radius minus dish radius) (in., m)	none
DP	Diameter of pellet (in., m)	none
DSPG	Diameter of spring, outside (in., m)	none
DSPGW	Diameter of spring wire (in., m)	none
ENRCH	Fuel enrichment (w/o U-235) used in flux depression estimate	if omitted, input flux depression (FLXDP)
FGPAV	Initial gas pressure (psia, N/m^2)	none
GØ	Mass flow rate ($lb/hr\text{-}ft^2$, $kg/s\text{-}m^2$)	= 0 , cladding surface temperature = TW at all increments. If NSP = 1, input one value for each power step

Variable	Description	Restrictions and Options
HDISH	Height of pellet end dish (in., m)	none
HPLT	Height of pellet (in., m)	none
ICM	Index for cladding material (presently the code does not distinguish between zircaloy-2 and zircaloy-4)	= 2, zircaloy-2 cladding = 4, zircaloy-4 cladding
IDXGAS	Index for initial fill gas	= 1, helium = 2, air = 3, nitrogen = 4, fission gas = 5, argon = 6, user specifies mole fractions of the above (see AMFAIR, etc. in the optional input section). If fission products are input, user should consider input of initial burnup, BUIN
IM	Number of power levels	must equal number of time steps (Maximum of 69)
IQ	Axial power shape index	= 0, shape input = 1, cosine shape
IPLANT	Index for LASER fit of radial power distributions. If IPLANT	= 1, PWR, uranium enriched if ENRCH >6 or

Variable	Description	Restrictions and Options
	is set to zero, FRAP-S3 makes use of the pellet temperature distribution calculation as described in Section 1.5.2	<2 set IPLANT = 0 = 2, BWR, uranium enriched if ENRCH >3.5 or <1.5 set IPLANT = 0 = 3, PWR, plutonium enriched UO_2 if ENRCH >10 or <2 set IPLANT = 0 = -1, user input radial power profile (see RAPØW) = 4, BWR, plutonium enriched UO_2 if ENRCH >6 or <1.5 set IPLANT = 0
JDLPR	Index for axial increments to be output	= 1, and NØPT = 0, peak power increment only ≠ 1, and NØPT = 0, all increments
JN	Number of entries in each set of QF and X tables	omit if IQ = 1. Maximum of 40. If more than one shape JST must be input. Number of values must equal number of axial shapes used.
NT	Number of equal length axial nodes	must be odd integer 3<NT <17

Variable	Description	Restrictions and Options
NUNITS	Units to be input (defaults to SI units)	= 0, SI units are input = 1, British units are input
P2	System pressure (psia, N/m^2)	if NSP = 1, input one value for each power level
QF	Pointwise axial heat flux normalization factors	number of entries must equal JN for each axial shape. 1 < Q < 41 for each shape up to 5 shapes. If more than one shape, normalize all shapes to the average
QMPY	Heat flux at each power ($Btu/hr\text{-}ft^2$) or (kW/ft, W/cm)	= kW/ft or W/cm if first value is less than 100. = $Btu/hr\text{-}ft^2$ if first value is greater than 100. Must be greater than zero however
TIME	Table of accumulated times. (end of step times) Corresponding to QMPY entries (sec) or (hours)	= seconds if first value greater than 17.0 = hours if first value >0.01 hour but, <1.0 hour
TØTL	Fuel stack height (ft, m)	none

Variable	Description	Restrictions and Options
TW	Inlet water temperature (°F, K)	if GØ = 0 TW is clad surface temperature. If NSP = 1, input one value for each power step
VS	Total number of spring turns	none
X	Table of axial stations corresponding to QF entries (ft, m)	number of entries must equal JN for each axial shape. 1 < X < 41 for each shape up to 5 shapes. First value must be 0.0 and last value must be equal to the total length TØTL

The following variables are predefined in the code. It is not necessary to include these cards in the input data deck unless a value other than that listed below is desired. The "additional" factors (i.e., ACOR, etc.) may be used in parametric or scoping studies.

2.2 Optional Input

Variable	Default Value	Description	Restrictions and Options
AFAL	1.0	Additional thermal expansion factor	≠

Variable	Default Value	Description	Restrictions and Options
AFCR	1.0	Additional creep acceleration factor	$\neq 0$
AFDN	1.0	Additional densification factor	none
AFGR	1.0	Additional fractional gas release multiplication factor	$\neq 0$
AFTC	1.0	Additional fuel thermal conductivity multiplication factor	$\neq 0$
AFSW	1.0	Additional fuel swelling multiplication factor	$\neq 0$
AMFAIR	0.0	Absolute mole fraction of air	use only if IDXGAS = 6
AMFARG	0.0	Absolute mole fraction of argon	use only if IDXGAS = 6
AMFFG	0.0	Absolute mole fraction of fission gas	use only if IDXGAS = 6
AMFKRY	0.0	Absolute mole fraction of krypton	use only if IDXGAS = 6 and AMFFG = 0.0
AMFXE	0.0	Absolute mole fraction of xenon	use only if IDXGAS = 6 and AMFFG = 0.0

Variable	Default Value	Description	Restrictions and Options
AMFHE	0.0	Absolute mole fraction of helium	use only if IDXGAS = 6
AMFH2	0.0	Absolute mole fraction of hydrogen	use only if IDXGAS = 6
AMFH2Ø	0.0	Absolute mole fraction of steam	use only if IDXGAS = 6
AMFN2	0.0	Absolute mole fraction of nitrogen	use only if IDXGAS = 6
AMI	0.0	Change in flux depression factor per unit burnup between BUCRIT and end of problem	= 0, constant flux depression factor
AMØ	0.0	Change in flux depression factor per unit burnup between zero burnup and BUCRIT	= 0, constant flux depression factor
BETA	1.0	Porosity correction to fuel thermal conductivity	none
BUIN	0.0	Initial fuel burnup (MWd/MtU, MWs/kg)	should include input of fission product mole fractions
BUCRIT	0.0	Burnup at which flux depression factor changes slope (MWd/MtU, MWs/kg)	= 0, AMØ not used

Variable	Default Value	Description	Restrictions and Options
CATEXF	0.05	Texture factor (fraction of cladding cells with basal poles parallel to the tube axis)	$0.0 \leq$ CATEXF ≤ 1.0
CØLDWK	0.0	Cold work of the cladding	none
CØMP	0.0	Weight percent of $PUØ_2$ in mixed oxide fuel	$0.0 \leq$ CØMP ≤ 100.0
CRDT	1.0	Initial crud thickness (mil, m)	
CRDTR	1.1415525×10^{-4}	Crud buildup rate (mil/hr, m/s)	used only if ICØR = 2
DENG	0.75	Porosity correction to pellet density (%) emersion (true) density to geometric density	none
EXØ	1.0	Surface roughness factor in gap conductance calculation	minimum of 1.0
FA	1.0	Nuclear axial hot channel factor (peak/average)	= 1.0, if QF table is normalized to the average, and QMPY = average heat flux. > 1.0, if IQ = 1 and QMPY = peak heat flux.

Variable	Default Value	Description	Restrictions and Options
			> 1.0, if IQ table is normalized to the peak, and QMPY = peak heat flux
FLXDP	0.9999	Initial value of flux depression factor	used only if ENRCH = 0.0 and IPLANT not specified. Must be less than 0.9999
			$FLXDP = \frac{2[I_0(\kappa a)-1]}{\kappa a[I_1(\kappa a)]}$
			a = pellet radius (in.) = reciprocal of thermal diffusion length ($in.^{-1}$) I_0 = zero order modified Bessel function (first kind) I_1 = first order modified function (first kind)
FLUX	$6x10^{17}$	Fast neutron flux experienced by rod	none
FQE	1.0	Heat flux engineering factor	multiplication factor on QMPY values
GRNSZ	5.0 microns	Initial grain size	none
ICØR	0	Index for crud model	= 0, corrosion model constant crud, no crud temperature drop if boiling. = 1, corrosion model, constant crud, crud temperature drop if boiling.

Variable	Default Value	Description	Restrictions and Options
			= 2, corrosion model, varying crud, crud temperature drop if boiling
JST	IM*1	Indicates type of axial power shape to be used for each time step	IQ must = 0. Must be one type number for each time step, (the first QF and X array is Type 1, the second is Type 2, etc.), maximum of five types. The axial shapes must be normalized to the average
LINKT	4	FRAP-T link index	= 1, link is to FRAP-T1 = 2. link is to FRAP-T2 = 3, link is to FRAP-T3 = 4, link is to FRAP-T4
MDBG	0	Summary power step debug output index	= 0, no debug output = 1, debug output
MØDE	0	Stack calculation selector	= 0, stack calculations are made = 1, stack calculations are not made
NDBG	0	Debug printout index	= 0, normal output = -1, full debug output. To obtain debug output at only one power level set NDBG equal to that power level number
NFR ØD	1	Number of like fuel rods being analyzed	None

Variable	Default Value	Description	Restrictions and Options
NGAPC	1	Gap conductance model selector	= 0, cracked pellet model = 1, annular gap model
NØFAIL	0	Failure Subcode switch	= 0, failure subcode is used and results output = 1, failure subcode is bypassed
NØPT	3	Printout selector	= 0, full output = 3, short (tabular) output
NPCYCL	0	Number of previous power cycles	None
NREAD	0	FRAP-S restart read index	= 0, no restart = 1, read restart tape
NRESTR	0	FRAP-S restart write index	= 0, no restart write = 1, write FRAP-S restart tape
NRØLL	0	Restart tape rewind index	= 0, rewrites in same storage space = 1, writes a string of restart information for each power step
NSP	0	Varying system parameter	= 0, constant system parameter (P2, TW, GØ) = 1, varying system parameters
NSTART	0	Timestep for start of debug output	0 ≤ NSTART ≤ IM
NSTØP	0	Timestep for end of debug output	0 ≤ NSTØP ≤ IM and NSTØP > NSTART

Variable	Default Value	Description	Restrictions and Options
NTAPE	0	FRAP-T restart index	= 0, no restart data stored = 1, restart data stored for FRAP-T use
PPMH2Ø	0	Fuel initial water content (PPM)	none
PPMN2	15.0	Fuel initial nitrogen content (PPM)	none
QEND	0.3	Normalized heat flux at top of fuel stack	must be one value for each axial shape. Used to determine heat flow into the plenum
RAPØW	1.0	Normalized radial power profile	IPLANT must be -1. Input eleven values from the fuel surface to the fuel center assuming equal areas between radial nodes
RC	0.0	Pellet core radius (in., m)	none
RØUGHC	4.8×10^{-5}	Arithmetic mean roughness height of cladding (in., m)	none
RØUGHF	8.5×10^{-5}	Arithmetic mean roughness height of fuel (in., m)	none

Variable	Default Value	Description	Restrictions and Options
RØ	DCØ/24	Cladding outside radius (ft, m)	do not input DCØ
RØF	DP/24	Pellet radius (ft, m)	do not input DP
SGAPF	30	Fission gas atoms per 100 fissions	none
TCC	(DCØ-DCI)/2	Clad thickness (in., m)	do not input DCI
TSINT	2912	Fuel sintering temperature (°F, K)	none
UMELT	MATPRO Compute-Value	User specified cladding failure melt temperature criterion	none
UØFD	17.0%	User specified cladding oxide failure depth criterion	none

2.3 Plot Input

The following is the input data for plotting. If no plots are desired, follow the "$END" card of the preceding input with card 1 below. It plots are desired, the "$END" card is followed with first, a full set of plot data, and then a set of plot JCL from SECTION III.

Card No. 1

Columns	Format	Name	Quantity
1 - 5	I	NPLTNØ	Number of axial nodes at which plots are desired. If no plots wanted, input the number 0.

Card No. 2 - Specification of axial nodes at which plots are wanted

Columns	Format	Name	Quantity
1 - 5	I	IAPLT(1)	Number of an axial node at which plots are wanted.
6 - 10	I	IAPLT(2)	Number of an axial node at which plots are wanted.

Repeat as necessary for IAPLT(K) (K being an axial node number)

Card No. 3 - Time axis

Columns	Format	Name	Quantity
1 - 10	F	TSTART	Minimum time on time axis (hr, sec).
11 - 20	F	TEND	Maximum time on time axis (hr, sec).
21 - 30	F	AXLT	Length of time axis (in.).
31 - 70	A	LABLT	Label to be given time axis.

Card No. 4 - Cladding surface temperaxis (°F, K)

Columns	Format	Name	Quantity
1 - 10	F	TSMIN	Minimum cladding surface temperature on axis (°F, K).
11 - 20	F	TSMAX	Maximum cladding surface temperature in axis (°F, K).
21 - 30	F	AXLTS	Length of surface temperature axis (in.).
31 - 70	A	LABLTS	Label to be given surface temperature axis.

Card No. 5 - Fuel centerline temperature axis

Columns	Format	Name	Quantity
1 - 10	F	TOLMIN	Minimum fuel centerline temperature on axis (°F, K).
11 - 20	F	TOLMAX	Maximum fuel centerline temperature on axis (°F, K).
21 - 30	F	AXLTMP	Length of centerline temperature axis (in.).
31 - 70	A	LABLTM	Label to be given centerline temperature axis.

Card No. 6 - Gas pressure axis

Columns	Format	Name	Quantity
1 - 10	F	PMIN	Minimum gas gap pressure on axis (psia, N/m^2).

Columns	Format	Name	Quantity
11 - 20	F	PMAX	Maximum gas gap pressure on axis (psia, N/m^2).
21 - 30	F	AXLP	Length of gas gap pressure axis (in.).
31 - 70	A	LABLP	Label to be given gas gap pressure axis.

Card No. 7 - Cladding hoop strain axis

Columns	Format	Name	Quantity
1 - 10	F	EPSMIN	Minimum cladding hoop strain on axis (dimensionless).
11 - 20	F	EPSMAX	Maximum cladding hoop strain on axis (dimensionless).
21 - 30	F	AXLEPS	Length of cladding hoop strain axis (in.).
31 - 70	A	LABLE	Label to be given cladding hoop strain.

Card No. 8 - Fuel axial displacement axis

Columns	Format	Name	Quantity
1 - 10	F	UZFMIN	Minimum fuel axial displacement on axis (ft, m).
11 - 20	F	UZFMAX	Maximum fuel axial displacement on axis (ft, m).

Columns	Format	Name	Quantity
21 - 30	F	AXLUZF	Length of fuel axial displacement axis (in.).
31 - 70	A	LABLUF	Label to be given fuel axial displacement axis.

Card No. 9 - Cladding axial displacement axis

Colums	Format	Name	Quantity
1 - 10	F	UZCMIN	Minimum cladding axial displacement on axis (ft, m).
11 - 20	F	UZCMAX	Maximum cladding axial displacement on axis (ft, m).
21 - 30	F	AXLUZC	Length of cladding axial displacement axis (in.).
31 - 70	A	LABLUC	Label to be given cladding axial displacement axis.

Card No. 10 - Fuel rod power axis

Columns	Format	Name	Quantity
1 - 10	F	PMIN	Minimum linear fuel rod power on axis (kW/ft, W/m).
11 - 20	F	PMAX	Maximum linear fuel rod power on axis (kW/ft, W/m).
21 - 30	F	PLEN	Length of linear fuel rod power axis (in.).

Columns	Format	Name	Quantity
31 - 70	A	PLABL	Label to be given fuel rod power axis.

Card No. 11 - Fuel surface temperature axis

Columns	Format	Name	Quantity
1 - 10	F	TFSMIN	Minimum fuel surface temperature on axis (°F, K).
11 - 20	F	TFSMAX	Maximum fuel surface temperature on axis (°F, K).
21 - 30	F	TFSLEN	Length of fuel surface temperature axis (in.).
31 - 70	A	TFSLAB	Label to be given fuel surface temperature axis.

Card No. 12 - Gap heat transfer coefficient axis

Columns	Format	Name	Quantity
1 - 10	F	HGMIN	Minimum gap heat transfer coefficient on axis (Btu/hr-°F-ft^2, W/m^2-K).
11 - 20	F	HGMAX	Maximum gap heat transfer coefficient on axis (Btu/hr-°F-ft^2, W/m^2-K).
21 - 30	F	HGLEN	Length of gap heat transfer coefficient axis (in.).
31 - 70	A	HGLABL	Label to be given gap heat transfer coefficient axis.

Card No. 13 - Surface heat transfer coefficient axis

Columns	Format	Name	Quantity
1 - 10	F	HSMIN	Minimum surface heat transfer coefficient on axis (Btu/hr-°F-ft^2, W/m^2-K).
11 - 20	F	HSMAX	Maximum surface heat transfer coefficient on axis (Btu/hr-°F-ft^2, W/m^2-K).
21 - 30	F	HSLEN	Length of surface heat transfer coefficient axis (in.).
31 - 70	A	HSLAB	Label to be given surface heat transfer coefficient axis.

Card No. 14 - Average cladding temperature axis

Columns	Format	Name	Quantity
1 - 10	F	TAMIN	Minimum average cladding temperature on axis (°F, K).
11 - 20	F	TAMAX	Maximum average cladding temperature on axis (°F, K).
21 - 30	F	TALEN	Length of average cladding temperature axis (in.).
31 - 70	A	TALABL	Label to be given average cladding temperature axis.

Card No. 15 - Zircaloy-Oxide thickness axis

Columns	Format	Name	Quantity
1 - 10	F	ZOMIN	Minimum ZrO_2 thickness (mil, m).
11 - 20	F	ZOMAX	Maximum ZrO_2 thickness (mil, m).
21 - 30	F	ZOLEN	Length of ZrO_2 thickness (in.).
31 - 70	A	ZOLABL	Label to be given zircaloy-oxide thickness axis.

Card No. 16 - Mole fraction of helium

Columns	Format	Name	Quantity
1 - 10	F	MFMIN	Minimum helium mole fraction on axis.
11 - 20	F	MFMAX	Maximum helium mole fraction on axis.
21 - 30	F	MFLEN	Length of helium mole fraction axis (in.).
31 - 70	A	MFLABL	Label to be given helium mole fraction axis.

Card No. 17 - Plenum temperature axis

Columns	Format	Name	Quantity
1 - 10	F	TPMIN	Minimum plenum temperature on axis (°F or K).
11 - 20	F	TPMAX	Maximum plenum temperature on axis (°F or K).

Columns	Format	Name	Quantity
21 - 30	F	TPLEN	Length of plenum temperature axis (in.).
31 - 70	A	TPLABL	Label to be given plenum temperature axis.

Card No. 18 - Rod gas increase

Columns	Format	Name	Quantity
1 - 10	F	RGMIN	Minimum gas increase on axis (% of initial).
11 - 20	F	RGMAX	Maximum gas increase on axis (% of initial).
21 - 30	F	RGLEN	Length of gas increase axis (in.).
31 - 70	A	RGLABL	Label to be given gas increase axis.

Card No. 19 - Mass flux axis (plot of average mass flux in coolant channels surrounding fuel rod)

Columns	Format	Name	Quantity
1 - 10	F	GMIN	Minimum mass flux on axis (lbm/ft^2-hr or kg/m^2-s).
11 - 20	F	GMAX	Maximum mass flux on axis (lbm/ft^2-hr or kg/m^2-s).
21 - 30	F	GLEN	Length of mass flux axis (in.).
31 - 70	A	GLABL	Label to be given mass flux axis.

Card No. 20 - Fuel stored energy

Columns	Format	Name	Quantity
1 - 10	F	SEMIN	Minimum stored energy on axis (Btu/lbm, Cal/gm).
11 - 20	F	SEMAX	Maximum stored energy on axis (Btu/lbm, Cal/gm).
21 - 30	F	SELEN	Length of average stored energy axis (in.).
31 - 70	A	SELABL	Label to be given average stored energy axis.

Card No. 21 - Coolant pressure axis (plot of average pressure in coolant channel surrounding fuel rod)

Columns	Format	Name	Quantity
1 - 10	F	PCMIN	Minimum pressure on axis (psia or N/m^2).
11 - 20	F	PCMAX	Maximum pressure on axis (psia or N/m^2).
21 - 30	F	PCLEN	Length of pressure axis (in.).
31 - 70	A	PCLABL	Label to be given coolant pressure axis.

Card No. 22 - Gap thickness axis

Columns	Format	Name	Quantity
1 - 10	F	THKMIN	Minimum gap thickness on axis (mil or m).

Columns	Format	Name	Quantity
11 - 20	F	THKMAX	Maximum gap thickness on axis (mil or m).
21 - 30	F	THKLEN	Length of gap thickness axis (in.).
31 - 70	A	THKLAB	Label to be given gap thickness axis.

Card No. 23 - Bulk temperature axis

Columns	Format	Name	Quantity
1 - 10	F	TBMIN	Minimum bulk temperature on axis (°F or K).
11 - 20	F	TBMAX	Maximum bulk temperature on axis (°F or K).
21 - 30	F	TBLEN	Length of bulk temperature axis (in.).
31 - 70	A	TBLAB	Label to be given bulk temperature axis.

3. JOB CONTROL LANGUAGE (JCL)

3.1 JCL Cards for Creating a FRAP-S3 Load Module on the INEL IBM 360/75 Computer

Card No.

1 Job Card

2 // CØR=360,CPU=003,WT=001,SR=T1

```
3    //STEP1 EXEC FTNHCL,CØSET='X1',MEMB='(X2)',
4    // DISP='(,CATLG)',UNIT=X3,SPACE='(TRK,(40,05,1),RLSE)',
5    // CREG=240K,CPGS=290,XREF=XREF
6    //C.SYSUT2 DD SPACE=(TRK,(40,10)),UNIT=SYSCRA
7    //C.SYSIN DD DSN='X4',UNIT=TP9ANY,DISP=(ØLD,KEEP),
8    // VØL=SER=X5
9    //L.ADD DD DSN =X6,DISP=(ØLD,KEEP)
10   11/L.SYSIN DD *
11   INCLUDE ADD (X7)
12   ENTRY MAIN
```

where

X1 is the data set name assigned to the load module (for example TEMP.GABFRAPS)

X2 is the member name associated with the load module name (for example FRAPS)

X3 is the storage unit on which the load module is to be stored (for example DKTEMP)

X4 is the tape identification name which contains card images of the source deck (for example ANCFRAPS)

X5 is the tape number corresponding to the tape identification name (for example T95246)

X6 is the name of the version of MATPRO, the material properties package (for example MATPRØ03)

X7 is the member name associated with the material properties package load module (for example MATPRO).

33-324

3.2 JCL Cards for Executing the Above Created Load Module on the INEL IBM 360/75 Computer.

Card No.

```
1    // Job Card
2    // CØR=360,CPU=Y1,WT=Y2
3    //STEP2 EXEC PGM=X2,REGIØN=360K
4    //STEPLIB DD DSN=X1,DISP=SHR
5    //FT06F001 DD SYSØUT=A,DCB=(RECFM-FBA,LRECL=133,BLKSIZE=1596),
6    // SPACE=(7980,(200,16),RLSE)
7    //FT01F001 DD DSN=Y3,UNIT=Y4,DISP=(,CATLG),
8    // DCB=(BLKSIZE=574,LRECL=104,RECFM=VBS),SPACE=(TRK,(5,5),RLSE)
```

NOTE: Include cards 9 through 12 only if plots are desired.

```
9    //FT17F001 DD DSN=Y5,DISP=(,PASS),UNIT=DKSCRA,
10   // DCB=(BLKSIZE=560,LRECL=56,RECFM=VBS),SPACE=(TRK,(1000,60))
11   //FT18F001 DD DSN=Y6,DISP=(,PASS),UNIT=DKSCRA,
12   // DCB=(BLKSIZE=560,LRECL=56,RECFM=VBS),SPACE=(TRK,(2,1))
13   //FT05F001 DD *
```

INPUT DATA:

where

Y1 is the total computer time required for the job in minutes

Y2 is the total wait time in minutes

Y3 is the name given to the restart data set (for example TEMP.LJSREST1)

Y4 is the storage unit on which the restart data is written (for example DKTEMP)

Y5 is a scratch data set name to be specified by the user (for example &&GAB00017)

Y6 is a scratch data set name to be specified by the user (for example &&GAB00018).

3.3 JCL Cards for Creating the Plot Code Load Module

If plots are desired an executable plot code load module should be available. The following cards are required to compile the plot package for FRAP-S2.

Card No.

```
1    // Job Card
2    // CØ=265,CPU=001,WT=001
3    //S1 EXEC FTNHCL,GØSET='Z1',MEMB='(Z2)',
4    // ØPT=2,DISP='(,CATLG)',UNIT=Z3,CREG=265K,
5    // SPACE='(TRK,(10,10),1),RLSE)',CPGS=100,
6    // XREF=XREF
7    //C.SYSUT2 DD SPACE=(TRK,(40,10)),UNIT=Z4
8    //C.SYSIN DD *
```

SOURCE CARDS:

where

Z1 is the name to be assigned to the load module (for example PLØTFRPS)

Z2 is the member name to be assigned to the compiled load module (for example PLØTCD)

Z3 is the name of the unit on which the load module is to be stored (for example DKTEMP)

Z4 is a scratch space unit (for example SYSCRA).

3.4 JCL Cards for Executing the Above Created Plot Load Module (to follow the plot input cards)

Card No.

```
1    //PLØTSTEP EXEC=Z2,REGIØN=200K
2    //STEPLIB DD DSN=Z1,DISP=(ØLD,KEEP)
3    //FT06F001 DD SYSØUT=A,DCB=(RECFM=FRA,LRECL=133,BLKSIZE=1596),
4    // SPACE=(TRK,(2,5))
5    //FT17F001 DD DSN=Y5,DISP=(ØLD,DELETE),UNIT=DKSCRA
6    //FT18F001 DD DSN=Y6,DISP=(ØLD,DELETE),UNIT=DKSCRA
7    //PLØT DD SYSØUT=(Y,,0003)
8    //FT05F001 DD *
```

where Z1, Z2, Y5, and Y6 are as defined in previous groups of JCL.

APPENDIX B

EXAMPLE PROBLEM INPUT AND OUTPUT

APPENDIX B

EXAMPLE PROBLEM INPUT AND OUTPUT

This section presents the general format used for input to FRAP-S2 and the output format showing the information a user would expect to receive from a run.

(1) Example Problem Input
A set of data for an example problem is presented in Table B-I and B-II.

(2) Example Problem Output

(a) Initial problem parameters and history information appear in the first three pages of output as shown in the first three pages of Table B-III.

(b) A typical set of output information for one axial station is shown in the fourth page of Table B-III.

(c) A power step summary of the entire rod is presented on the fifth page of Table B-III.

(d) A problem summary of information calculated at the peak power axial level along with other information provided at a problem's completion are shown on the seventh and eighth pages of Table B-III.

TABLE B-I

EXAMPLE PROBLEM DATA (PCM-20 PBF ROD)

Coolant Conditions:

mass flux, 1.0×10^6 (lbm/hr-ft^2)
inlet temperature, 642 (°F)
hydraulic diameter, 0.348 (in.)
pressure, 2250 (psia)

Fuel Rod Geometry:

fuel stack length, 3.0 (ft)
fuel rod outside diameter, 0.422 (in.)
fuel pellet diameter, 0.366 (in.)
plenum length, 2.0 (in.)

Fuel Initial Conditions:

density, 93.5 (% theoretical density)
pressure, 300 (psia)
enrichment, 35 (%)

Power History:

a power ramp from 5 kW/ft to 10 kW/ft in 10 hours

TABLE B-II

EXAMPLE PROBLEM

FORTRAN CODING FORM

```
      PBF SINGLE ROD PCM-20
$FRAPS
 CPL   =2.0   , ORDTR= 0.0, DCI   = .374, DCO   = .422, DE    =0.348,
 DEN   =93.5  , DENG = 5.0, DISHSD= .062, DP    = .366, DSPG  =0.355,
 DSPGW=0.04   , ENRCH= 35.0, FGPAV = 600., GO(1) =1.E6, HDISH=0.015,
 HPLT  =.6545, ICM  =   4, ICOR  =   1, IDXGAS=   1, IM    =   2,
 IPLANT=1     , IQ   =   0, JDLPR =   0, JN(1) =  19, NT    =   9,
 NTAPE=   0, P2(1)= 2250, NOPT  =   0, NOTL  = 3.0, VS    = 17.0,
 TW(1)= 642., QMPY=5., 10., TIME=.01, 10., ROUGHF=8.5E-5, ROUGHC=4.5E-5,
 QF    = 0.62  , .705  , .875  , 1.065 , 1.215 , 1.31  , 1.37  , 1.38  , 1.375
       , 1.335 , 1.275 , 1.18  , 1.06  , 0.94  , 0.815 , 0.685 , 0.55  , 0.44  , 0.38 ,
 X     = 0.0   , .1667 , .3333 , 0.5   , .6667 , .8333 , 1.0   , 1.1667, 1.3333,
       1.5     , 1.6667, 1.8333, 2.0   , 2.1667, 2.3333, 2.5   , 2.6667, 2.8333, 3.0,
$END
```

TABLE B-III

EXAMPLE PROBLEM OUTPUT

```
            FRAP-S MOD 002  VERS 02J* STEADY-STATE FUEL PERFORMANCE CODE*11/29/76*G A BERNA* AEROJET NUCLEAR COMPANY
  RUN DATE IS -  12/18/76                             MAT PRO MODULE MOD007                                              PAGE   1
XXXXXXXXXXXXXXXXXXXXXXXXXXXXXXXXXXXXXXXXXXXXXXXXXXXXXXXXXXXXXXXXXXXXXXXXXXXXXXXXXXXXXXXXXXXXXXXXXXXXXXXXXXXXXXXXXXXXXXXXXXXXXX
                                                      PBF SINGLE ROD  PCM-20
      XXXXXXXXXXXXXXXXXXXXXXXXXXXXXXXXXXXXXXXXXXXXXXXXXXXXXXXXXXXXXXXXXXXXXXXXXXXXXXXXXXXXXXXXXXXXXXXXXXXXXXXXXXXXXXXXXXX
 ******PWR SYSTEM  U-235 RODS

 CLAD MATERIAL IS ZIRCALOY-4
 CLAD YIELD STRENGTH  (660 F , 588.7 K) = 54200. (PSI)
                                        = .37369E+09 (N/M**2)
 COLD CLAD O.D. =  .422000(IN)                        .0107188 (M)
 COLD CLAD I.D. =  .374000(IN)                        .0094996 (M)
 COLD CLAD THICKNESS =  .0240 (IN)                    .00061 (M)

 COLD DIAMETRAL GAP =  8.0000(MILS)                  .20320E-03 (M)

 COLD INTERNAL HELIUM PRESSURE =  300.00(PSIA)
                               =  .20684E+07 (N/M**2)
 COLD PELLET DIAMETER =  .366000(IN)                  .00929642 (M)
 COLD PELLET LENGTH =   .65455(IN)                    .0166255 (M)
 PELLET TRUE DENSITY = 93.500(PERCENT)
 ENRICHMENT = 35.0000(WEIGHT PERCENT)
 FUEL STACK HEIGHT =  3.0000(FT)                       .9144 (M)
 DISH SPHERICAL RADIUS =   .49553(IN)                 .012587 (M)
 DISH DEPTH =   .01500(IN)                           .0003810 (M)
 DISH SHOULDER WIDTH =   .06200(IN)                  .0015748 (M)
 PELLET CORE RADIUS =  0.00000(IN)                   0.0000000 (M)
 COLD FUEL VOLUME =   3.74938(CU.IN.)            .61442E-04 (M**3)
 DISH VOLUME FRACTION OF FUEL =   .01007
 FUEL ROUGHNESS VOLUME =   .0019(PERCENT)
 FUEL SINTERING TEMP  =2912.0  (F)                    1873.2 (K)
 COLD PLENUM LENGTH =   2.0000(IN)                   .050800 (M)
 SPRING DIAMETER =   .35500(IN)                      .0090170 (M)
 SPRING WIRE DIAMETER =   .04000(IN)                 .0010160 (M)
 TOTAL SPRING TURNS =  17.00000
 INITIAL BURNUP =  0.           (MWD/MTU)    0.            (MWS/KG)
 SPRING VOLUME =   .02114(CU.IN.)              .34644E-06 (M**3)
 PLENUM VOLUME =   .19856(CU.IN.)              .32541E-05 (M**3)
 TOTAL COLD VOID VOLUME =   .41914(CU.IN.)  .68685E-05 (M**3)
 ARITHMETIC MEAN ROUGHNESS(FUEL)= .0000850(IN)   .00000216 (M)
 ARITHMETIC MEAN ROUGHNESS(CLAD)= .0000450(IN)   .00000114 (M)
 CHANNEL EQUIVALENT DIAMETER =  .02900(FT)       .0088392 (M)
 FISSION GAS ATOMS PER 100 FISSIONS =   30.0
 INITIAL WATER CONCENTRATION =   0.00(PPM)
 INITIAL NITROGEN CONCENTRATION =   15.00(PPM)

 AFCR =  1.0000      AFAL =  1.0000
 AFGR =  1.0000      AFSW =  1.0000
 AFTC =  1.0000      BETA =  1.0000
 EXO  =  1.0000      ACOR =  1.0000
 FA   =  1.0000      FQE  =  1.0000

 FLXDP =   .70319    AMU =  0.00000
 BUCRIT =     0.0    AMI =  0.00000
```

STEP	TIME(HRS)	QMPY(KW/FT)	PZ(PSI)	TW(F)	GO(LBM/HR-FT2)
1	.90	5.000	2250.0	642.00	1000000.0
2	10.00	10.000	2250.0	642.00	1000000.0
3	0.00	0.000	0.0	0.00	0.0
4	0.00	0.000	0.0	0.00	0.0
5	0.00	0.000	0.0	0.00	0.0
6	0.00	0.000	0.0	0.00	0.0
7	0.00	0.000	0.0	0.00	0.0
8	0.00	0.000	0.0	0.00	0.0
9	0.00	0.000	0.0	0.00	0.0
10	0.00	0.000	0.0	0.00	0.0
11	0.00	0.000	0.0	0.00	0.0
12	0.00	0.000	0.0	0.00	0.0
13	0.00	0.000	0.0	0.00	0.0
14	0.00	0.000	0.0	0.00	0.0
15	0.00	0.000	0.0	0.00	0.0
16	0.00	0.000	0.0	0.00	0.0
17	0.00	0.000	0.0	0.00	0.0
18	0.00	0.000	0.0	0.00	0.0
19	0.00	0.000	0.0	0.00	0.0
20	0.00	0.000	0.0	0.00	0.0
21	0.00	0.000	0.0	0.00	0.0
22	0.00	0.000	0.0	0.00	0.0
23	0.00	0.000	0.0	0.00	0.0
24	0.00	0.000	0.0	0.00	0.0
25	0.00	0.000	0.0	0.00	0.0
26	0.00	0.000	0.0	0.00	0.0
27	0.00	0.000	0.0	0.00	0.0
28	0.00	0.000	0.0	0.00	0.0
29	0.00	0.000	0.0	0.00	0.0
30	0.00	0.000	0.0	0.00	0.0
31	0.00	0.000	0.0	0.00	0.0
32	0.00	0.000	0.0	0.00	0.0
33	0.00	0.000	0.0	0.00	0.0
34	0.00	0.000	0.0	0.00	0.0
35	0.00	0.000	0.0	0.00	0.0
36	0.00	0.000	0.0	0.00	0.0
37	0.00	0.000	0.0	0.00	0.0
38	0.00	0.000	0.0	0.00	0.0
39	0.00	0.000	0.0	0.00	0.0
40	0.00	0.000	0.0	0.00	0.0
41	0.00	0.000	0.0	0.00	0.0
42	0.00	0.000	0.0	0.00	0.0
43	0.00	0.000	0.0	0.00	0.0
44	0.00	0.000	0.0	0.00	0.0

TABLE B-III (continued)

```
              FRAP-S MOD 002  VERS 02J* STEADY-STATE FUEL PERFORMANCE CODE*11/29/76*G A BERNA* AEROJET NUCLEAR COMPANY
  RUN DATE 15 -  12/18/76                              MAT PRO MODULE MOD007                                                  PAGE   2
XXXXXXXXXXXXXXXXXXXXXXXXXXXXXXXXXXXXXXXXXXXXXXXXXXXXXXXXXXXXXXXXXXXXXXXXXXXXXXXXXXXXXXXXXXXXXXXXXXXXXXXXXXXXXXXXXXXXXXXXXXXXXXXXXX
                                                                 45        0.00      0.000       0.0     0.00          0.0
    ANGI =   .0003356  H2UMI = 0.0000000                         46        0.00      0.000       0.0     0.00          0.0
    IPLANT =   1                                                 47        0.00      0.000       0.0     0.00          0.0
    ICOR =     1                                                 48        0.00      0.000       0.0     0.00          0.0
    CRUD THICKNESS= 1.00 (MILS)     .25400E-04 (M)               49        0.00      0.000       0.0     0.00          0.0
    CRUD RATE= 0.00 (MILS/C.Y.)                                  50        0.00      0.000       0.0     0.00          0.0
    PCTPRE = 15.0                                                51        0.00      0.000       0.0     0.00          0.0
    PCTPOST= 35.0                                                52        0.00      0.000       0.0     0.00          0.0
                                                                 53        0.00      0.000       0.0     0.00          0.0
    BRITISH UNITS ARE USED                                       54        0.00      0.000       0.0     0.00          0.0
    GAP CONDUCTANCE = 0                                          55        0.00      0.000       0.0     0.00          0.0

PLOTS NOT REQUESTED
```

TABLE B-III (continued)

```
          FRAP-S MOD 002  VERS 02J* STEADY-STATE FUEL PERFORMANCE CODE*11/29/76*G A BERNA* AEROJET NUCLEAR COMPANY
 RUN DATE IS -  12/18/76                            MAT PRO MODULE MOD007                                                      PAGE   3
XXXXXXXXXXXXXXXXXXXXXXXXXXXXXXXXXXXXXXXXXXXXXXXXXXXXXXXXXXXXXXXXXXXXXXXXXXXXXXXXXXXXXXXXXXXXXXXXXXXXXXXXXXXXXXXXXXXXXXXXXXXXXXXXXXXX
                              XXXXXXXXXXXXXXX  AXIAL POWER SHAPE INFORMATION  XXXXXXXXXXXXXXX

   AXIAL DISTRIBUTION IS INPUT          ROD AVERAGE POWER IS INPUT          NUMBER OF INCREMENTS =  9
                                                           X'S  IN FEET

                             XXXXXXXXXXXXXXXXXXX  INPUT AXIAL SHAPE NUMBER    1  XXXXXXXXXXXXXXXXXXX

   X( 1)=  0.0000  X( 2)=   .1667  X( 3)=   .3333  X( 4)=   .5000  X( 5)=   .6667  X( 6)=   .8333  X( 7)=  1.0000  X( 8)=  1.1667
X( 9)=  1.3333  X(10)=  1.5000  X(11)=  1.6667  X(12)=  1.8333  X(13)=  2.0000  X(14)=  2.1667  X(15)=  2.3333  X(16)=  2.5000
X(17)=  2.6667  X(18)=  2.8333  X(19)=  3.0000  X(
  QF( 1)=   .6200 QF( 2)=   .7050 QF( 3)=   .8750 QF( 4)=  1.0650 QF( 5)=  1.2150 QF( 6)=  1.3100 QF( 7)=  1.3700 QF( 8)=  1.3800
QF( 9)=  1.3750 QF(10)=  1.3350 QF(11)=  1.2750 QF(12)=  1.1600 QF(13)=  1.0600 QF(14)=   .9400 QF(15)=   .8150 QF(16)=   .6850
QF(17)=   .5500 QF(18)=   .4400 QF(19)=   .3800 QF(

INCREMENT      AXIAL STATION          UNNORMALIZED
              FEET      METERS         HEAT FLUX
    1        .1667      .05080           .7262
    2        .5000      .15240          1.0550
    3        .8333      .25400          1.3013
    4       1.1667      .35560          1.3762
    5       1.5000      .45720          1.3300
    6       1.8333      .55880          1.1737
    7       2.1667      .66040           .9388
    8       2.5000      .76200           .6838
    9       2.8333      .86360           .4525

                               AVGQI =  1.004167

    NORMALIZED HEAT FLUX AT TOP OF STACK =  .3000


                    ROD AVE BURNUP AT END OF LIFE (AMWDT) =      21.6
                    ROD TIME AVE HEAT FLUX (QBAR) =  294952.



                             XXXXXXXXXX  INITIAL PLENUM GASES (MOLES)  XXXXXXXXXX
AIR =  0.           NITROGEN =  0.           ARGON =  0.           FISSION GAS =  0.           HELIUM =   .57931E-02
```


1569 104

TABLE B-III (continued)

```
          FRAP-S MOD 002  VERS 02J* STEADY-STATE FUEL PERFORMANCE CODE*11/29/76*G A BERNA* AEROJET NUCLEAR COMPANY
 RUN DATE IS -  12/18/76                                   MAT PRO MODULE MOD007                                          PAGE   7
XXXXXXXXXXXXXXXXXXXXXXXXXXXXXXXXXXXXXXXXXXXXXXXXXXXXXXXXXXXXXXXXXXXXXXXXXXXXXXXXXXXXXXXXXXXXXXXXXXXXXXXXXXXXXXXXXXXXXXXXXXXXXXXXXX
XXXXXXXXXXXXXXXXXXXXXXXXXX  AXIAL INCREMENT   4  XXXXXXXXXX  POWER LEVEL   1  XXXXXXXXXX  GAS ITERATION  2  XXXXXXXXXXXXXXXXXXXXX

   START STEP AT          .00 HOURS            17. SECONDS       END STEP AT          .90 HOURS       3240. SECONDS
   POWER DURING STEP    6.883 KW/FT     22561.7 W/M           HEAT FLUX DURING STEP  212579.99 BTU/HR-FT2          .12063E+07 W/M**2
   FLUX DEPRESSION FACTOR    .7032
   BURNUP AT START OF STEP         .00 MWD/MTU      .1234E-02 MWS/KG     BURNUP DURING STEP       1.39 MWD/MTU    .1204E+03 MWS/KG

XXXXXXXXXXXXXXXXXXXXXXXXXXXXXXXXXXXXXXXXXXXXXXXXXX  COOLANT CONDITIONS  XXXXXXXXXXXXXXXXXXXXXXXXXXXXXXXXXXXXXXXXXXXXXXXXXXXXXX
   INLET TEMP.  642.00 (F)       BULK TEMP.  652.75 (F)       AVERAGE BULK TEMP.  652.75 (F)          COOLANT DENSITY   37.77 (LB/FT3)
                612.04 (K)                   618.01 (K)                           618.01 (K)                            605.1 (KG/M**3)

XXXXXXXXXXXXXXXXXXXXXXXXXXXXXXXXXXXXXXXXX FILM,CRUD AND OXIDE CONDITIONS  XXXXXXXXXXXXXXXXXXXXXXXXXXXXXXXXXXXXXXXXXXXXXXXXX
          DITTUS-BOELTER FILM COEF.    3267.33 (BTU/HR-FT2-F)   FORCED CONVECTION FILM COEF.    2115.38 (BTU/HR-FT2-F)
                                    .16540E+05 (W/M**2-K)                                     .12004E+05(W/M**2-K)
          DITTUS-BOELTER TEMP. DROP    65.06 (F)     36.15 (K)   FORCED CONVECTION TEMP. DROP  100.49 (F)    55.83 (K)
          JENS-LOTTES TEMP. DRUP        3.35 (F)      1.86 (K)
          CRUD THICKNESS   1.0000 (MILS)     .2540E-04 (M)        CRUD TEMPERATURE DROP ,  35.43 (F)     19.68 (K)
  ZR-OXIDE...  SURFACE TEMP.  691.53 (F)       639.55 (K) , THICKNESS    .0000071 (IN)     .1809E-06 (M) , WEIGHT GAIN     2.64 (MGMS/DM2)
          HYDROGEN    2.94 (PPM)      TEMP. DROP  .10812 (F)      .0600678 (K)

XXXXXXXXXXXXXXXXXXXXXXXXXXXXXXXXXXXXXXXXXXXXXXXXXX CLAD CONDITIONS  XXXXXXXXXXXXXXXXXXXXXXXXXXXXXXXXXXXXXXXXXXXXXXXXXXXXXXXXXX
 INSIDE DIAM.  .37436 (IN)      .0095087 (M)                  VOLUME     .4427 (CU.IN.)      .7255E-05 (CU.M.)
 O.D. TEMP.  691.64 (F)    639.61 (K)           AVG. TEMP.  714.48 (F)    652.30 (K)              I.D. TEMP.  737.32 (F) 664.99 (K)
        HOOP: STRESS -14037. (PSIA)             AXIAL: STRESS  -7788. (PSIA)              RADIAL: STRESS         0.   (PSIA)
              -.96784E+08(N/M**2)                      -.53698E+08 (N/M**2)                              0.          (N/M**2)
             STRAIN    .1077 (PCT)                    STRAIN    .1823 (PCT)                  STRAIN          .2675 (PCT)
 BOS EFFECTIVE CREEP STRAIN  0.            AXIAL NODE LENGTH  4.0000 (IN)  .101601 (M)         AXIAL GAP  0.0000 (IN) 0.000000 (M)

XXXXXXXXXXXXXXXXXXXXXXXXXXXXXXXXXXXXXXXXXXXXXXXXX  GAP CONDITIONS  XXXXXXXXXXXXXXXXXXXXXXXXXXXXXXXXXXXXXXXXXXXXXXXXXXXXXXXXXX
DIAMETRAL GAP  5.9242 (MIL) CONDUCTANCE,    2641.(BTU/HR-FT2-F)  AVG. TEMP.   782.93 (F) TEMP. DROP  91.17 (F) VOLUME   .0140IN**3
          .15048E-03 (M)                  14985.(W/M**2-K)                    690.33 (K)              50.65 (K)        .2295E-06 M**3
        CONTACT PRESSURE      0.(PSIA)    0.             (N/M**2)  GAS CONDUCTIVITY =         .151 (BTU/HR-FT-F)            .262 (W/M-K)

XXXXXXXXXXXXXXXXXXXXXXXXXXXXXXXXXXXXXXXXXXXXXXXXXX  FUEL CONDITIONS  XXXXXXXXXXXXXXXXXXXXXXXXXXXXXXXXXXXXXXXXXXXXXXXXXXXXXXXXXX
OUTSIDE DIAM.  .36843 (IN)      .009358 (M)                    SURFACE TEMP.  828.49 (F)    715.64 (K)
  STORED ENERGY AT TAVE =  1266.43 (F)  960.05 (K)  IS         77.10 (BTU/LB)          42.84 (CAL/GM)
```

RING RADIUS (IN)	RING RADIUS (M)	TEMPERATURE (F)	TEMPERATURE (K)	EXPANSION (PCT)	SWELLING (PCT)	POROSITY (PCT)	DENSIFICATION (PCT)	GRAIN SIZE (MICRONS)
0.000000	0.000000	1761.21	1233.82	0.000000	0.00000	0.0000	0.000000	5.00
.058358	.001482	1652.64	1173.50	.844259	0.00000	2.1667	0.000000	5.00
.082514	.002096	1547.76	1115.24	.772901	0.00000	2.1667	0.000000	5.00
.101037	.002566	1446.43	1058.94	.705886	0.00000	2.1667	0.000000	5.00
.116643	.002963	1348.53	1004.56	.642922	0.00000	2.1667	0.000000	5.00
.130384	.003312	1253.98	952.03	.583753	0.00000	2.1667	0.000000	5.00
.142800	.003627	1162.68	901.30	.528145	0.00000	2.1667	0.000000	5.00
.154211	.003917	1074.56	852.35	.475880	0.00000	2.1667	0.000000	5.00
.164828	.004187	989.54	805.12	.426755	0.00000	2.1667	0.000000	5.00
.174794	.004440	907.54	759.56	.380583	0.00000	2.1667	0.000000	5.00
.184217	.004679	828.49	715.64	.337184	0.00000	2.1667	0.000000	5.00

```
VOLUMES,(CU.IN.) ... FUEL      .4245      DISH      .0042       CRACK       .0009     OPEN POROSITY     .0008
        (CU.M. ) ...         .6957E-05           .6817E-07             .1393E-07                     .1243E-07
NITROGEN CONCENTRATION    .36558E-04 (MOLES)
 RADIUS OF COLUMNAR GRAIN ZONE = 0.000000 (IN)  0.000000 (M)        THRESHOLD TEMP. =3391.2 (F) 2139.4 (K)
 COLUMNAR GRAIN ZONE DENSITY =    .935
```


23-330

TABLE B-III (continued)

```
          FRAP-S MOD 002  VERS 02J* STEADY-STATE FUEL PERFORMANCE CODE*11/29/76*G A BERNA* AEROJET NUCLEAR COMPANY
  RUN DATE IS -  12/18/76                              MAT PRO MODULE MOD007                                              PAGE  23
XXXXXXXXXXXXXXXXXXXXXXXXXXXXXXXXXXXXXXXXXXXXXXXXXXXXXXXXXXXXXXXXXXXXXXXXXXXXXXXXXXXXXXXXXXXXXXXXXXXXXXXXXXXXXXXXXXXXXXXXXXXXXX
  XXXXXXXXXXXXXXXXXXXXXXXX     POWER LEVEL   2      XXXXXXXXXXXXXXXXXXXXXXXX     AXIAL SHAPE NUMBER  1    XXXXXXXXXXXXXXXXXXXX

  BURNUP TO END OF STEP    22. (MWD/MTU)       BURNUP DURING STEP          21. (MWD/MTU)     ROD AVERAGE HEAT FLUX 308927. (BTU/HR-FT2)
                  .16662E+04.(MWS/KG)                            .17787E+04 (MWS/KG)                        .17530E+07 (W/M)
RAD. + AX. CLAD AVG TEMP  741.35 (F)  667.23 (K) CLAD VOL    .2541 CU.IN.    .416E-05 CU.M. POROS VOL    .0153 CU.IN.  .2525E-06 CU.M.
RAD. + AX. GAP  AVG TEMP  833.73 (F)  716.56 (K) GAP VOL     .1005 CU.IN.    .163E-05 CU.M. DISH VOL     .0374 CU.IN.  .6123E-06 CU.M.
RAD. + AX. FUEL AVG TEMP 1627.62 (F) 1159.72 (K) FUEL VOL  3.8577 CU.IN.    .632E-04 CU.M. ROUGH VOL    .0072 CU.IN.  .1172E-06 CU.M.
AVG. FUEL SURFACE TEMP.    893.14 (F)  751.56 (K) CRACK VOL  .0160 CU.IN.    .263E-06 CU.M.
STACK HEIGHT    36.276 (IN)     .9214 (M)   PCT. INCREASE    .7675    ROD LENGTH   36.070 (IN)     .9162 (M) PCT. INCREASE   .1939

   NITROGEN CONCENTRATION   .28155E-03 (MOLES)  HELIUM PRODUCTION   .16115E-06 (MOLES)  FISSION GAS PRODUCTION   .16115E-04 (MOLES)

   GASES RELEASED --          WATER                NITROGEN               HELIUM                FISSION
                (MOLES)     0.                     .54256E-04             .28644E-07            .10312E-05
             (FRACTION)     0.                     .16157E+00             .17775E+00            .63991E-01

   XXXXXXXXXXXXXXXXXXXXXXXXXXXXXXXXXXXXXX    MOLE FRACTIONS OF GAS    XXXXXXXXXXXXXXXXXXXXXXXXXXXXXXXXXXXXXXXXXX

             AIR       0.                  HYDROGEN   0.                  WATER        0.
             ARGON     0.                  HELIUM      .99055E+00         NITROGEN      .92771E-02
             KRYPTON    .26449E-04         XENON       .14988E-03         FISSION       .17632E-03

   CUMULATIVE QUANTITY OF GAS IN GAP     .58484E-02 (MOLES)

  PLENUM LENGTH             1.8116 (IN)    .04602 (M)          PLENUM VOLUME                    .1785 CU.IN.      .2925E-05 CU.M.
  GRASHOFF NUMBER OF PLENUM  10611.46                          HEAT FLOW FROM TOP OF STACK  4.0131 (BTU/HR)     .1175E+01 (W)
  HEAT GENERATED IN SPRING   4.3303 (BTU/HR)  .1268E+01 (W)    PLENUM TEMPERATURE              695.20 (F)    641.59 (K)
  COOLANT SATURATION TEMP.   652.75 (F)   618.01 (K)           TOTAL HOT VOID VOLUME            .3549 CU.IN.      .5815E-05 CU.M.
INTERNAL PRESSURE = (GASMOL)(40.8) /((HPV / TPLEN +460.)   +   SUMDH   +   SUMGP   +   SUMCK   +   SUMRG   +   SUMPOR)
                     .0058484        .1785    695.             .0000185    .0000786    .0000116    .0000057    .0000068     =    865.79

          CLADDING TEMP. IN DEG F  , STRESSES + INTERFACIAL PRESSURE IN PSIA   , + RADIAL GAP IN INCHES
XXXXXXXXXXXXX  CLAD TEMP., AXIAL + HOOP STRESS,STRAIN,+ PLASTIC STRAIN, GAP WIDTH, AND INTERFACIAL PRESSURE  XXXXXXXXXXXXX
```

J	T CLAD	SIG HOOP	SIG AXIAL	EPS HOOP	EPS AXIAL	EPP HOOP	EPP AXIAL	GAP	PINT
1	.71784E+03	-.13022E+05	-.73114E+04	.11740E-02	.18551E-02	0.	0.	.24658E-02	0.
2	.74577E+03	-.13022E+05	-.73114E+04	.13079E-02	.19539E-02	0.	0.	.18634E-02	0.
3	.76651E+03	-.13022E+05	-.73114E+04	.14099E-02	.20286E-02	0.	0.	.12943E-02	0.
4	.77280E+03	-.13022E+05	-.73114E+04	.14413E-02	.20516E-02	0.	0.	.11124E-02	0.
5	.76893E+03	-.13022E+05	-.73114E+04	.14220E-02	.20374E-02	0.	0.	.12246E-02	0.
6	.75579E+03	-.13022E+05	-.73114E+04	.13566E-02	.19896E-02	0.	0.	.15997E-02	0.
7	.73593E+03	-.13022E+05	-.73114E+04	.12604E-02	.19190E-02	0.	0.	.20974E-02	0.
8	.71421E+03	-.13022E+05	-.73114E+04	.11568E-02	.18423E-02	0.	0.	.25309E-02	0.
9	.69433E+03	-.13022E+05	-.73114E+04	.10636E-02	.17722E-02	0.	0.	.28403E-02	0.

1569 106

TABLE B-III (continued)

FRAP-S MOD 002 VERS 02J* STEADY-STATE FUEL PERFORMANCE CODE*11/29/76*G A BERNA* AEROJET NUCLEAR COMPANY
RUN DATE IS - 12/18/76 MAI PRO MODULE M00007 PAGE 24

CLADDING TEMP. IN DEG F , STRESSES + INTERFACIAL PRESSURE IN PSIA , + RADIAL GAP IN INCHES
CLAD TEMP.+ AXIAL + HOOP STRESS,STRAIN,+ PLASTIC STRAIN, GAP WIDTH, AND INTERFACIAL PRESSURE

J	T CLAD	SIG HOOP	SIG AXIAL	EPS HOOP	EPS AXIAL	EPP HOOP	EPP AXIAL	GAP	PINT
1	.71784E+03	-.13022E+05	-.73114E+04	.92372E-03	.18337E-02	-.25025E-03	-.21380E-04	.24128E-02	0.
2	.74577E+03	-.13022E+05	-.73114E+04	.95056E-03	.19234E-02	-.35743E-03	-.30536E-04	.17876E-02	0.
3	.76651E+03	-.13022E+05	-.73114E+04	.94905E-03	.19893E-02	-.46040E-03	-.39375E-04	.11965E-02	0.
4	.77280E+03	-.13022E+05	-.73114E+04	.94432E-03	.20091E-02	-.49700E-03	-.42460E-04	.10070E-02	0.
5	.76893E+03	-.13022E+05	-.73114E+04	.94749E-03	.19969E-02	-.47447E-03	-.40535E-04	.11240E-02	0.
6	.75579E+03	-.13022E+05	-.73114E+04	.95223E-03	.19551E-02	-.40457E-03	-.34563E-04	.15139E-02	0.
7	.73593E+03	-.13022E+05	-.73114E+04	.94454E-03	.18920E-02	-.31583E-03	-.26982E-04	.20304E-02	0.
8	.71421E+03	-.13022E+05	-.73114E+04	.91816E-03	.18219E-02	-.23862E-03	-.20386E-04	.24803E-02	0.
9	.69433E+03	-.13022E+05	-.73114E+04	.88070E-03	.17566E-02	-.18291E-03	-.15626E-04	.28015E-02	0.

CHANGE IN CLADDING LENGTH = .68713E-01 (IN) .17453E-02 (M)
LENGTH CHANGE RELATIVE TO THE FUEL CHANGE = -.20757E+00 (IN) -.52724E-02 (M)

TABLE B-III (continued)

FRAP-S MOD 002 VERS 02J* STEADY-STATE FUEL PERFORMANCE CODE*11/29/76*G A BERNA* AEROJET NUCLEAR COMPANY

RUN DATE IS - 12/18/76 MAI PRO MODULE MOD007 PAGE 25

PBF SINGLE ROD PCM-20

********** PEAK POWER INCREMENT OUTPUT **********

	TIME HOURS	BURNUP MWD/TU	POWER KW/FT	CLAD TEMP (F) OD.	AVG	ID.	GAP MILS	GAP (F)	FUEL TEMP (F) OD.	AVG	CEN	CONT. PSI	CLAD STRESS HOOP	AXIAL	STRAIN PCT	FUEL OD INCH	GAP CONDCT	FGAS PSI	ZRO2 MIL	H2 PPM
1	1.	1.	6.68	692.	714.	737.	5.92	783.	828.	1268.	1761.	0.	-14037.	-7788.	.1077	.36843	2641.	736.	.01	2.9
2	10.	30.	13.77	728.	773.	817.	3.14	892.	967.	2057.	3366.	0.	-13022.	-7311.	.1441	.37135	3247.	866.	.02	7.2

TABLE B-III (continued)

FRAP-S MOD 002 VERS 02J* STEADY-STATE FUEL PERFORMANCE CODE*11/29/76*G A BERNA* AEROJET NUCLEAR COMPANY
RUN DATE 1> - 12/16/76 MAT PRO MODULE MOD007 PAGE 26

END OF LIFE STRAIN RANGE (PCT) = .0751

FISSION GAS CUMULATIVE FRACTION RELEASE = .063991

ZRO2 WEIGHT GAIN , (MG/DM2) = 6.46

APPENDIX C

FRAP-S LINK TO FRAP-T

APPENDIX C

FRAP-S LINK TO FRAP-T

A sample problem is presented to show the use of FRAP-S2 results as initial conditions for the transient accident analysis code FRAP-T2.

A typical PWR fuel rod is modeled for FRAP-S2 and an analysis is made for a 2000 hour burnup on the rod. At 2000 hours, the rod is subjected to a full-size break loss-of-coolant accident (LOCA).

Table C-I contains pertinent data on the rod. Figure C-1 shows the response of the fuel rod for the two time scales defining long-term operational behavior and short-term accident response.

The discontinuities evident in Figure C-1 at the transition between normal and accident conditions are due to slight differences in similar models of versions of FRAP-S and FRAP-T. Most of these differences have been removed as part of the continuing development effort of versions of FRAP-S and FRAP-T.

This link capability allows the user to initiate accidents at any time during the operating cycle of a reactor and use a realistic set of initial conditions as input for the accident analysis code.

TABLE C-I

FRAP-S LINK TO FRAP-T EXAMPLE PROBLEM SPECIFICATIONS

(PWR UO_2 ENRICHED)

Coolant Conditions:	
mass flux	1.917×10^6 (lbm/ft-ft^2)
pressure	2273 (psia)
inlet temperature	540 (°F)
hydraulic diameter	0.534 (in.)
Rod Geometry:	
fuel stack length	12 (ft)
fuel outside diameter	0.366 (in.)
cladding outside diameter	0.422 (in.)
plenum length	7.0 (in.)
Rod Initial Conditions:	
internal pressure	600 (psia)
enrichment	3 (%)
density	93.288% theoretical
Power History:	
linear ramp from 0.0 kW/ft to 11.08 kW/ft in 50 hours, then held for the remainder of 2000 hours	

EARLY LINK RESULTS

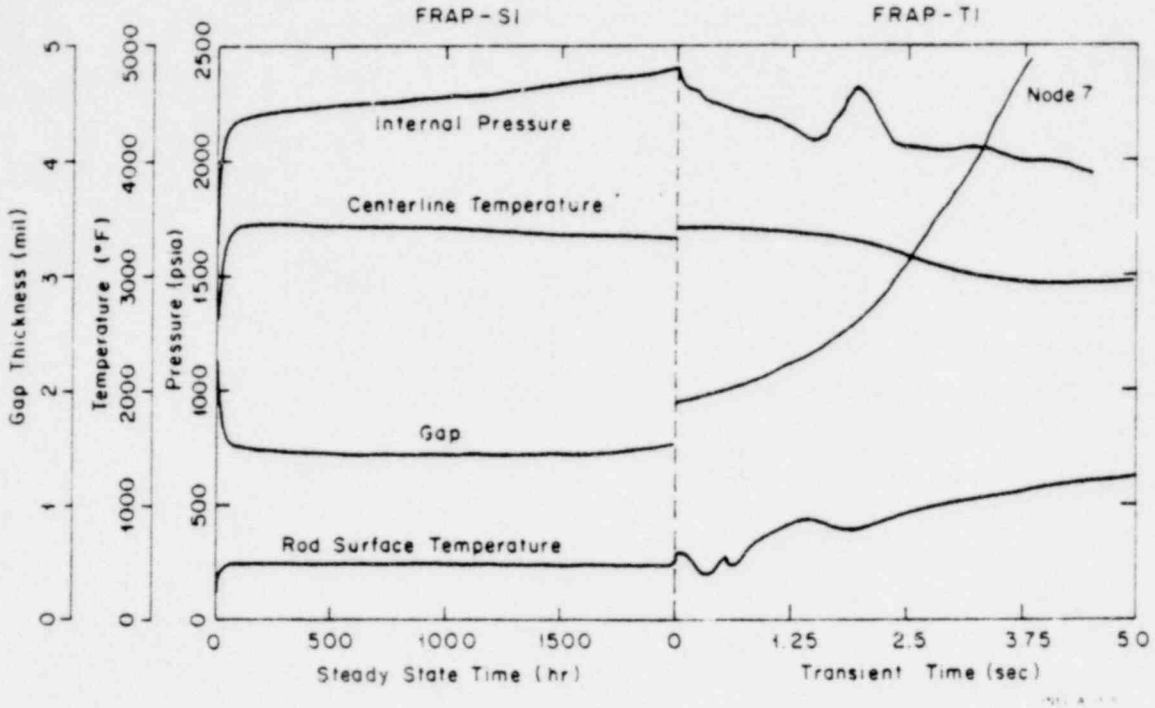

Fig. C-1 Early link results.

APPENDIX D

CONFIGURATION CONTROL PROCEDURE

APPENDIX D

CONFIGURATION CONTROL PROCEDURE

A Configuration Control Procedure (CCP) has been defined to maintain a traceability of results from developing computer codes. During the development process of a computer code, requirements exist for using the code for generating both checkout results and production results, depending on the stage of development.

The Configuration Control Procedure consists of a method by which changes can be made to the code and traceability of results maintained. Any time a modification to the code is made, the following data are taken:

(1) Version of code to which modification was made
(2) Reason for modification
(3) Results affected by modification
(4) Date of modification
(5) Person responsible for modification
(6) The change cards used to modify the original version of the code.

A tape update routine is used to modify the code. This routine requires only those computer cards defining new statements or deleting old statements. These "change cards" are kept on file so any version of the code can be reproduced if necessary.

A new identification number is assigned to the modified version of the code and this new number is programmed into the code where it will be listed at the top of each page of output and on each plot produced by the code.

APPENDIX E

MATERIALS PROPERTIES CORRELATIONS EMPLOYED BY FRAP-S3

APPENDIX E

MATERIALS PROPERTIES CORRELATIONS EMPLOYED BY FRAP-S3

A materials properties subcode is used to provide the computational subcodes of FRAP-S3 with gas, fuel, and cladding properties. Table E-I lists those properties from one of the two references which are used by FRAP-S3 given below.

1. P. E. MacDonald et al, MATPRO - A Handbook of Materials Properties for Use in the Analysis of Light Water Reactor Fuel Rod Behavior, ANCR-1263 (February 1976).

2. P. E. MacDonald et al, MATPRO - Version 09 - A Handbook of Materials Properties for Use in the Analysis of Light Water Reactor Fuel Rod Behavior, TREE-NUREG-1005 (December 1976).

TABLE E-I

PROPERTIES INCLUDED IN MATPRO USED BY FRAP-S3

Property	Subcode	Reference
Fuel Material Properties		
1. Specific Heat Capacity	FCP	2
2. Thermal Conductivity	FTHCON	2
3. Emissivity	FEMISS	2
4. Thermal Expansion	FTHEXP	2
5. Fuel Swelling	FSWELL	2
6. Densification	FUDENS	2
7. Restructuring	FRESTR	2
Cladding Material Properties		
1. Axial Growth	CAGROW	2
2. Thermal Conductivity and Its Uncertainty	CTHCON	2
3. Zr-Oxide Thermal Conductivity	ZOTCON	2
4. Axial Thermal Expansion	CATHEX	2
5. Diametral Thermal Expansion	CDTHEX	2
6. Elastic Modulus	CELMOD	2
7. Strain versus Stress	CSTRAN	1
8. Stress versus Strain	CSTRES	1
9. Poisson's Ratio	CPOIR	2
10. Meyer Hardness	CMHARD	2
Gas and Fuel Rod Material Properties		
1. Gas Thermal Conductivity	GTHCON	2
2. Gas Viscosity	GVISCO	2
3. Gap Heat Transfer	GAPHTR	2
4. Physical Properties	PHYPRO	2